The Hydrological System of Storglaciären, Sweden: Integrating Modelling with Observations

Andrew G. Williamson

SCOTT POLAR RESEARCH INSTITUTE,
UNIVERSITY OF CAMBRIDGE
&
GIRTON COLLEGE

This thesis is submitted for the degree of
Master of Philosophy
2014

Declaration

I declare that this thesis is entirely my own work, and includes nothing that is the outcome of work done in collaboration with others, except where clearly acknowledged in the text or Acknowledgements. It has not been submitted in whole or in part for a degree at this or any other University. This thesis does not exceed 20,000 words, excluding Figures and their captions, Tables and their captions, Cover Page, Declaration, Acknowledgements, Appendices, References, and Lists of Contents, Figures, Tables, Abbreviations and Mathematical Notation.

Andrew G. Williamson

June 2014

Acknowledgements

Firstly, and most importantly, I thank my supervisor Neil Arnold (University of Cambridge) for his unfailing support and insights over the year. Most especially, he helped solve numerical-modelling issues, often given all too short a notice. Thanks too must go to Ali Banwell (University of Cambridge) who advised on running and helped solve technical problems with the subglacial-hydrology model.

Helen Dahlke (University of California, Davis) permitted my involvement with two field seasons on Storglaciären, allowing data collection that rendered this thesis possible. Helen has been, and continues to be, a role model for me: her enduring care, enthusiasm and, above all, friendship, are matched by few others, and I'm extremely fortunate that I've come to know her so well.

Some of the data in this study were provided or originally collected by staff and field assistants at the remarkable Tarfala Research Station. I particularly thank Peter Jansson, Ninis Rosqvist and Andrew Mercer (University of Stockholm) for speedily answering questions on several aspects of these data. The supreme hospitality experienced at the Tarfala Research Station was probably asymptomatic of many fieldwork experiences, and for this I am grateful.

For providing some MPhil funding, I am appreciative of Girton College. For helping fund fieldwork, I acknowledge the Girton College K.J. Baker Travel Award, the University of Cambridge Department of Geography, the David Richards Travel Scholarship, the Dr Jean Grove Memorial Fund, and my family and friends. Helen's ability to conduct, and thus my invitation to be involved with, 2013 fieldwork was only possible due to NSF Award #0853809, the Göran Gustafsson Foundation and the Helge Ax:son Johnsons Foundation. For making fieldwork so gratifying, I thank field companions from both years: Helen, Fanny, Isy, Todd, Steve, Asha and Selene; we made 'epic' field teams.

It is the people with whom we surround ourselves that have the largest impact on our lives. I've been very blessed then to be encircled by individuals who have offered me such profound motivation and inspiration. I thank all of my friends and family, in Cambridge and elsewhere, who were there for me over this study's derivation, execution and completion; I'm quite certain that I wouldn't have remained sane (and perhaps I haven't) without them. Thanks to everyone at SPRI for making it such a rewarding place to study, but a special thank you to fellow MPhils or 'sports fans' (the title we appear to have given ourselves): Tom, Mike, Charles, John and Corinne. Even though they remind me all too often of my overuse of superlatives, they can believe me when I say that they helped make this my *best ever* year in Cambridge. Finally, I shall be forever indebted to three special individuals who kept me going when nobody else could thanks to their continuing care and words of reassurance: Philip, Vicky and Marcus.

This thesis is dedicated to my Aunty, one of the kindest and most selfless people I know, and without whose staggering generosity, I could not have funded this year.

Abstract

There is a need for more studies in glacier hydrology that integrate numerical models with detailed empirical data collected over one/multiple summer(s). This is especially true for physically based models whose main advantage lies in ability to predict basal water pressure because of its significance for ice dynamics, thus helping inform knowledge of runoff and ultimately sea-level rise both presently and, when forced with climate projections, into the future. This study helped fulfill this requirement by applying a physically based glacier-hydrology model to the predominantly temperate ~3.22km^2 Storglaciären, Sweden, forced with 2012 empirical data. The model has three sub-elements: a high temporal (hourly) and spatial (20-m) resolution surface-energy-balance model to generate meltwater across Storglaciären's surface for the entire summer, a surface-routing model to route this meltwater (and precipitation) across the surface either until it runs off Storglaciären's edges or is intercepted by moulins extending into the internal system, and a subglacial-hydrology model where inflow from moulin hydrographs is routed in R-channels from moulins to the terminus to produce proglacial discharge. The surface-energy-balance model was validated using Storglaciären's summer mass-balance data and measurements of surface lowering at an automatic weather station on its surface. It performed well, though slightly (~4%) underestimated melt. The surface-routing model was qualitatively evaluated using estimates of direct supraglacial runoff derived from previous studies and reproduced these to within 2%. The subglacial-hydrology model's outputs of proglacial discharge and subglacial flow-routing times were quantitatively compared with empirical discharge measurements in the three proglacial streams Nordjåkk, Centerjåkk and Sydjåkk, and with flow-routing times from ~25 tracer injections across Storglaciären in 2012 and 2013. To replicate these data, the subglacial model required high conduit roughnesses to be specified (Manning's $n = 0.125$ for conduits leading to Centerjåkk/Sydjåkk and $n = 0.075$ for the conduit producing outflow at Nordjåkk). However, this is encouraging and follows postulations of braided, broad and low H-channels beneath Storglaciären, which cannot be explicitly accounted for by the model, so rough R-channels are instead required. Overall, the subglacial model performed well, though slightly underestimated discharge and overestimated flow-routing times. The internal drainage system was reevaluated, with suggestion that the englacial network in the upper ablation and firn areas may feed Centerjåkk/Sydjåkk, not Nordjåkk, contrasting with suggestions in previous studies. The physically based model performed less favourably than simpler linear-reservoir models applied to Storglaciären; however, its key worth was in generating continuous basal water pressure for the entire summer, the first data of this kind to be generated for this glacier. These data compared well with suggestions from empirical borehole measurements in previous years. Specifically, the 'Spring Event' (marked by a high-pressure period at the end of May), continuously high pressures (at/above ice-overburden) within the overdeepened (up to ~230m) area and the response of water pressures to major meteorological forcings were captured. The fact that continuously high pressures within the overdeepening were reproduced despite the model's inherent specification of R-channels suggests this flow morphology is possible here, informing our understanding of processes within overdeepenings.

List of Contents

List of Figures

List of Tables

List of Abbreviations

a.s.l.	above sea level
AWS	Automatic weather station
BTC	Breakthrough curve
CSA	Cross-sectional area
DDF	Degree-day factor
DEM	Digital elevation model
ELA	Equilibrium-line altitude
EXTRAN	Extended Transport block (of SWMM)
FDA	Flow-delay algorithm
GIC	Glaciers and ice caps
GlaDS	Glacier Drainage System (model)
GrIS	Greenland Ice Sheet
GS	Gauging station
H-	Hooke-(channel)
HGd'A	Haut Glacier d'Arolla
IPCC	Intergovernmental Panel on Climate Change
JD	Julian Day Number
LWR	Longwave radiation
N-	Nye-(channel)
PDD	Positive-degree-day
PMP	Pressure-melting point
R-	Röthlisberger-(channel)
RH	Relative humidity
RMSE	Root Mean Square Error
SEB	Surface-energy-balance
SL	Sea level
SLR	Sea-level rise
SROUT	Surface-routing
SUBHYD	Subglacial-hydrology
SWMM	Storm Water Management Model
SWR	Shortwave radiation
TRS	Tarfala Research Station
w.e.	water equivalent

List of Mathematical Notation

$\boldsymbol{\beta}$	Degree-day factor (mm w.e. d^{-1} $°C^{-1}$)
$\boldsymbol{\delta e}$	Difference between vapour pressure of air and glacier-surface vapour pressure (Pa)
$\boldsymbol{\theta}$	Surface slope (^{o})
$\boldsymbol{\mu}$	Water viscosity (Pa s)
$\boldsymbol{\rho_i}$	Ice density (kg m^{-3})
$\boldsymbol{\rho_s}$	Snow density (kg m^{-3})
$\boldsymbol{\rho_w}$	Water density (kg m^{-3})
$\boldsymbol{\sigma}$	Stefan-Boltzmann constant (W m^{-2} K^{-4})
$\boldsymbol{\varphi}$	Hydraulic potential (Pa)
$\boldsymbol{a}$	Surface albedo
$\boldsymbol{a_i}$	Ice albedo
$\boldsymbol{a_s}$	Snow albedo
$\boldsymbol{A_c}$	Conduit cross-sectional area (m^2)
$\boldsymbol{B}$	Arrhenius parameter in Glen's Flow Law (N m^{-2} $s^{1/m}$)
$\boldsymbol{c}$	Specific heat capacity (J kg^{-1})
$\boldsymbol{C}$	Rate of conduit closure by ice deformation (m^2 t^{-1})
$\boldsymbol{C_i}$	Horizontal flow velocity across ice-covered cells (m s^{-1})
$\boldsymbol{C_s}$	Horizontal flow velocity across snow-covered cells (m s^{-1})
$\boldsymbol{CSA_{fp}}$	Mean cross-sectional area of flow pathway (m^2)
$\boldsymbol{d}$	Snow depth (m)
$\boldsymbol{d_s}$	Surface-layer depth (m)
$\boldsymbol{d_2}$	Subsurface layer depth (m)
$\boldsymbol{D}$	Vertical travel time to the base of the snowpack (s)
$\boldsymbol{D_{fp}}$	Diameter of flow pathway (m)
$\boldsymbol{E}$	Surface grid cell elevation (m a.s.l.)
$\boldsymbol{ET_{sky}}$	Emissive temperature of the sky
$\boldsymbol{f_r}$	Frictional coefficient
$\boldsymbol{f_s}$	Proportion of sky visible from a grid cell (%)
$\boldsymbol{F}$	Thermal diffusivity of ice or snow (m^2 s^{-1})
$\boldsymbol{g}$	Gravitational acceleration (m s^{-2})
$\boldsymbol{G}$	Degrees of freedom
$\boldsymbol{h}$	Glacier-surface elevation (m a.s.l.)
$\boldsymbol{k}$	Uniform flotation factor (P_w/P_i)

K	Porosity of the snowpack
K_e	Effective porosity of the snowpack
K_l	Latent heat scalar (of ice or snow) (m kg^{-1} K^{-1} s^2)
K_s	Sensible heat scalar (of ice or snow) (m kg^{-1} K^{-1} s^2)
L_f	Latent heat of fusion of water (J kg^{-1})
$LW\downarrow$	Incoming longwave radiation (W m^{-2})
$LW\downarrow_{AWS}$	Measured incoming longwave radiation at the weather station (W m^{-2})
$LW\downarrow_{sky}$	Incoming longwave radiation from the sky (W m^{-2})
$LW\downarrow_{terr}$	Incoming longwave radiation from the surrounding terrain (W m^{-2})
$LW\uparrow$	Outgoing longwave radiation (W m^{-2})
m	Exponent in Glen's Flow Law
M	Total melt (mm w.e.)
n	Manning's roughness coefficient ($m^{-1/3}$ s)
N	Effective pressure (Pa)
P	Air pressure (Pa)
P_a	Atmospheric pressure (Pa)
P_i	Ice-overburden pressure (Pa)
P_w	Water pressure (Pa)
q	Water flux through the snowpack (m^3 s^{-1})
Q_{fp}	Mean sum of water flowing along a pathway over summer (m^3 s^{-1})
Q_L	Latent heat flux
Q_M	Energy available for melt
Q_R	Heat flux from rain
Q_S	Sensible heat flux
R	Hydraulic radius of a channel (m)
$SW\downarrow$	Incoming shortwave radiation (W m^{-2})
$SW\uparrow$	Outgoing shortwave radiation (W m^{-2})
t	Time step (s)
T	Air temperature at ~2m above the ice surface (°C)
T_{pdd}	Sum of positive daily mean temperatures (°C)
T_s	Glacier-surface temperature (°C)
T_{terr}	Average temperature of the surrounding terrain (°C)
u_{fp}	Mean throughflow velocity (m s^{-1})
U	Water velocity through a conduit (m s^{-1})

$\boldsymbol{V}$	Wind speed (m s^{-1})
$\boldsymbol{V_m}$	Modelled value
$\boldsymbol{V_o}$	Mean of observed values
$\boldsymbol{V_o^t}$	Observed value at time *t*
$\boldsymbol{w}$	Snow permeability (m^2)
$\boldsymbol{X}$	Rate of conduit-wall melting (kg t^{-1})
$\boldsymbol{Y}$	Nash-Sutcliffe Model Efficiency Coefficient
$\boldsymbol{z}$	Glacier-bed elevation (m a.s.l.)

1. Introduction

"Water is the driving force of all nature."

– Leonardo da Vinci

1.1. Rationale

Perhaps the most concerning consequence of climate change is accelerating sea-level rise (SLR), which, intrinsically linked to processes within the cryosphere, may have profound societal impacts (Church and White, 2006; Church *et al.*, 2008; Vaughan *et al.*, 2013). Glaciers and ice caps (GIC), excluding the Greenland (GrIS) and Antarctic Ice Sheets, contain an estimated 0.412 m SL equivalent (Vaughan *et al.*, 2013), the mean of values given in studies by Huss and Farinotti (2012), Marzeion *et al.* (2012), Grinsted (2013), and Radić *et al.* (2013). GIC are likely to raise global SL 0.124±0.037 m by 2100 (Radić and Hock, 2011). Recent glaciological research has arguably been diverted from GIC towards ice sheets, as their contribution to SLR is more uncertain on centurial/millennial timescales (due to dynamic feedbacks) and they could ultimately raise SL by >65 m (Shepherd *et al.*, 2012; Bamber and Aspinall, 2013; Vaughan *et al.*, 2013). Yet, on decadal timescales, GIC will likely continue their ~60% current domination of SLR (Meier, 1984; Dyurgerov and Meier, 1997; Cogley and Adams, 1998; Bamber and Payne, 2004; Meier *et al.*, 2007; Gardner *et al.*, 2013; Kerr, 2013). Understanding processes governing GIC mass balance and their response to climatic change is therefore imperative for informing policymakers, at least over the coming century (Bahr *et al.*, 2009; Bahr and Radić, 2012).

Numerous factors control GIC's contribution to SLR, with hydrology crucially important due to its profound influence on other elements of the glacial system. Most especially, glacier-sliding rates strongly depend upon high-pressure water at the ice-bed interface, which can increase basal sediment deformation (Clarke, 1987; Boulton and Hindmarsh, 1987; Iverson *et al.*, 1995), promote 'hydraulic jacking' (Kamb, 1970; Iken, 1981; Iken *et al.*, 1983; Bindschadler, 1983; Iken and Bindschadler, 1986), and permit 'enhanced basal sliding' (Iken and Bindschadler, 1986). Any/all of these mechanisms can cause speed-ups at various timescales, including diurnal (Schuler *et al.*, 2004; Schuler and Fischer, 2009), seasonal, such as in 'Spring Events' (Kavanaugh and Clarke, 2001; Mair *et al.*, 2003; Bingham *et al.*, 2003), intra-annual (Willis, 1995; Mair *et al.*, 2002; Rippin *et al.*, 2005; Bartholomaus *et al.*, 2008; Purdie *et al.*, 2008; Fudge *et al.*, 2009) and on longer timescales (e.g., Hambrey *et al.*, 2005; Anderson *et al.*, in press), and during 'surging' (e.g., Kamb *et al.*, 1985). Higher rates of motion transport more of GIC's mass to lower elevations where melting is higher, thus leading to positive feedbacks. Models predicting basal water pressure (P_w) variations are thus a fundamental requirement in glaciology. Our understanding derived from these models and from empirical observations on GIC can be applied to ice sheets, useful since GIC are logistically easier to research (e.g., Zwally *et al.*, 2002; Jansson and Näslund, 2009; Bartholomew *et al.*, 2010; Chandler *et al.*,

2013). This is especially true when GIC resemble ice sheets, whether because of their latitudes (and thus environmental response), because they have predominantly 'cold' (<0°C) thermal regime (e.g., Bingham *et al.*, 2003; van der Veen, 2007; Irvine-Fynn *et al.*, 2011), because they have calving fronts, or because they have overdeepened areas, similar to many ice-sheet outlet glaciers, potentially hastening their response to climatic change (e.g., Schoof, 2007; Howat *et al.*, 2008; Nick *et al.*, 2009; Cook and Swift, 2012).

In addition to its control on dynamics, glacier hydrology moderates streamflows through temporal storage following snowfall, with water released during otherwise low flows (Jansson *et al.*, 2003; Dahlke *et al.*, 2012). One sixth of the world's population has this runoff as its major water supply (Barnett *et al.*, 2005) and it is important for hydropower, especially in the Alps/Scandinavia (Willis and Bonvin, 1995; Sharp, 2005; Willis, 2005; Benn and Evans, 2010; Huss, 2011; Baraer *et al.*, 2011; Bolch *et al.*, 2012; Schaner *et al.*, 2012). Runoff can present hazards to populations, including through glacial-lake outburst floods (e.g., Nye, 1976; Hubbard *et al.*, 2005; Huss *et al.*, 2007). Meltwater is also important for erosion and thus sediment entrainment, impacting water quality (e.g., Schneider and Bronge, 1996; Tranter *et al.*, 1996; Alley *et al.*, 1997). Finally, local biodiversity is often enhanced by glacial runoff (Jacobsen *et al.*, 2012). Thus, accurate runoff forecasts represent a socio-economical and environmental necessity.

This discussion indicates having sound understanding of glacier hydrology is vitally important. Yet, glacier-hydrological systems are highly spatiotemporally heterogeneous and transient, and have many inaccessible elements (Hubbard and Nienow, 1997; Hock and Jansson, 2005). Therefore, much knowledge must be derived from indirect empirical observations or modelling-based studies, which have typically been focused on temperate glaciers. Many studies have fulfilled these purposes, but the two are seldom integrated to yield comprehensive understanding of glaciers' hydrological systems. Specifically, studies are lacking using detailed datasets from a single/multiple summer season(s) and integrating them with models. This approach would offer greater insight into glacier hydrology, allowing higher confidence in numerical models' ability to replicate its complexity.

1.2. Approach and Aims

Given need for further studies integrating extensive empirical data with modelled outputs, this thesis applies a physically based glacier-hydrology model to a small, predominantly temperate, valley glacier: Storglaciären, Sweden. This site is selected since extensive empirical data were collected during 2012 and because, although Storglaciären has been intensively researched over several decades, to date no study has applied a physically based glacier-hydrology model here. Furthermore, alternative glacier-hydrology models have been used here, thus making it a valuable location for comparing simpler empirically based models with more advanced physically based ones. Storglaciären presents other promising research opportunities because it lies within the Arctic, which has experienced more rapid warming than elsewhere recently (IPCC, 2013). It also has an

overdeepening, where glacier-hydrology knowledge is poor, but from which understanding could be applicable to ice-sheet outlet glaciers' troughs, so representing an important research area (Cook and Swift, 2012).

Towards fulfilling this objective, the aims are:

- To apply the physically based glacier-hydrology model developed by Arnold *et al.* (1998). This model has high spatial (20-m) and temporal (hourly) resolution, is forced with 2012 empirical data, and combines three sub-elements:
    - a surface-energy-balance (SEB) model to generate distributed meltwater across the glacier surface,
    - a surface-routing (SROUT) model to route water across the glacier, and
    - a subglacial-hydrology (SUBHYD) model to route flow in conduits.
- The model's performance is evaluated by comparing modelled outputs, specifically of meltwater production, surface lowering, supraglacial runoff, proglacial discharge, and subglacial water flow-routing times, with empirical observations from one intensive field campaign during summer 2012, supplemented with several observations from summer 2013. In contrast to Arnold *et al.*'s (1998) study, modelled flow-routing times are compared with observations from the same season, representing improvement.
- To use the results to then examine:
    - inferences of drainage within Storglaciären's overdeepening,
    - whether reevaluation of Storglaciären's internal hydrology is needed,
    - spatio-temporal basal P_w variations, evaluating this model's ability to predict seasonal changes, and alignment with major meteorological/glaciological events and,
    - performance of this model compared with simpler glacier-hydrology models.

1.3. Thesis Structure

This thesis has seven Chapters. This Chapter introduced justification for glacier-hydrology studies, how this study furthers previous work, and the approach it takes. Chapter 2 reviews existing knowledge of glacier hydrological systems, focusing on temperate glaciers. Chapter 3 outlines the study site and previous research conducted here. Chapter 4 details methods and justification behind them. Modelled outputs, including sensitivity tests, are in Chapter 5, with qualitative/quantitative comparisons with observations. Chapter 6 discusses the models' ability to replicate empirical observations, outlining reasons for discrepancies. It also examines key knowledge acquired and how this contradicts/complements existing understanding. Chapter 7 synthesises this study's findings, proposing future research for Storglaciären and more broadly.

2. Glacier Hydrology: A Review

2.1. Introduction

This Chapter reviews key theories/models in temperate valley-glacier hydrology; polythermal valley-glacier hydrology is largely omitted since Storglaciären's hydrological system behaves like temperate glaciers' (Seaberg *et al.*, 1988; Fountain *et al.*, 2005; Benn and Evans, 2010).

2.2. The Glacier Hydrological System

Glaciers' systems are divided into supraglacial, englacial, subglacial and proglacial hydrology (Figure 2.1). The main inputs are meltwater and precipitation, however subaerial and basal water (generated, usually, by geothermal heat) may contribute (Hubbard and Nienow, 1997; Sharp, 2005). A key process is storage at various timescales, permitting runoff delay and later release during periods of otherwise low flow (Jansson *et al.*, 2003; Hock and Jansson, 2005). Overall, glacier-hydrology knowledge remains comparatively limited, though advances in modelling/observation are underway.

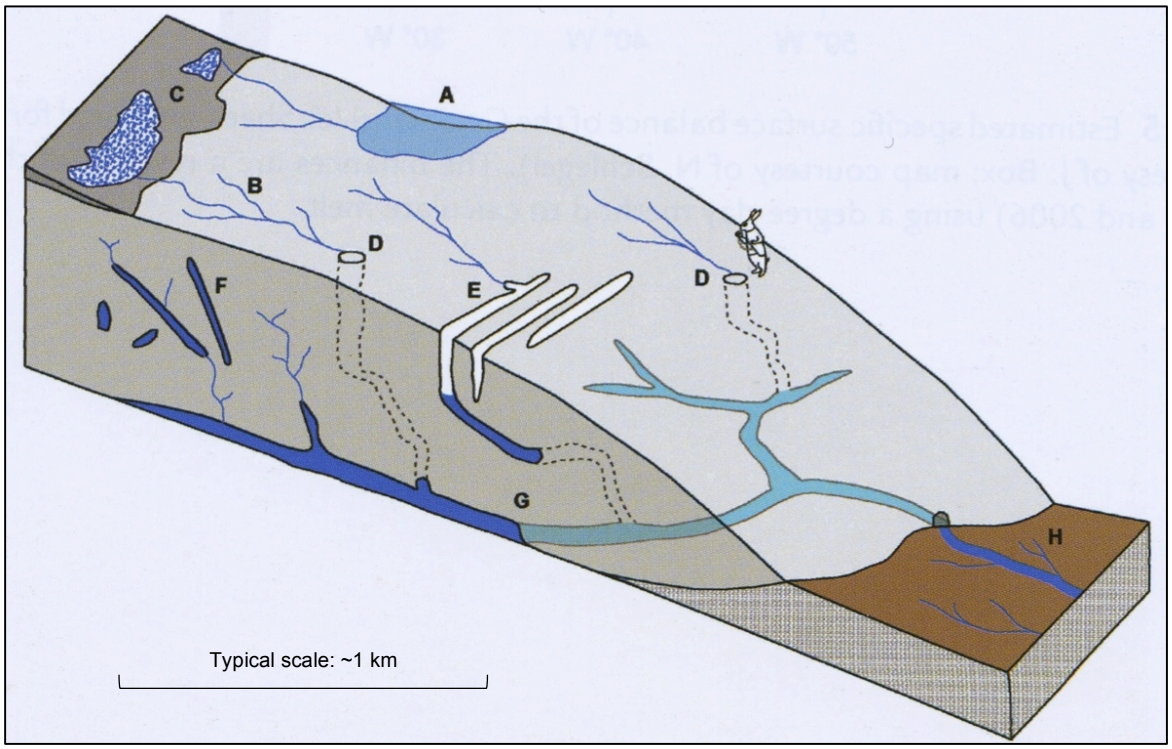

***Figure 2.1**. The hydrological system of an idealised glacier (Cuffey and Paterson, 2010, p.177). The major elements of a glacial system are shown: (**A**) a supraglacial lake (only formed if surface depressions exist and if 'cold' ice prevents meltwater penetration into the glacier), (**B**) a supraglacial stream emerging from a firn/snow reservoir (**C**) and going on to be captured by a moulin (**D**) extending from the surface; a similar situation is shown in (**E**), except the stream is captured by a crevasse field. The (~10-m tall) white rabbit gives vertical scale. The englacial system is represented by moulins and crevasses extending from the surface, and by voids (**F**), where water may be temporarily stored. Subglacially, flow is often routed in conduits (**G**), with other flow morphologies possible, until it reaches the terminus, where it forms proglacial streams (**H**), to which groundwater and direct supraglacial runoff over the snout may also contribute.*

2.2.1. Supraglacial Hydrology

Supraglacial flow morphologies are largely determined by the presence of snow, firn or ice. Early season, supraglacial flow is slow due to snow, through which percolation must first occur to the snow-ice interface. The snowpack's key effect, then, is dampening diurnal to seasonal melt-rate variations (Willis *et al.*, 2002; Campbell *et al.*, 2006). Water may refreeze or be held between snow crystals, forming a 'firn aquifer', storing up to 44% total seasonal meltwater (Östling and Hooke, 1986; Fountain and Walder, 1998). As snow is melted during a season, the delay on meltwater runoff is reduced as flow rates are ~3–5 orders of magnitude higher over ice than snow/firn (Willis *et al.*, 2002; Nienow and Hubbard, 2005). A positive feedback is also induced because ice has lower albedo than snow, so melting accelerates (Gordon *et al.*, 1998; Willis *et al.*, 2002).

Flow over ice is typically in arborescent, highly sinuous channel networks; low roughnesses enable rapid flow and incision (Knighton, 1981, 1985). Water either runs off glacier edges or is intercepted by fractures and moulins, which typically form at the upper end of crevasse fields (Holmlund, 1988b).

Occasionally, these fractures overflow, adding complexity to the relationship between the system's englacial and supraglacial elements. If thermal regime and surface topography permit their formation, supraglacial lakes can form, like on the GrIS (e.g., Lüthje *et al.*, 2006; McMillan *et al.*, 2007).

2.2.2. Englacial Hydrology

Having been routed supraglacially, considerable water enters the englacial system, with numerous flow pathways and storage elements possible. Many englacial observations are from boreholes (e.g., Hooke and Pohjola, 1994; Copland *et al.*, 1997; Fountain *et al.*, 2005) and ground-penetrating radar (e.g., Stuart *et al.*, 2003), supplemented by limited speleological investigation (e.g., Holmlund, 1988b; Gulley *et al.*, 2009). Water may be present in macroscopic/microscopic englacial systems. The macroscopic system comprises principally decimetre-sized fractures, crevasses and moulins, which route water from the surface to the glacier's bed. Moulins characteristically dip at 40–45^{o} from the glacier surface, before levelling some distance into the glacier (Holmlund, 1988b). They spatially concentrate water inputs in the basal system (Gulley *et al.*, 2012b). Contrastingly, the microscopic system comprises water inclusions in veins/nodes along crystal intersections (e.g., Mader, 1992). Inclusions are first generated in the accumulation area because water percolates into snow, and is then included when crystallisation to ice occurs (Gusmeroli *et al.*, 2010). This microscopic system is only present where ice reaches pressure-melting point (PMP), and the amount of flow occurring here is trivial compared with flow through fractures (Raymond and Harrison, 1975; Fountain *et al.*, 2005; Cuffey and Paterson, 2010).

2.2.3. Subglacial Hydrology

If englacial water reaches the subglacial system, it is routed anywhere the bed is at PMP (Sharp, 2005). Much understanding is from indirect observations, including dye tracing (e.g., Seaberg *et al.*, 1988; Willis *et al.*, 1990; Sharp *et al.*, 1993; Hock and Hooke, 1993; Nienow *et al.*, 1996, 1998; Schuler *et al.*, 2004; Willis *et al.*, 2008, 2012), proglacial-ion content (e.g., Fountain, 1992; Tranter *et al.*, 1996; Tranter, 2005), former glacier beds (e.g., Walder and Hallet, 1979), borehole water-level measurements (e.g., Hubbard *et al.,* 1995; Smart, 1996; Stone and Clarke, 1996; Copland *et al.*, 1997; Gordon *et al.*, 1998, 2001), radio-echo sounding (e.g., Copland and Sharp, 2001), or modelling (e.g., Arnold *et al.*, 1998; Schuler and Fischer, 2004; Schoof, 2010; Werder *et al.*, 2013). Yet, "a complete theory of subglacial drainage evolution remains an important but elusive goal" (Benn and Evans, 2010, p.68), partly because surface-fed subglacial systems are extremely spatiotemporally heterogeneous, responding to variations in surface-water inputs and ice deformation (Fountain and Walder, 1998).

Subglacial drainage is 'distributed' or 'channelised' (Fountain and Walder, 1998). Distributed (channelised) systems convey water slowly and inefficiently (rapidly and efficiently) (Figure 2.2).

These subglacial systems may co-exist, with pronounced variable pressure axes (Murray and Clarke, 1995).

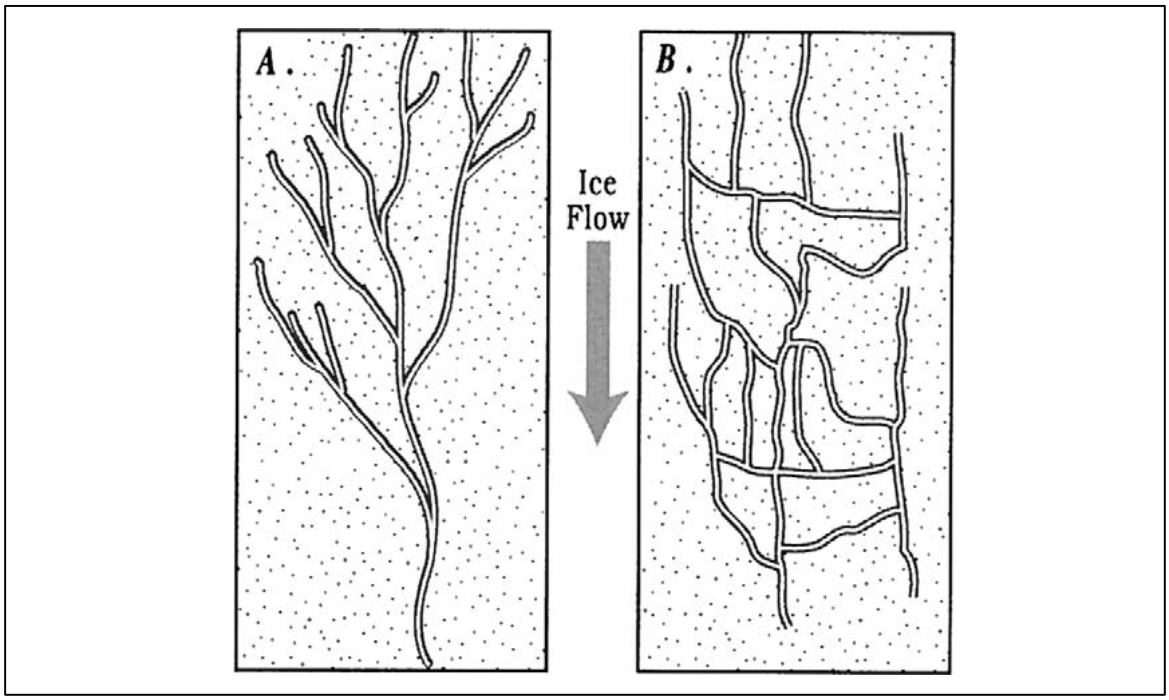

***Figure 2.2**. Idealised plan view of (**A.**) a fast 'channelised' arborescent network conveying flow efficiently and (**B.**) a slow 'distributed' linked-cavity network conveying flow inefficiently (from Fountain and Walder, 1998, p.308).*

Within these categories, numerous flow morphologies exist. In distributed systems, flow can be in sheets/thin films (Weertman, 1964, 1972; Creyts and Schoof, 2009; Creyts and Clarke, 2010) or linked-cavity systems (Figure 2.3(b); Lliboutry, 1968; Kamb, 1970, 1987; Walder, 1986). Alternatively, flow may be through a porous medium if sediment underlies a glacier (e.g., Boulton and Hindmarsh, 1987; Walder and Fowler, 1994). Channelised systems can have Röthlisberger- (R-) channels (Figure 2.3(a); Röthlisberger, 1972), which are idealised circular pipes incised upwards into ice, or Nye- (N-) channels (Nye, 1976), their equivalents cut into bedrock/sediment. Hooke- (H-) channels are also possible, with flow in shallow, wide conduits, based on observed rapid closure with low water fluxes (Hooke, 1984; Hooke *et al.*, 1990). Arborescent networks are expected since larger channels have lower P_w than smaller ones, preferentially capturing their flow (Cuffey and Paterson, 2010).

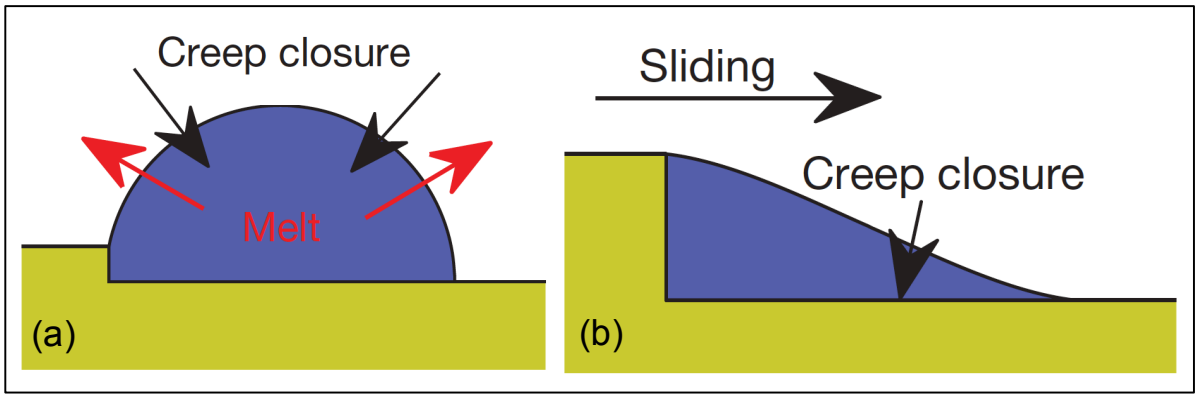

***Figure 2.3**. Theoretical representations of (a) a R-channel, in an arborescent network, and (b) a cavity, which will likely be linked to other subglacial cavities (from Schoof, 2010, p.803). R-channels are maintained by the balance between wall melting by flowing meltwater and creep closure by ice deformation; cavities are formed when ice is forced upwards by bumps at the bed of a glacier.*

Relationships between discharge and P_w differ in these systems. In distributed systems, as discharge increases, P_w increases because the system is unable to evacuate meltwater sufficiently quickly; this decreases effective pressure (N), defined as:

$$N = P_i - P_w \tag{2.1}$$

because P_w is typically close to/above P_i. Glacial velocity therefore increases. Speed-ups are most pronounced during 'Spring Events' (Kavanaugh and Clarke, 2001; Mair *et al.*, 2003; Bingham *et al.*, 2003; Anderson *et al.*, in press) or glacier 'surging' (Kamb *et al.*, 1985), when water input to the distributed system is high. Transitions to channelised systems occur since distributed systems are too inefficient, expanding insufficiently quickly to accommodate water (Figure 2.4). The initial channelised system is probably highly braided, with braids cut off as the season progresses (e.g., Röthlisberger and Lang, 1987). Channels have two competing effects: enlargement by the viscous energy dissipated by flowing water and channel closure by ice deformation. In steady-state systems, enlargement exactly balances closure; in practice, this is rarely achieved because of fluctuations in water input at varying timescales. Closure is highest beneath thick ice (permitting higher deformation) and with low water quantities present (not allowing expansion by energy dissipation by flowing water). In channelised systems, with increasing discharge, P_w decreases because the system can expand quickly from channel enlargement by flowing water, evacuating water inputs, so N increases and velocity decreases (Figure 2.4; Nienow *et al.*, 1998; Schoof, 2010). Transitions from distributed to channelised systems represent important negative feedbacks since otherwise glaciers' velocities would inexorably increase with increasing water inputs. More rapid water transit occurs as melt seasons progress (e.g., Nienow *et al.*, 1998; Swift *et al.*, 2005; Jobard and Dzikowski, 2006). Channelised systems' P_w varies between atmospheric (P_a) and ice-overburden (P_i) depending upon the filling of channels. 'Spikes' in water input can still cause speed-ups because channels cannot enlarge quickly enough; it is thus variability in meltwater input rather than its absolute magnitude that is most important (e.g., Iken *et al.*, 1983; Schoof, 2010; Pimentel and Flowers, 2011; Sundal *et al.*, 2011; Bartholomew *et al.*, 2011a, 2011b, 2012; Colgan *et al.*, 2012; Banwell *et al.*, 2013). During

winter, with limited water inputs, conduits are expected to collapse (most effectively below thick ice) and distributed systems form (e.g. Seaberg *et al.*, 1988; Cutler, 1998).

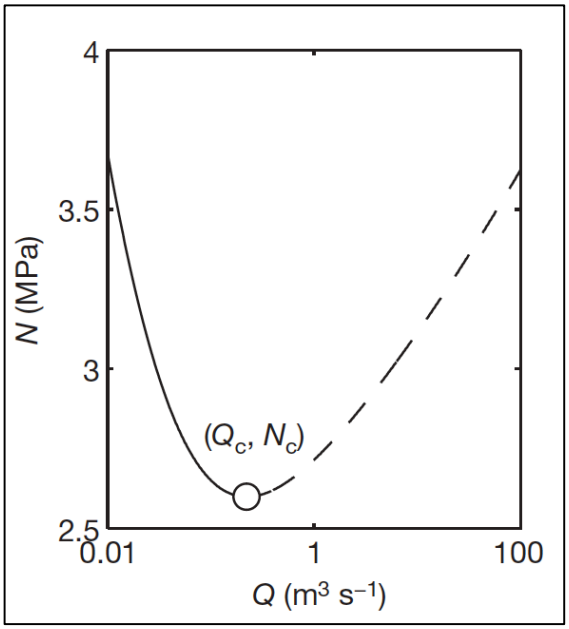

***Figure 2.4**. The relationship between steady-state effective pressure (N, in MPa) and discharge (Q, in m^3 s^{-1}) for a subglacial drainage system from Schoof's (2010, p.803) recent unified description of cavities and channels. The solid line represents a distributed system, where increases in Q cause decreases in N, and the dashed line represents a channelised system, where increases in Q cause increases in N. The critical discharge for conduit formation (i.e., the point at which 'distributed' cavities become unstable and a channelised system forms) is represented by point Q_c, N_c on the graph.*

The key idea is subglacial drainage occurs in many ways, is highly transient, and evolves seasonally due to changing meltwater inputs. If modelling subglacial hydrology, these observations need incorporating.

2.2.4. Proglacial Hydrology

Water normally emerges at glaciers' termini in several channels, often converging shortly downstream (Cuffey and Paterson, 2010; Figure 3.4). Runoff principally constitutes meltwater/precipitation routed through the glacier, though groundwater may contribute (Röthlisberger and Lang, 1987). Proglacial hydrographs vary on diurnal to interannual timescales, reflecting changes in all aspects of hydrology, including supraglacial recharge, subglacial storage, and routing efficiency (Flowers, 2008; Willis, 2011; Covington *et al.*, 2012). Many polythermal glaciers, including Storglaciären, are drained over winter, likely from release of englacially stored water (e.g., Stenborg, 1969; Irvine-Fynn *et al.*, 2011). Understanding complex variations in proglacial runoff is crucial for glacierised catchments' populations, and thus models reliably predicting runoff are required (Willis, 2005).

2.3. Modelling Glacier Hydrological Systems

Glacier-hydrology models must capture numerous aspects of the system, including its storage and delay; modelling is complex because it requires incorporating the transition of water between phases (e.g., Jansson and Näslund, 2009). Two elements are needed: estimation of the system's water inputs, determined with melt modelling, and understanding of supraglacial, englacial and subglacial routing (Hock and Jansson, 2005).

2.3.1. Melt Modelling

Firstly, reliable estimates of the system's water inputs need generating. Melt in glaciers' catchments depends upon numerous atmospheric factors (Hock, 2005). Many melt models have been developed from positive-degree-day (PDD) approaches based on empirical relationships to SEB approaches grounded in physics (Hock, 2005).

2.3.1.1. Positive-degree-day Approaches

PDD approaches rely on the strong relationship between air temperatures and melt rates (Hock, 2003). Because of widely available temperature data, both for the present and with future climate projections, PDD approaches are often chosen. These models have performed extremely favourably compared with empirical data (e.g., Hock, 1999). Occasionally, extra meteorological data, including shortwave radiation (SWR), can be incorporated (Hock, 1999). PDD approaches use the following equation:

$$M = \beta T_{pdd} \tag{2.2}$$

where M is total melt, β the degree-day factor (DDF), and T_{pdd} the sum of all positive daily mean temperatures over the time period (Hock, 2003). PDD models can be distributed across elevation bands with lapse rates (Hock, 2003). Many DDFs have been generated using empirical relationships; Cuffey and Paterson (2010) summarise them. DDFs are glacier-specific and it is unclear how they will vary into the future, thus reducing reliability for determining melting (Hock, 2003).

2.3.1.2. Surface-energy-balance Approaches

In overcoming these problems, SEB models were developed. These are point-based or fully distributed (Hock, 2005). The latter calculates melt over a grid, used because of increased computer power and availability of digital elevation models (DEMs) (Hock, 2005). DEMs are required for distributing meteorological data and for determining cells' slopes, aspects and shading. In glacier hydrology, fully distributed models are particularly important since lack of knowledge of the locations of water inputs to the system increases uncertainty, probably producing unrealistic representations

(e.g., Gulley *et al.*, 2012b). SEB models are forced with extrapolated/interpolated meteorological data (e.g., Schneeberger *et al.*, 2001) from automatic weather stations (AWSs) or with downscaled, bias-corrected climate-reanalysis data (e.g., Radić and Hock, 2006; Rye *et al.*, 2010).

SEB models calculate the sum of components contributing to melting. They determine the energy available for melt (Q_M) from five elements:

$$Q_M = (SW\downarrow - SW\uparrow) + (LW\downarrow - LW\uparrow) + Q_S + Q_L + Q_R \quad (2.3)$$

where $SW\downarrow$ is incoming SWR, $SW\uparrow$ outgoing SWR (defined as: $(1-\alpha) \times SW\downarrow$, where α is surface albedo for snow/ice), $LW\downarrow$ incoming longwave radiation (LWR), $LW\uparrow$ outgoing LWR, Q_S the sensible heat flux, Q_L the latent heat flux, and Q_R the (normally omitted) heat flux from rain (Cuffey and Paterson, 2010).

Once the energy available for melting is determined, and assuming a surface at melting point (0°C), melt rates (M) are then calculated:

$$M = \frac{Q_M}{\rho_w L_f} \quad (2.4)$$

where ρ_w is water density and L_f latent heat of fusion of water (Hock, 2005).

2.3.1.3. Choice of Melt Model

Choosing a PDD or SEB model for a study depends principally upon data availability; where detailed meteorological data exist, SEB approaches are preferred (e.g., Hock *et al.*, 2007). Yet, because temperature data are so widely available, PDD models remain most convenient for determining melt for many purposes (Hock, 2005). However, by lumping SEB into few parameters, they neglect physics and cannot be applied between sites without calibration (Hock, 2005).

2.3.2. Early Glacier-hydrology Models

Earlier models were either stochastic (based on statistical relationships) or conceptual, lumping together elements of the glacier's system. Stochastic models (e.g., Baker *et al.*, 1982; Willis *et al.*, 1993) lack conceptual basis, requiring glacier-specific calibration, so cannot easily be transferred nor predict future changes (Hock and Jansson, 2005). This led to conceptual-model development, placing more emphasis on physics. Linear-reservoir models are most widespread, only requiring limited data inputs (Chow *et al.*, 1988). They route meltwater through glaciers, with different elements of the system having storage times defined by constants (Figure 2.5). Normally, two/three reservoirs are used and meltwater is routed through the system to produce proglacial runoff (e.g., Hock and Noetzli, 1997; Span and Kuhn, 2003; Flowers, 2008; Hodgkins *et al.*, 2013; Gravelle, 2013). Storage constants are often assumed spatiotemporally invariant and, though linear-reservoir models perform

well in replicating observed discharge, they often cannot capture high transience of glaciers' hydrology, and omit physics. This does not allow prediction of the system's internal state; perhaps most significantly, they cannot model basal P_w, fundamental in glaciology because it profoundly affects dynamics.

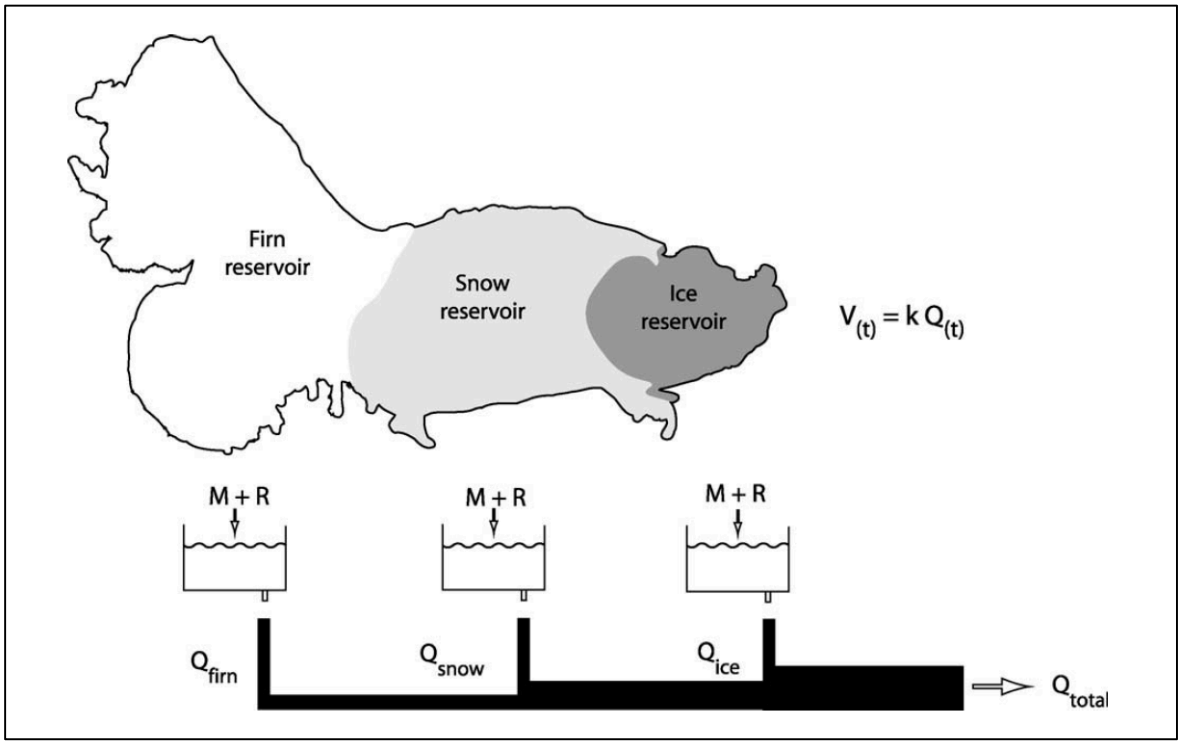

***Figure 2.5**. Diagrammatic representation of a linear-reservoir model as applied to Storglaciären, following Hock and Noetzli (1997) (from Jansson* et al.*, 2003, p.123). Three parallel 'coupled' reservoirs, supplied by melt (M) and rainfall (R), are used here, each having different storage constants associated with them. The firn reservoir area was kept constant, while the snow and ice reservoirs varied inversely: i.e., the snow reservoir decreased in size over the melt season as the snowline retreated, and the ice reservoir increased in size. The total outflow (Q_{total}) is proportional to the reservoir volumes (V).*

2.3.3. Physically Based Glacier-hydrology Models

Physically based models have been recent research focuses since they are non-site-specific, incorporating physics.

2.3.3.1. Early Models

Early work (e.g., Shreve, 1972; Röthlisberger, 1972) assumed steady-state subglacial drainage systems, later developed for unsteady ones (e.g., Nye, 1976; Spring and Hutter, 1981, 1982). Röthlisberger (1972) modelled flow in circular pipes, thus in 'channelised' form. Shreve's (1972) model assumed the primary driver of subglacial routing is the hydraulic potential (φ) gradient (Equation 4.14), which determines subglacial pressure fields based on bed and ice-surface slopes, with the latter crucially important. This theory allows uphill water flow from overdeepenings assuming

the pressure gradient is higher than the elevation-potential gradient (Sharp, 2005). Subglacial drainage system structure has been inferred using Shreve's (1972) method, assuming all meltwater reaches the bed *in situ*, for assumptions of steady-state P_w from P_a to P_i (e.g., Holmlund, 1988a; Sharp *et al.*, 1993; Flowers and Clarke, 1999; Hagen *et al.*, 2000; Pälli *et al.*, 2003; Rippin *et al.*, 2003; Fischer *et al.*, 2005; Willis *et al.*, 2008, 2012). Realistic representations were produced.

Early theories did not account for 'distributed' morphologies, developed by others (e.g., Kamb, 1987). Much of this early work modelled specific elements of glacier hydrology rather than the entire system and assumed steady-state systems, rather than time-dependent ones.

2.3.3.2. Early Time-dependent Models

Arnold *et al.* (1998) first attempted holistic, time-dependent modelling of glacier hydrology. Their model was developed for the temperate Haut Glacier d'Arolla (HGd'A), Switzerland, applied here to Storglaciären, Sweden. It incorporates a SEB model to generate melt at high spatio-temporal resolution (Arnold *et al.*, 1996), and SROUT and SUBHYD models. The SROUT model incorporates the snowpack's delaying effect in determining flow across the surface and defines the catchments and upstream-contributing areas for all moulins. The SUBHYD model routes flow in R-channels, with attempts made at replicating distributed flow using 'bundles' of eight, small, rough conduits. Chapter 4 gives further model details and its application in this study. This model broadly replicated observations (Richards *et al.*, 1996) of proglacial discharge, subglacial water-flow routing times and borehole P_w for HGd'A, with best matches mid-melt season. This likely resulted from its inability to replicate distributed drainage, believed to exist at the beginning and end of the season (Arnold *et al.*, 1998). It was recently applied to the GrIS's 'Paakitsoq region' (Banwell *et al.*, 2013) and Franz Josef Glacier, New Zealand (Anderson *et al.*, in press). Its P_w predictions were especially valuable for the GrIS, helping confirm suggestions of P_w 'spikes' following lake-drainage events (e.g., Das *et al.*, 2008) and consistently high P_w in the GrIS's interior.

To partially fulfill requirements to represent distributed subglacial flow, Flowers and Clarke (2002a), furthering Clarke's (1996) model, developed a model for Trapridge Glacier, Canada, incorporating a PDD model, an englacial-storage component (omitted by Arnold *et al.*, 1998), and subglacial flow in a sheet and subsurface aquifer (Figure 2.6). The model replicated borehole P_w well (Flowers and Clarke, 2002b). It was applied to Vatnajökull, Iceland (Flowers *et al.*, 2003), producing realistic models of drainage, with high water flux predicted beneath major outlet glaciers, following expectations.

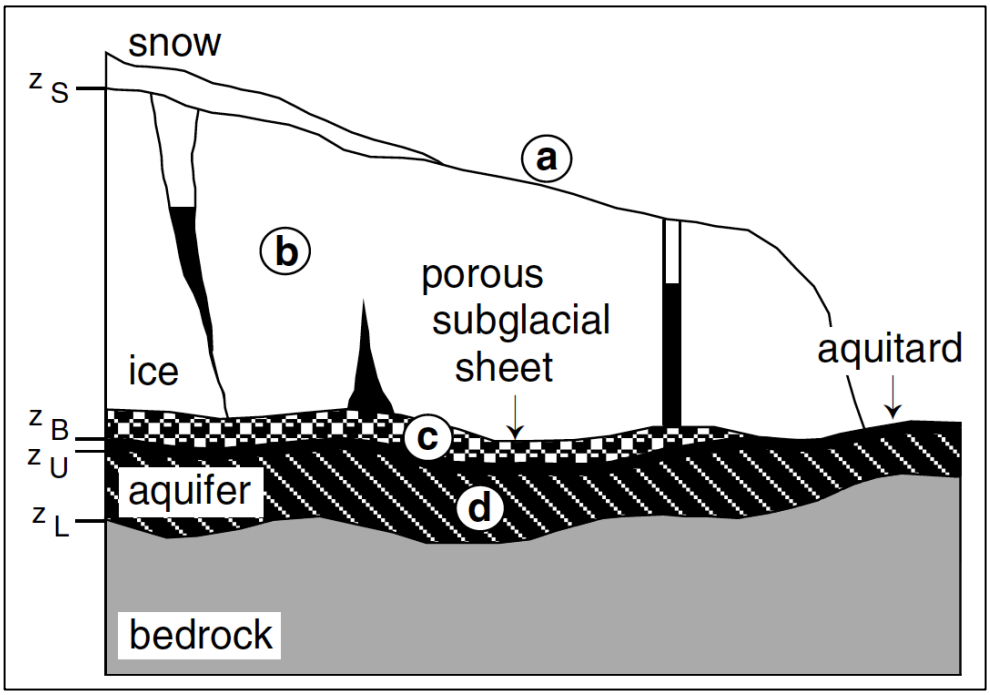

***Figure 2.6**. Diagrammatic representation of the glacier-hydrology model developed by Flowers and Clarke (2002a, p.9-2) with four coupled models: (a) surface melting from a PDD model, (b) an englacial storage component, (c) a distributed subglacial water sheet and (d) a subsurface aquifer within sediments. Z_S = the ice surface, Z_B = the bed surface, Z_U = the upper aquifer interface, and Z_L = the lower aquifer interface.*

2.3.3.3. Recent, Unified Models

Modelling advances continue. Schoof (2010) unified the description of cavities and channels, allowing switching between them at critical-discharge thresholds (Figure 2.4). This means, in contrast to Arnold *et al.*'s (1998) and Flowers and Clarke's (2002a) approaches, there is no need for specifying one subglacial-drainage morphology. Schoof's (2010) model was developed by Hewitt (2011), Schoof *et al.* (2012) and Hewitt *et al.* (2012), to allow 'hydraulic jacking' and partially filled channels, however models remained one-dimensional. Werder *et al.* (2013) developed the model to two dimensions, incorporating dynamic switching between distributed and channelised flow, localised water inputs from moulins (deemed crucial by Gulley *et al.* [2012b]) and englacial storage. Channels form on an unstructured mesh, so avoiding directional bias and better representing reality than Schoof's (2010) structured mesh or models (e.g., Arnold *et al.*, 1998) where channel locations need specifying. The resultant Glacier Drainage System (GlaDS) model was successfully applied to a replication of the GrIS margin and to Gornergletscher, Austria. This model represents the 'best' glacier-hydrology model presently, however, GlaDS has not been quantitatively compared with observations, not allowing it to be constrained and developed further, representing a key future research area (de Fleurian *et al.*, 2013). Moreover, incorporating modelled basal P_w from models like this into ice-flow models is a fundamental requirement, only beginning to be addressed using finite-element models

like Elmer/Ice (Pimentel and Flowers, 2011; Schoof and Hewitt, 2013; de Fleurian *et al.*, 2013). Such models could also inform glacier-erosion models (Werder *et al.*, 2013).

2.3.3.4. Choice of Glacier-hydrology Model

Though ideally all studies would now employ unified glacier-hydrology models, using other physically based models is still justified in some situations since such models' ability to reproduce basal P_w is hugely advantageous over linear-reservoir models. If it is known that distributed/channelised subglacial drainage exists, using models like Arnold *et al.*'s (1998) and Flowers and Clarke's (2002a) can be justified and understanding of glacier-hydrological systems furthered. This is especially true if extensive empirical data can validate models. Presently, no study has applied differing models at the same site using uniform input data.

3. Study Site

3.1. Introduction

Storglaciären (67°55'N, 18°35'E) is a 3.22 km^2 (Koblet *et al.*, 2010) sub-polar valley glacier located in the Kebnekaise massif of Lapland, Sweden (Figure 3.1). It lies within the 30%-glacierised Tarfala valley (Dahlke *et al.*, 2012), and has a ~4.55 km^2 drainage basin (Östling and Hooke, 1986). Storglaciären ranges from ~1130 to ~1730 m above sea level (a.s.l.), flowing eastwards from a branched accumulation area encompassing two corries, bounded in the east by Kebnekaise peak. A riegel (resistant rock ridge), comprising Mylonite Gneiss (Andréasson and Gee, 1989), divides the ablation zone into upper and lower areas (cf. Figure 4.16), with extensional forces causing moulins to form above it. Storglaciären's mean thickness is ~95 m, with a ~0.5 km^2 overdeepening (up to ~230 m) in the upper ablation area below the current equilibrium-line altitude (ELA) (Figure 3.2; Bjørnsson, 1981; Eriksson *et al.*, 1993; Cook and Swift, 2012). The overdeepening formed because of the locality's structural geology and preferential erosion of weaker strata over ~300,000 years (Andréasson and Gee, 1989; Bronge, 1996).

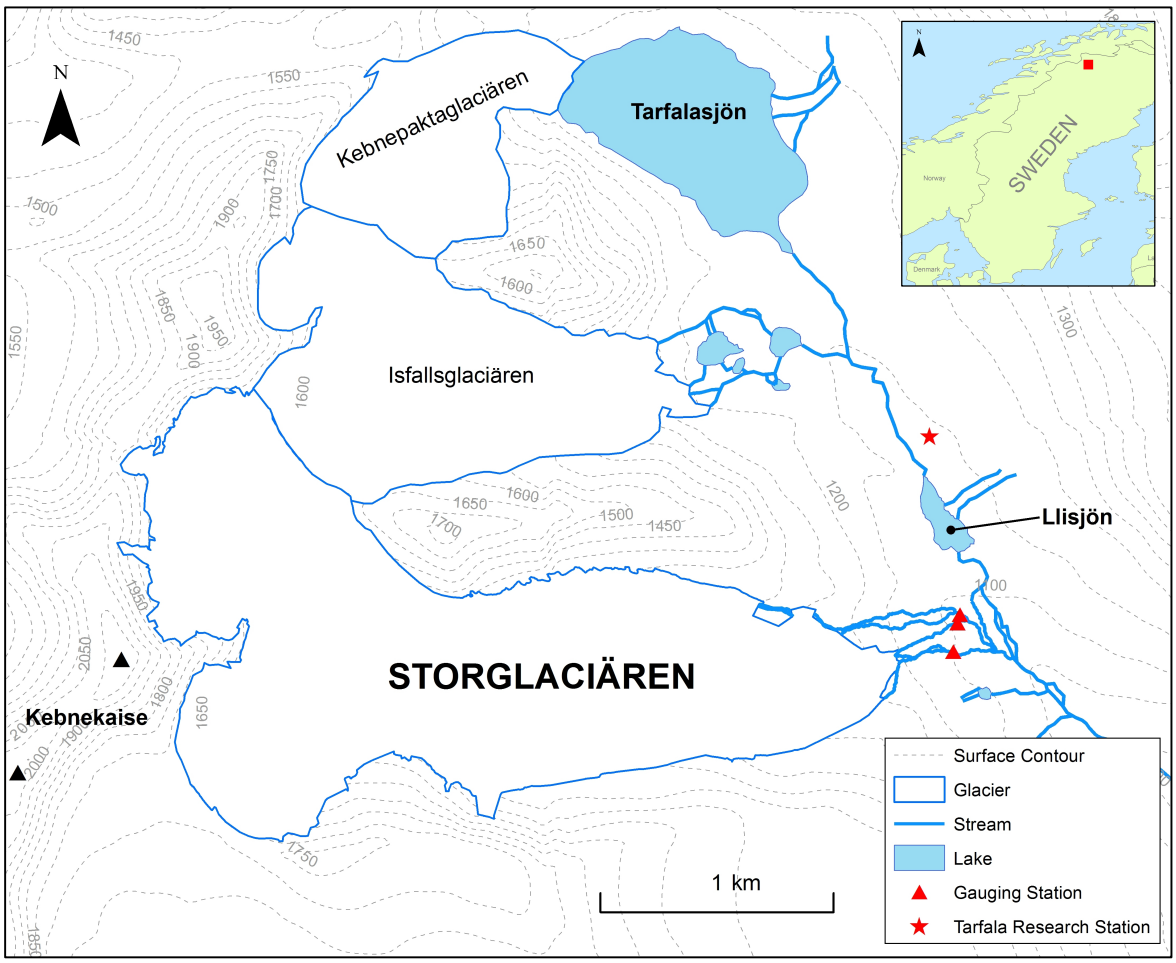

***Figure 3.1**. The location of Storglaciären within the Tarfala valley, and with respect to surrounding glaciers, major streams, lakes, peaks and topography. The location of the Tarfala Research Station is also shown. The inset shows its location within Sweden and Scandinavia.*

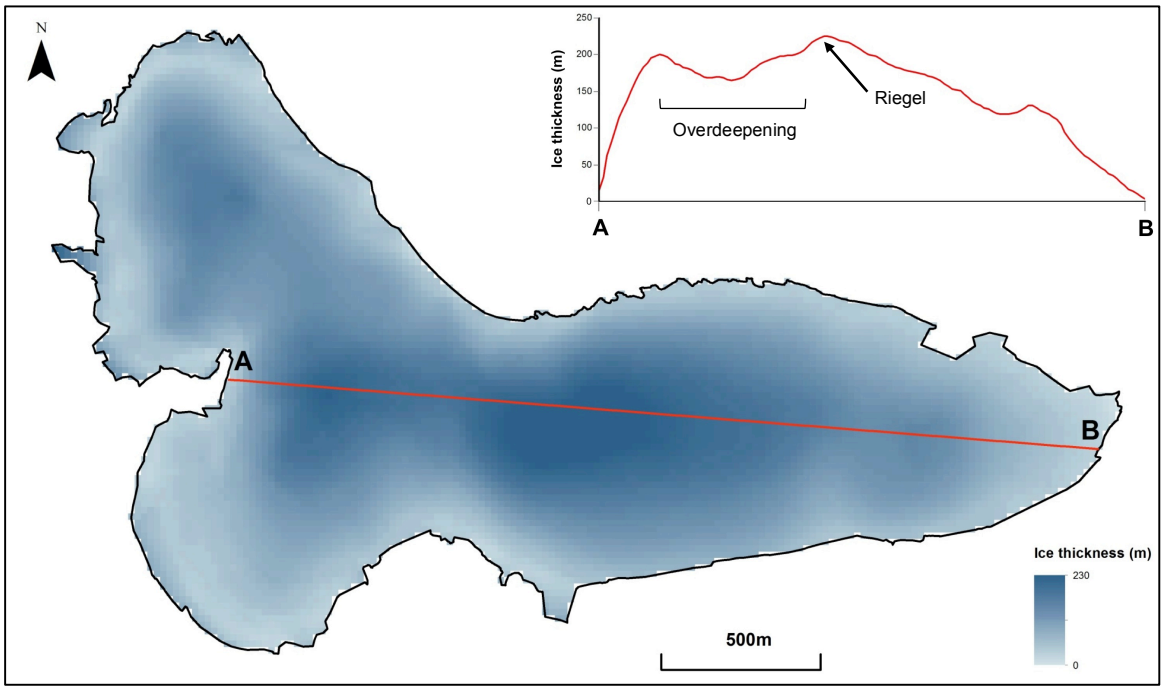

***Figure 3.2**. Storglaciären's ice thickness (m), with a profile of ice thickness along line A–B (the approximate centreline), with the locations of the main overdeepening and riegel also shown.*

3.2. Mass Balance

Owing to Tarfala Research Station's (TRS) close proximity, Storglaciären is one of the world's best-researched glaciers. Photographic records of its front extend back to ~1880 (Svenonius, 1910) and continuous glaciological mass-balance measurements to 1946 (Schytt, 1959; Holmlund, 1987; Østrem and Brugman, 1991; Holmlund and Jansson, 1999; Jansson and Pettersson, 2007). Figure 3.3 displays recent mass balance. Storglaciären thus provides an almost unique prospect for examining the cryosphere's temporal response to climate change and for studies requiring extensive empirical data (e.g., Holmlund *et al.*, 1996, 2005; Brugger, 2007).

Storglaciären is in quasi-equilibrium with current climate (Brugger *et al.*, 2005). Recent temperature increases were 0.055°C a^{-1} (Evans *et al.*, 2008), paralleling the trend of double the rate of Arctic warming compared with elsewhere (e.g., Dowdeswell *et al.*, 1997; IPCC, 2013), mainly from increased summer temperatures (Linderholm and Jansson, 2007). 300 m terminus retreat and 30% mass loss is predicted by 2050 (Schneeberger *et al.*, 2001), with 50–90% volume loss estimated by 2100 using climate-reanalysis data (Radić and Hock, 2006).

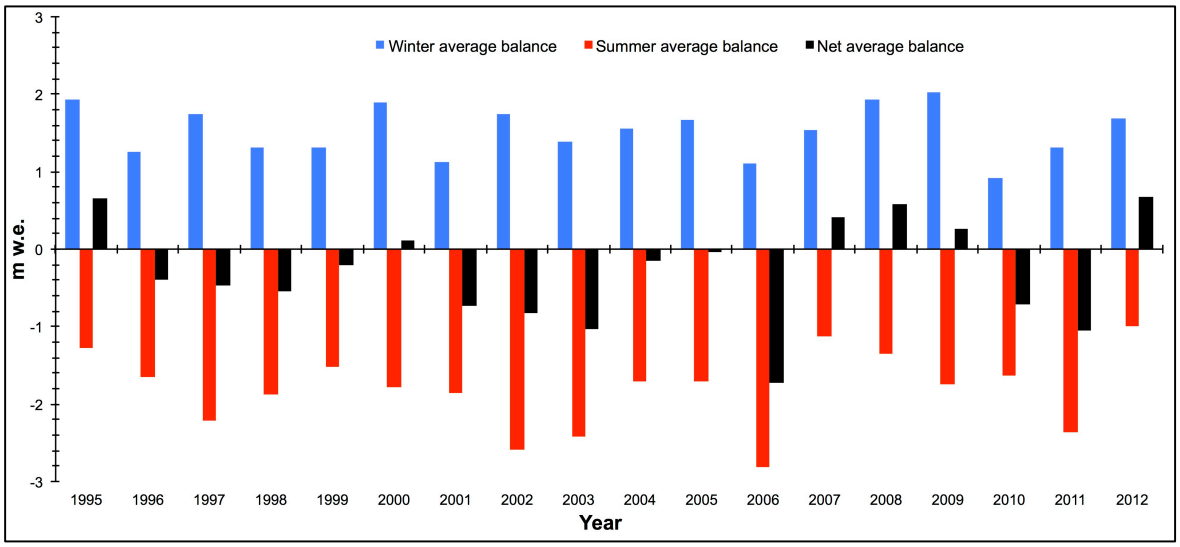

***Figure 3.3**. Storglaciären's average (i.e., average over the entire glacier surface) winter, summer and net mass balance from 1995 to 2012, which is the most recently processed year. Figure adapted from Jansson and Pettersson (2007).*

3.3. Thermal Regime

Storglaciären, like other glaciers on the drier side of Scandinavian mountains, is polythermal because of its cold (<0°C) surface layer, thickest (~60 m) at the terminus/margins (Holmlund and Eriksson, 1989; Pettersson *et al.*, 2003; Gusmeroli *et al.*, 2010). Besides this, ~85% ice is maintained temperate by meltwater percolation into firn in the accumulation area, which is then advected downglacier (Evans *et al.*, 2008). The cold layer is maintained by rapid runoff over its impermeable surface (Gusmeroli *et al.*, 2012). This means, in the ablation zone, water must principally reach the englacial system through moulins/crevasses near the ELA or above the riegel, since inter-crystal water transfer is impossible (Holmlund, 1988a; Mader, 1992; Hanson *et al.*, 1998; Fountain *et al.*, 2005). This layer is currently thinning at 0.80±0.24 m a^{-1} (Figure 3.4; Gusmeroli *et al.*, 2012), continuing earlier trends (Pettersson *et al.*, 2003). Thinning will likely impact Storglaciären's future hydrology.

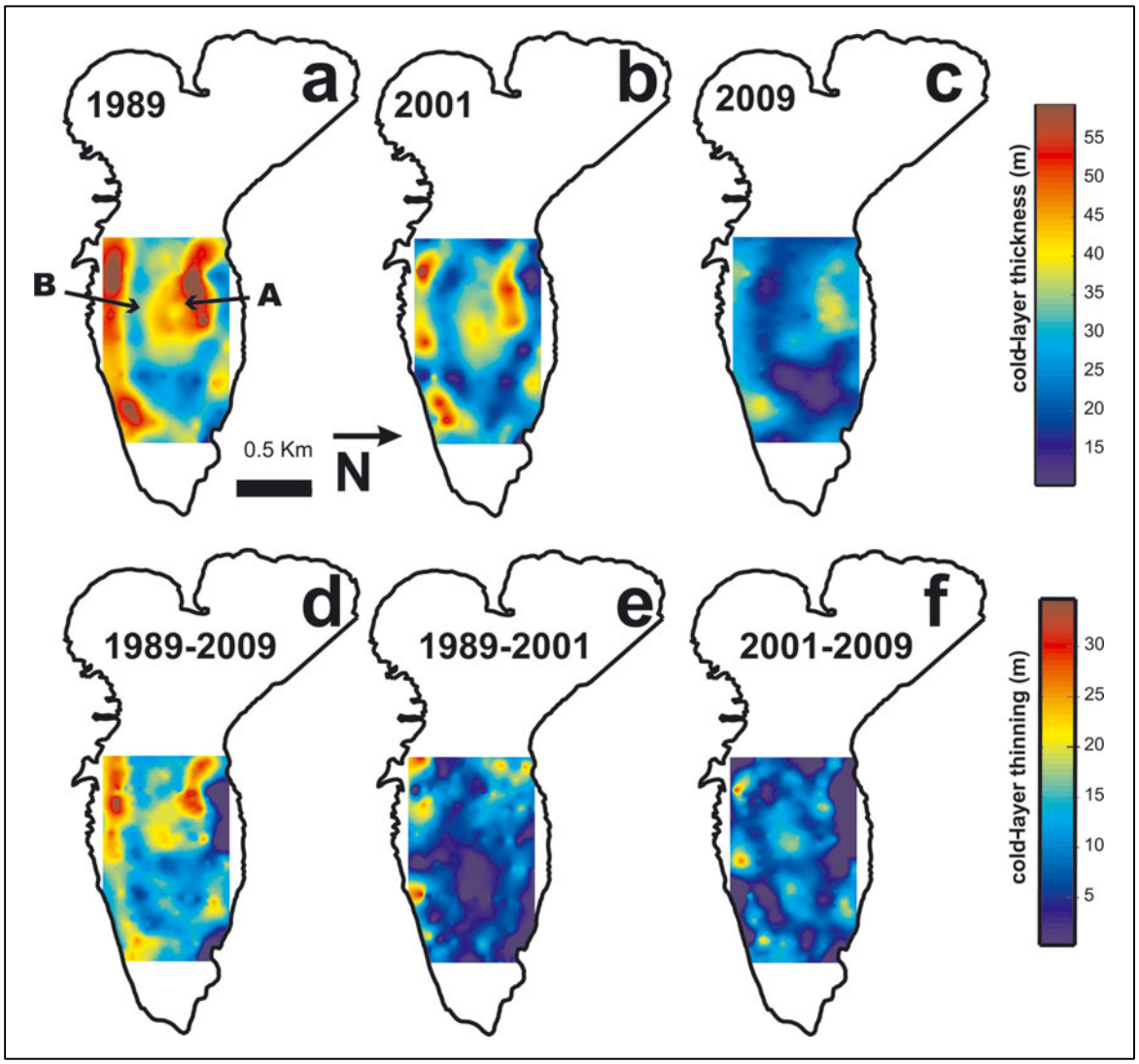

***Figure 3.4**. Maps showing the cold surface layer thickness in (a) 1989 (Holmlund and Eriksson, 1989), (b) 2001, and (c) 2009, and changes in layer thickness (d) from 1989 to 2009, (e) from 1989 to 2001, and (f) from 2001 to 2009. Figure from Gusmeroli* et al. *(2012, p.7), based on radio-echo sounding surveys in the ablation area.*

3.4. Previous Hydrology Research on Storglaciären

3.4.1. Drainage

Three proglacial streams – Nordjåkk, Centerjåkk and Sydjåkk – drain Storglaciären (Figures 3.1, 3.5 and 4.16). Nordjåkk is normally clear, while Centerjåkk and Sydjåkk are both highly turbid, indicating extensive subglacial travel, permitting sediment entrainment, before emerging at the terminus (Östling and Hooke, 1986; Hock and Hooke, 1993). These streams transport $\sim 1.85 \times 10^6$ kg km^{-2} a^{-1} (=0.7 mm a^{-1} erosion) from Storglaciären's basin (Schneider and Bronge, 1996). These streams are supplemented by direct supraglacial runoff, representing ~15% Storglaciären's water balance (Rudensky, unpublished, in Seaberg *et al.*, 1988; Kohler, 1992; Gravelle, 2013). Their discharges are

ablation-dominated, with some contributions from major rainfall events, especially for Sydjåkk (Gravelle, 2013). Recently, runoff from the valley has become more rapid due to lower snow and ice quantities within the basin (Dahlke *et al.*, 2012; Gravelle, 2013).

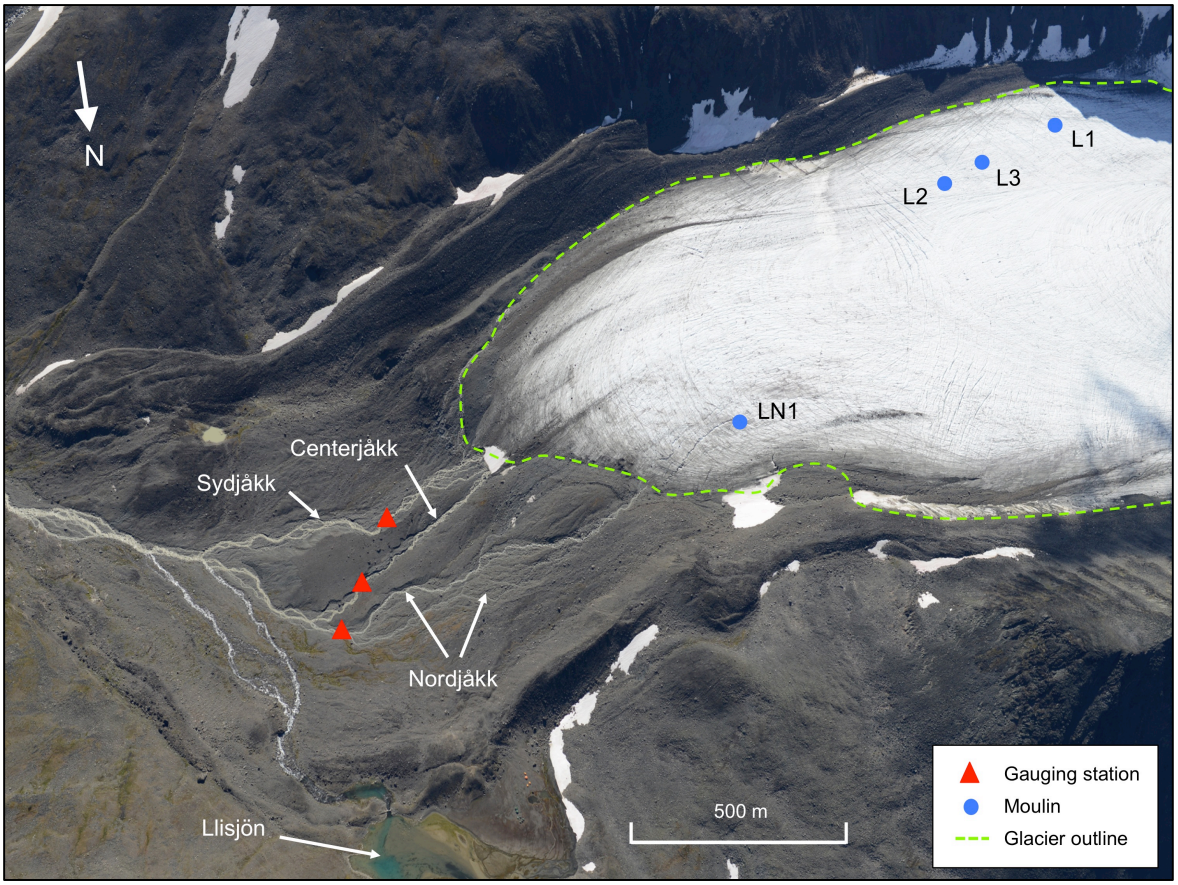

***Figure 3.5**. Storglaciären's lower ablation area and proglacial drainage viewed from above; also shown are four locations used for tracing experiments (cf. Figure 4.16). Photo taken by Per Holmlund, 10 August 2013, with additional labels and symbols added by the author.*

3.4.1.1. Internal Drainage

Early work (Stenborg, 1965, 1969) showed drainage through winter and postulated proglacial streams drain dissimilar areas of Storglaciären. Greater knowledge was acquired during the 1980s/1990s to describe the complex drainage system; however, recent studies have been few. Storglaciären has extensive englacial and subglacial networks, including an overdeepening, uncommon to many glaciers (Jansson and Näslund, 2009). The lower ablation, upper ablation and firn areas are drained differently.

3.4.1.1.1. Lower Ablation Area

Sydjåkk and Centerjåkk subglacially drain the lower ablation area; drainage probably evolves from numerous smaller conduits early in the melt season to a single homogenously braided stream later,

responding to increasing water inputs (Figure 3.6; Hock and Hooke, 1993). Braiding decreases as water overflows stream bends and drowns channel divides (Seaberg *et al.*, 1988; Hock and Hooke, 1993; Mercer, 2004; Williamson, 2013). Flow-routing times thus decrease. Channels are likely broad and low since observations show rapid closure with low water inputs (Hooke *et al.*, 1990). Inferences were made mainly from tracer studies (Zimmerer, 1987; Hooke *et al.*, 1988; Seaberg *et al.*, 1988; Hooke, 1991; Kohler, 1992; Hock and Hooke, 1993; Williamson, 2013).

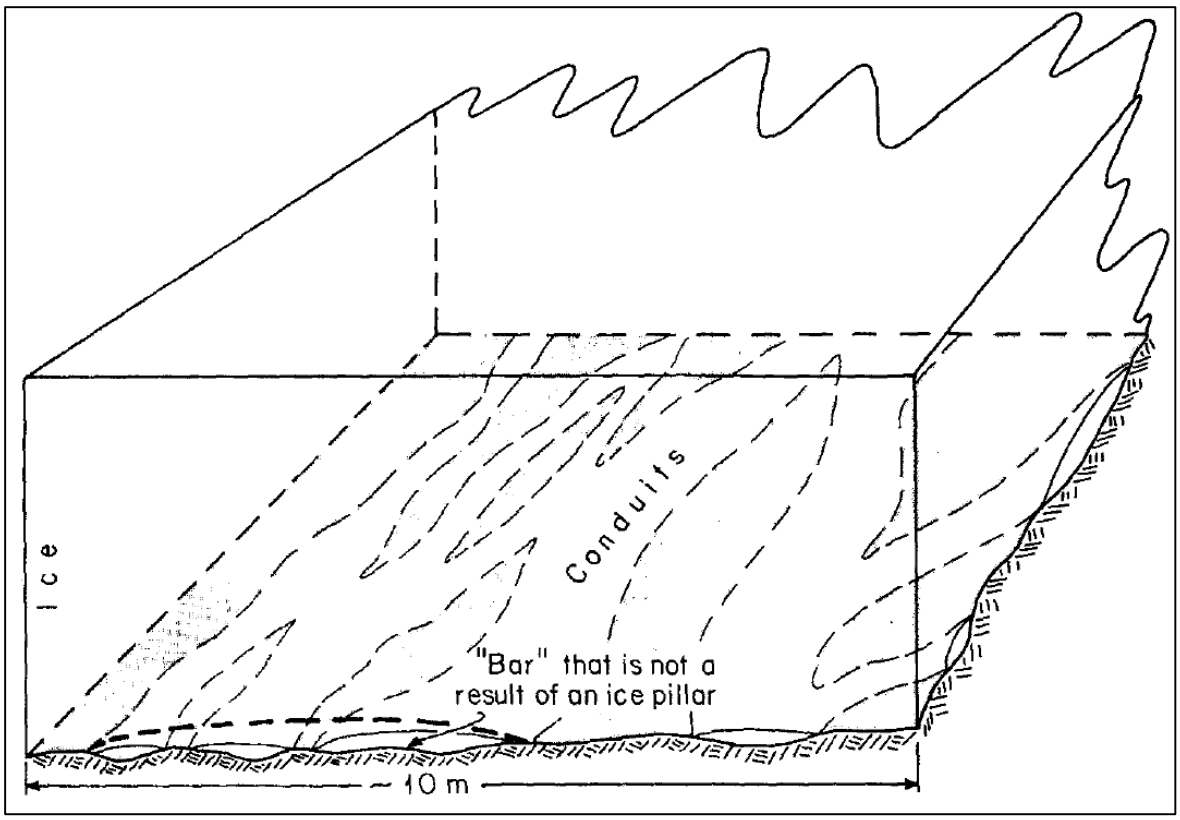

***Figure 3.6**. A schematic diagram of a homogeneously braided stream, believed to prevail beneath Storglaciären (from Hock and Hooke, 1993, p.541). Dotted lines show locations where ice would probably be in contact with the bed, forming elongate pillars dividing water flow. During higher flows (which may be consistent later in the season), flow is likely in the channel represented by the heavy dashed line, due to channel enlargement.*

3.4.1.1.2. Upper Ablation Area

The riegel represents a division in Storglaciären's drainage since, contrasting with the lower ablation area, the upper area (above the overdeepening; cf. Figure 4.16) probably has extensive englacial drainage towards Nordjåkk, inferred from boreholes and borehole-video investigations (Pohjola, 1994; Hooke and Pohjola, 1994). If subglacial drainage occurs here (and it may not), it may be in extremely broad, low conduits since excess energy dissipated by flowing water would keep the water ascending from the overdeepening at PMP rather than enlarging conduits; conduits must therefore be maintained by high basal P_w (Hooke *et al.*, 1990; Hooke, 1991). ~0.2–0.7 m thick subglacial till is present here, which deforms, blocking subglacial channels that may form, contributing to the requirement for englacial drainage (Brand *et al.*, 1987; Hooke *et al.*, 1989; Hooke and Pohjola, 1994).

Our understanding of processes here, and in overdeepenings generally, remains poor. No consensus exists, for example, on whether subglacial drainage, if it even occurs, is in shallow, braided canals, as for Matanuska Glacier, Alaska (Ensminger *et al.*, 1999), or whether poor subglacial connectivity exists and storage prevails, as for Gornergletscher, Switzerland (Iken *et al.*, 1996). Further model- and empirical-based studies of overdeepenings are crucially required given overdeepenings' profound influence in glaciology: specifically their potential inefficiency at transporting ice, water and sediment along adverse bed gradients (Cook and Swift, 2012). This is even more important since many ice-sheet outlet glaciers drain overdeepened troughs (Cook and Swift, 2012).

3.4.1.1.3. Firn Area

Here, drainage is probably englacial, inferred from a single dye-tracer injection, appearing over 35 days, with 0.02 m s^{-1} maximum transit velocity, in Nordjåkk (Hooke *et al.*, 1988; Kohler, 1992). Further research is necessary.

3.4.2. Subglacial Water Pressures

Storglaciären's subglacial P_w varies at numerous timescales, being linked to ice-velocity changes. Most understanding was from boreholes. The following is known:

- Winter P_w is almost consistently high, but can fluctuate occasionally (Jansson and Näslund, 2009). Fluctuations may result from release of englacially stored water or because large water fluxes (e.g., during major storms) can still somehow affect the basal system, though understanding of this process remains low (Jansson and Näslund, 2009).
- High moulin P_w correlates with temperature/precipitation peaks (e.g., Holmlund and Hooke, 1983). However, this response is not uniform: some moulins were insensitive to these forcings, demonstrating no apparent correlation (Jansson and Näslund, 2009).
- Within the overdeepening, P_w is consistently high during the summer: often >75% P_i, with small-amplitude fluctuations at ~80–100% P_i, despite pronounced surface-melt variations (e.g., Hooke, 1991; Hooke and Pohjola, 1994; Jansson, 1995; Fountain *et al.*, 2005; Jansson and Näslund, 2009; Cook and Swift, 2012). P_w here can exceed P_i (Hooke, 1991). Observations match those for other overdeepenings from borehole and tracer studies (e.g., Hock *et al.*, 1999).
- Downglacier of the riegel, consistently high P_w is observed early melt season, then replaced by diurnally varying P_w later, probably indicating transition to more efficient drainage (Kohler, 1995; Jansson and Näslund, 2009). High P_w values here are then $\sim P_i$, and low values $\sim P_a$ (Jansson, 1996). $P_w > 50\% P_i$ is probably needed to cause velocity increases. P_w 'spikes' (those at $\sim P_i$) are pronounced at first, but decline seasonally, probably because water is evacuated more efficiently (Jansson and Näslund, 2009). Several boreholes drilled here overflowed with turbid water, indicating subglacial $P_w > P_i$ (Jansson, 1996).

3.4.3. Ice Dynamic Interactions

Research has linked hydrology, through its effect on basal P_w, and coupling between the bed and glacier, to explain multi-temporal velocity variations observed on Storglaciären (Iverson *et al.*, 1994, 1995).

Velocity patterns in Storglaciären's lower ablation area mirror other glaciers': there is abrupt increase in late spring and early summer, following gradual winter decline (Hooke *et al.*, 1983, 1989; Jansson, 1995). Exact timing of this depends upon when air temperature is consistently >0°C (Jansson, 1995). Velocity then decreases over summer, but occasional 'spikes' are observed during high water flux to the subglacial system with high temperature/precipitation (Hooke *et al.*, 1983; Jansson, 1995). These 'spikes' occur on other GIC and the GrIS (e.g., Vieli *et al.*, 2004; Das *et al.*, 2008; Banwell *et al.*, 2013). If temperature/precipitation peaks occur when the system is poorly developed, they are especially effective at increasing velocities (Hooke *et al.*, 1989; Vieli *et al.*, 2004) and are probably due to basal decoupling/increased till deformation (Hanson *et al.*, 1998; Jansson and Näslund, 2009). The upper ablation area may also respond to basal P_w fluctuations. Here, short-lived increases in water input increase basal sliding by 16–40% relative to winter velocities, probably occurring because of increased till deformation and possible ice-till decoupling, permitting efficient sliding (Hooke *et al.*, 1989, 1992; Iverson *et al.*, 1995). In the firn area, short-term velocity variations have been observed close to the headwall, believed to be caused by limited water input to the bergschrund (Hanson *et al.*, 1994).

Some longitudinal coupling may help explain velocity variations, whereby changes occurring in one area of the bed impact elsewhere (Hooke *et al.*, 1989; Hanson and Hooke, 1994; Jansson, 1996). This coupling is inferred because often velocities in one area increase before the area's P_w increases.

3.4.4. Melt Modelling

Hock and Holmgren (1996) developed a SEB model for Storglaciären, finding net radiation supplied 66% total melt energy, with the remainder contributed by sensible (29%) and latent (5%) heat fluxes. Agreement between measured and calculated ablation was good on most days, with ~10% underestimation by the model compared with observations (Hock and Holmgren, 1996). They noted that a major error might be in assuming 0°C surface temperature, not accounting for nocturnal freezing at the surface (Hock and Holmgren, 1996). Employing the bulk aerodynamic approach also likely introduced errors.

Hock and Holmgren (2005) developed this SEB model. It calculated melt for each 30-m cell, including direct and diffuse radiation modifications based on slope and shading. It replicated well observations of snowline retreat and stake ablation, though overpredicted 1994 melt, and underpredicted high and overpredicted low ablation in 1993 (Hock and Holmgren, 2005). It was coupled to Hock and Noetzli's (1997) linear-reservoir model to compare modelled and observed proglacial discharges. The model

replicated well diurnal/seasonal discharge fluctuations: Nash-Sutcliffe values were 0.83 and 0.86 for 1993 and 1994, respectively (Hock and Holmgren, 2005). The key conclusion was importance of including surrounding topography since modelled melt varied substantially from topographic shading. Diurnal melt variations captured by this model would not have been reproduced as well by PDD approaches (Hock, 2003). Reijmer and Hock (2008) coupled this to a subsurface model for internal accumulation (namely refreezing within the snowpack); this performed reasonably well, although melt was overestimated (underestimated) high in the accumulation area (low in the ablation area).

3.4.5. Hydrological Modelling

Nilsson and Sundblad (1975) used a linear-reservoir model on Storglaciären, demonstrating water does not reach proglacial streams only by supraglacial runoff since delays existed between melt generation and detection at gauging stations (GSs). Hock and Noetzli (1997) furthered this by incorporating a SEB model, routing water through Storglaciären using three reservoirs (Figure 2.5). Modelled discharges replicated observations: in 1993, the R^2 was 0.82 and, in 1994, 0.88; total discharge was underestimated by 8% (6%) in 1994 (1993) (Hock and Noetzli, 1997). However, peak flows were underestimated mid-melt season (Hock and Noetzli, 1997). This could be because melt was underestimated, because empirical discharges were overestimated during peak flows (due to difficulty of accurate measurement in proglacial streams) or because storage constants were temporally invariant, when seasonal evolution occurs, especially for the ice reservoir. Bulk water storage was also unaccounted for by the model. This shows that accurately modelling meltwater is fundamental (Hock and Noetzli, 1997).

Recently, Gravelle (2013) used linear-reservoir modelling to determine the contributions of different reservoirs to proglacial streams. However, melt was not modelled using meteorological data, but determined using 'implied input' calculated from flow-recession analysis (following Hodgkins *et al.*, 2013) of proglacial streams' discharge; the modelled and observed values were 'tuned' until a best fit was obtained, generating near-perfect matches of modelled and observed data. However, this approach does not allow future discharge predictions as a physically based model would, nor did it integrate modelled with empirical data to verify the model.

3.5. Summary and Research Gaps

Collectively, there has been much effort to determine, using theoretical and empirical studies, Storglaciären's hydrology. Much focus has been on collecting extensive empirical observations, principally with dye-tracing and borehole experiments. While hydrological modelling has been conducted here, no study has applied a physically based model, allowing detailed consideration of the internal-drainage-system state, including P_w predictions, and being able to be forced with future-climate data. Moreover, previously applied linear-reservoir models have been compared with, at best,

one/two empirical dataset(s) for one/two summer season(s). Better integration with observations is needed. In addition, no model included surface routing to determine delays to supraglacial travel and produce spatially concentrated water inputs. This study therefore builds on this research by using physically based modelling, integrating it with detailed empirical observations, determining the model's applicability for Storglaciären.

4. Data and Methods

4.1. Introduction

Three coupled models are used (Figure 4.1):

1) a SEB model calculating meltwater across Storglaciären's surface,
2) a SROUT model routing water supraglacially either until it runs off Storglaciären or is intercepted by moulins feeding the glacier's internal system, and
3) a SUBHYD model routing the moulin inputs subglacially in an inherently channelised system.

Models are written in the FORTRAN-77 programming language; the SEB and SROUT models form a single program and the SUBHYD model a separate one.

Models run for 139 days from 17/04/2012 (Julian Day Number [JD] 108).

This chapter now has five sections: one for each of the three models, including required input data, a fourth detailing empirical data used for model calibration/validation, and a fifth describing the experimental design.

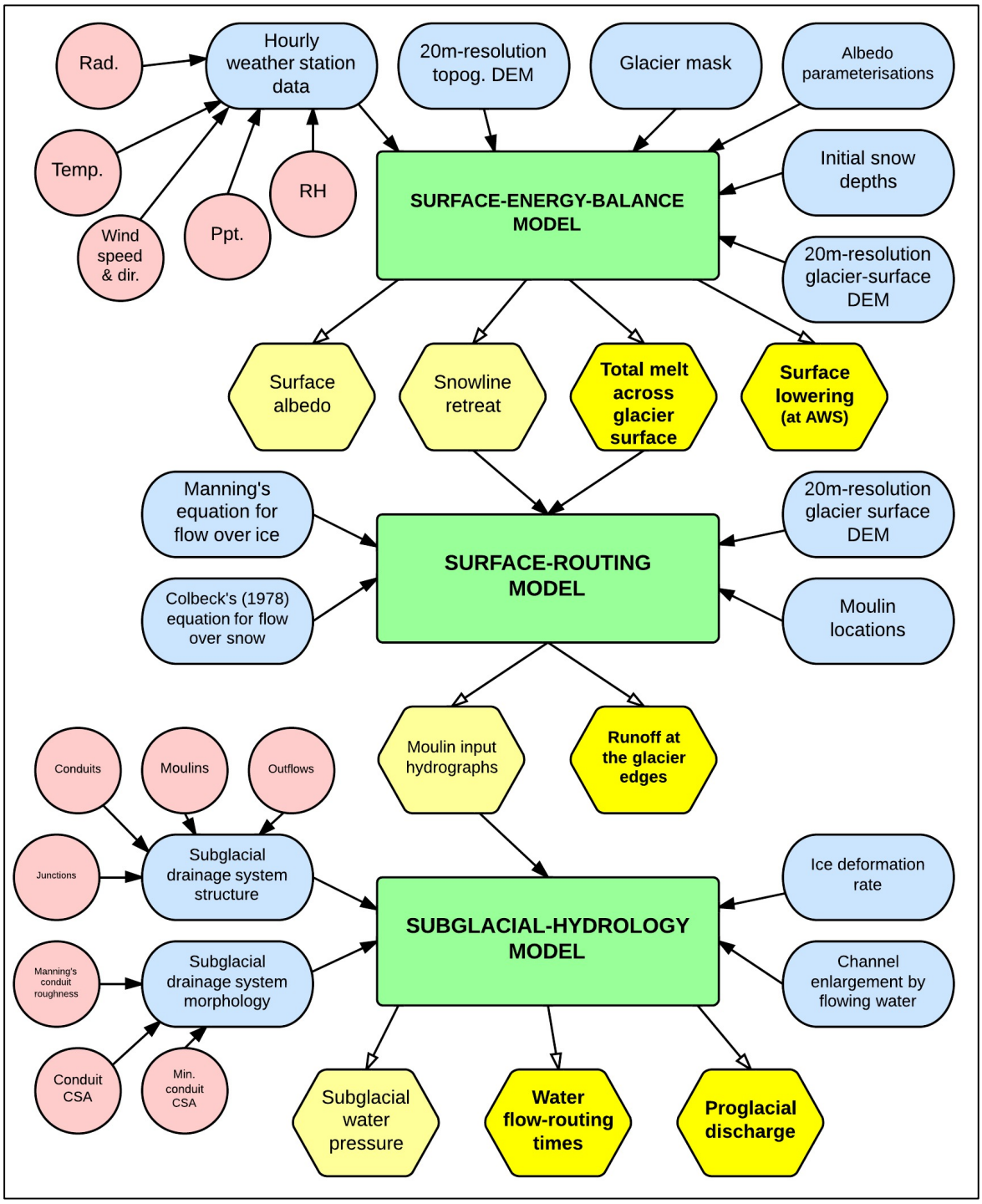

***Figure 4.1**. A summary of the models used in this study, their input data requirements and output data. Green boxes indicate the three (SEB, SROUT and SUBHYD) submodels coupled in this study. Blue boxes indicate model input data, with red circles indicating subsets within these input datasets. Yellow hexagons indicate modelled outputs; the darker yellow hexagons containing bold text indicate modelled outputs that are compared with empirical datasets for validation purposes. (Abbreviations: DEM = digital elevation model; Rad. = (shortwave and longwave) radiation, Ppt. = precipitation, Temp. = temperature, dir. = direction, topog. = topography, AWS = Automatic Weather Station, and CSA = cross-sectional area.) For further details on generating input datasets and for detailed descriptions of each model, see subsequent sections.*

4.2. Surface-energy-balance Model

This study uses the SEB model developed by Arnold *et al.* (1996) for HGd'A, tested with Richards *et al.*'s (1996) empirical data. Its outputs were used to force SROUT and SUBHYD models (Arnold *et al.*, 1998). The SEB model was applied, with developments, to Midre Lovénbreen, Svalbard (Arnold *et al.*, 2006; Rye *et al.*, 2010), the 'Paakitsoq region' of the GrIS (Banwell *et al.*, 2012a), and in other studies (Brock *et al.*, 2002; Arnold, 2005; Arnold and Rees, 2009). It always performed well, increasing confidence in its use for multiple glaciers and thus Storglaciären.

The model's key output is high temporal (hourly) and spatial (20-m) resolution melt across Storglaciären's surface, used by the SROUT model (Section 4.3). The model is validated by comparing cumulative modelled ablation with observed mass-balance data, and modelled surface lowering with lowering observations at the glacier-surface AWS.

4.2.1. Model Description

Basic equations and parameters (Table 4.1) are maintained from earlier model versions. The major difference between the model used here and Arnold *et al.*'s (1996) version is this model allows variable glacier-surface temperatures (following Arnold *et al.*, 2006).

4.2.1.1. Introduction

The model deals with SWR in most detail, but includes turbulent heat fluxes and LWR, which make smaller, but still significant, contributions (Arnold *et al.*, 1996; Arendt, 1999; Cuffey and Paterson, 2010). This model uses Equation 2.3 (Section 2.3.1.2), but omits Q_R. A subsurface refreezing scheme (e.g., Reijmer and Hock, 2008; Rye *et al.*, 2010; Banwell *et al.*, 2012a) is not included. The SEB components are calculated for each hourly timestep for every glacier-surface DEM cell.

***Table 4.1**. Values of parameters used in the SEB model.*

Parameter	Symbol	Value	Units
Sensible heat scalar (ice)	K_s	6.34×10^{-6}	m kg^{-1} K^{-1} s^2
Sensible heat scalar (snow)	K_s	4.42×10^{-6}	m kg^{-1} K^{-1} s^2
Latent heat scalar (ice, condensation)	K_l	9.83×10^{-3}	m kg^{-1} s^2
Latent heat scalar (ice, evaporation)	K_l	11.14×10^{-6}	m kg^{-1} s^2
Latent heat scalar (snow, condensation)	K_l	6.86×10^{-6}	m kg^{-1} s^2
Latent heat scalar (snow, evaporation)	K_l	7.77×10^{-6}	m kg^{-1} s^2
Latent heat of fusion of water	L_f	3.34×10^{-5}	J kg^{-1}
Density of water	ρ_w	1000	kg m^{-3}
Density of ice	ρ_i	900	kg m^{-3}
Density of snow	ρ_s	331	kg m^{-3}
Stefan-Boltzmann constant	σ	5.7×10^{-8}	W m^{-1} K^{-4}
Atmospheric lapse rate		0.0065	K m^{-1}
Surface layer depth	d_s	0.22	m
Subsurface layer depth	d_2	2.78	m
Thermal diffusivity (ice)	F	1.16×10^{-6}	m^2 s^{-1}
Thermal diffusivity (snow)	F	0.4×10^{-6}	m^2 s^{-1}
Specific heat capacity	c	2097	J kg^{-1}

4.2.1.2. Shortwave Radiation

The model assumes incoming SWR measured at the AWS is representative of the entire catchment. It then follows Oerlemans (1993), Arnold *et al.* (1996) and Banwell *et al.* (2012a) in assuming diffuse radiation from the sky is one-fifth of measured global SWR. If detailed cloud-cover records existed, this assumption would be unnecessary. The incoming SWR flux is modified at each grid cell based on aspect, slope angle, shading from surrounding grid cells and for the sky-view factor for diffuse radiation, accounting for the variation in sky proportion visible from a given grid cell, deemed important for SEB (Arnold *et al.*, 2006). Arnold *et al.* (1996) give full details of calculating slope angles, aspects, shading from surrounding cells, and sky-view factors; these are the same here.

4.2.1.3. Albedo

Albedo is a surface's average reflectivity, significant for total SEB (Escher-Vetter, 1985; Hock, 2005). Albedo is controlled by numerous factors, including water content, grain size, impurity content, surface roughness, and crystal orientation and structure (Hock, 2005). Typical albedos are <0.1 for

debris-rich dirty ice to >0.9 for fresh snow (Brock *et al.* 2000; Hock, 2005; Cuffey and Paterson, 2010). Many possible albedo paramaterisations exist (Brock *et al.*, 2000).

This study uses differing snow and ice albedos. Following Arnold *et al.* (2006), snow albedo (α_s) is calculated using a relation between snow depth and albedo, with 92 measurements from the AWS during 2012 on albedo variation with snow depth (Figure 4.2).

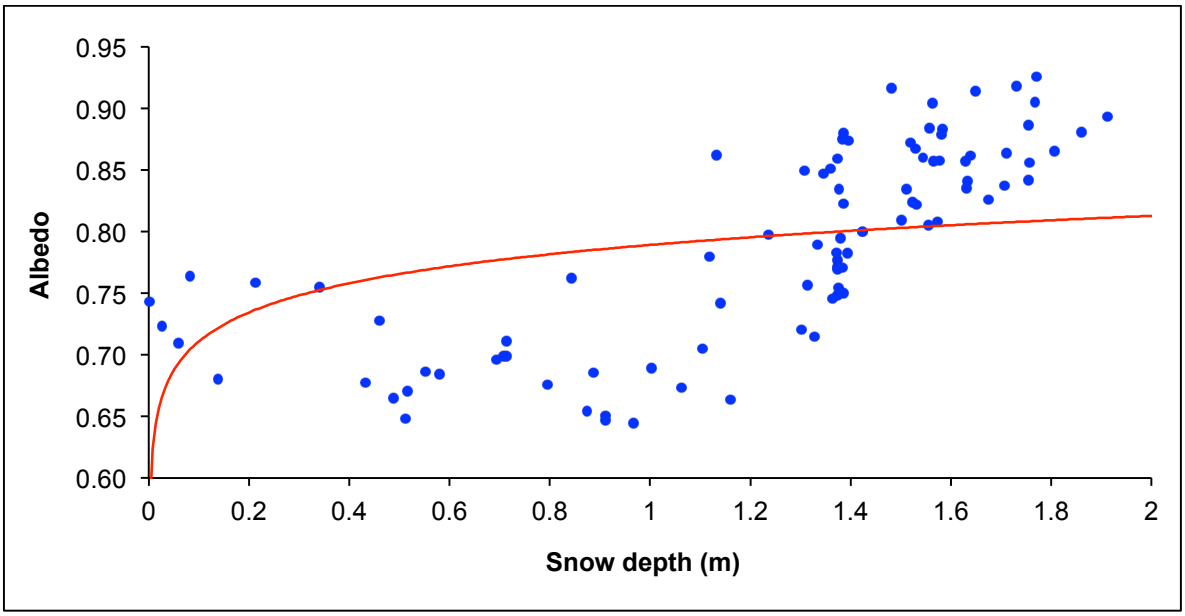

***Figure 4.2**. The albedo to snow depth relation used in this study. The red line shows the logarithmic relationship used to generate Equation 4.1.*

With these data, a logarithmic relationship was deemed appropriate ($R^2 = 0.183$, p-value $= 0.000$ at the 95% significance level). While other (e.g., linear) relationships produced slightly higher R^2 values, they overpredicted albedo at higher snow depths (values generated were often >1), resulting from bias in empirical measurements towards lower snow depths.

α_s is calculated by:

$$\alpha_s = 0.034 \ln(d) + 0.7892 \quad (4.1)$$

where d is snow depth.

To determine ice albedo (a_i), data were used from Jonsell *et al.*'s (2003) Storglaciären study: 216 a_i measurements over nine summers were made and mean values presented for different glacier-surface elevations. Overall mean a_i was 0.353, close to the value for 'clean ice' (Cuffey and Paterson, 2010). An albedo-elevation relationship was used for these data (Figure 4.3; $R^2 = 0.478$, p-value $= 0.027$ at the 95% significance level).

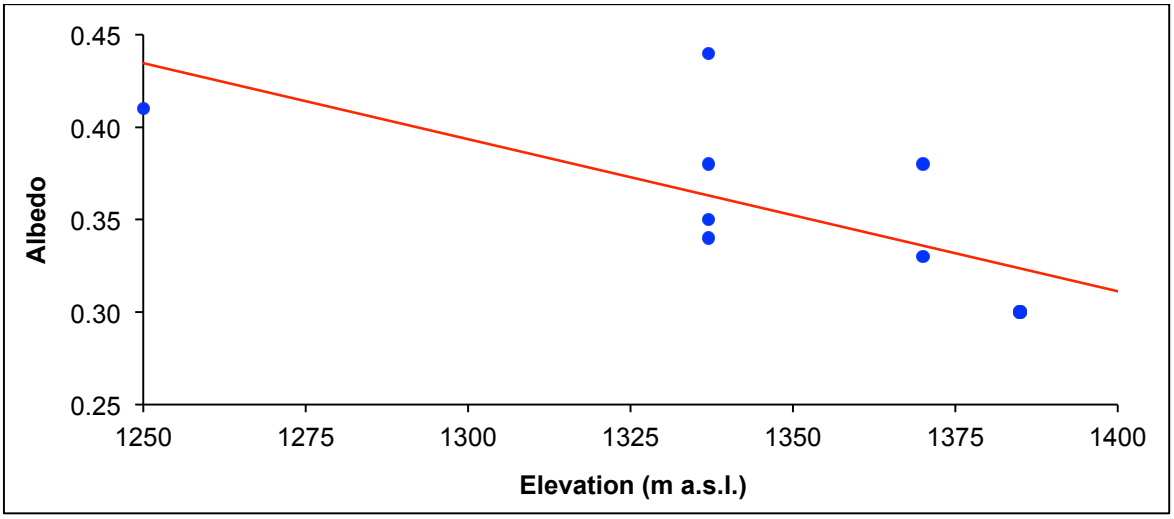

***Figure 4.3**. The ice albedo relation used in this study. The red line shows the linear relationship used to derive Equation 4.2.*

Albedo is expectedly lower at lower surface elevations due to lengthier exposure to melting, concentrating debris on the surface, thus absorbing more insolation (e.g., Oerlemans, 1992, 1993; Klok and Oerlemans, 2002; Cuffey and Paterson, 2010; Scherler *et al.*, 2011; Zhang *et al.*, 2011; Fyffe *et al.*, 2014).

a_i is calculated by:

$$a_i = (-0.0008\,E) + 1.4629 \tag{4.2}$$

where E is the surface DEM's cell elevation.

For each grid cell, the a_s relation (Equation 4.1) is used for every timestep until the entire snow depth is melted, whence the a_i relation (Equation 4.2) is employed. $SW\uparrow$ is then calculated with Equation 2.3.

4.2.1.4. Longwave Radiation

Net LWR sums that received from the sky and surrounding terrain ($LW\downarrow$) and that emitted by the glacier surface ($LW\uparrow$).

Incoming LWR is calculated following Arnold *et al.* (2006). This is due to lacking cloud-cover data, making estimating LWR from the sky using relations to atmospheric factors such as temperature and humidity difficult.

Thus, the 'effective emissive temperature of the sky' (ET_{sky}) is first calculated:

$$ET_{sky} = \left(\frac{LW\downarrow_{AWS}}{\sigma}\right)^{1/4} \quad (4.3)$$

where σ is the Stefan-Boltzmann constant and $LW\downarrow_{AWS}$ measured incoming LWR at the AWS.

A lapse rate corrects for elevation differences of DEM cells, generating elevation-corrected incoming LWR ($LW\downarrow_c$). Total incoming LWR from the sky for each grid cell ($LW\downarrow_{sky}$) is determined from:

$$LW\downarrow_{sky} = LW\downarrow_c f_s \quad (4.4)$$

where f_s is the proportion of sky visible from each DEM cell. f_s was not calculated in this study, and so was left constant at 0.95 (i.e., from each DEM cell, 95% sky is visible). This is a simplification but is justified since Storglaciären is not surrounded by high mountains (such as in the Alps) likely to have a disproportionate effect on the proportion of visible sky, and also because LWR makes relatively unimportant contributions to SEB (Arnold *et al.*, 2006).

LWR emitted by the surrounding terrain ($LW\downarrow_{terr}$) is then calculated:

$$LW\downarrow_{terr} = (1 - f_s)\sigma T_{terr}^4 \quad (4.5)$$

where T_{terr} is average temperature of the surrounding terrain visible from the grid cell. Given the lack of temperature data for surrounding terrain, and the difficulty this would be to compute (as temperatures need calculating for each different terrain type), this study follows Arnold *et al.* (2006) in assuming T_{terr} is the same as the elevation-corrected temperature (calculated using a lapse rate with measurements from the AWS) in each grid cell for each time step. This is an oversimplification, but $LW\downarrow_{terr}$ again makes small contributions to total SEB.

Total $LW\downarrow$ is then the sum of $LW\downarrow_{terr}$ and $LW\downarrow_{sky}$.

$LW\uparrow$ is determined as a function of the glacier-surface temperature (T_s):

$$LW\uparrow = \sigma T_s^4 \quad (4.6)$$

Section 4.2.1.5 gives details of computing surface temperatures.

Net LWR is $LW\downarrow$ minus $LW\uparrow$ (Equation 2.3).

4.2.1.5. Glacier-surface Temperature

Following Arnold *et al.* (2006), this study allows varying glacier-surface temperatures, contrasting with earlier models assuming constant 0°C temperatures (Arnold *et al.* 1996, 1998). Arnold *et al.* (2006) outline this scheme. Briefly, it follows Klok and Oerlemans (2002) in assuming a two-layer subsurface scheme. The total SEB is allowed to warm the surface layer, and heat loss to the sub-surface layer is calculated based on the temperature gradient between the surface and subsurface layer; this subsurface layer can then lose heat to glacier's body. The glacier-body temperature therefore needs specifying to determine the magnitude of the flux between the two. To this end, the average 2012 air temperature of –3.2°C at TRS is used, slightly higher than the 1965–1995 mean of –3.9°C, therefore representing a valid long-term value (Grudd and Schneider, 1996).

4.2.1.6. Turbulent Fluxes

Q_S and Q_L are calculated following Arnold *et al.* (1996) and Ambach (1986). The model assumes a melting glacier surface (at 0°C, with vapour pressure equal to the saturated vapour pressure at 0°C) and adiabatic stratification in a Prandtl-type boundary layer. The equations then are:

$$Q_S = K_S \, P \, T_2 \, V_2 \tag{4.7}$$

and

$$Q_L = K_l \, \delta e_2 \, V_2 \tag{4.8}$$

where K_S and K_l are coefficients, P air pressure, T air temperature, V wind speed and δe the difference between vapour pressure of the air and saturation vapour pressure at the glacier surface (Arnold *et al.*, 1996). Measurements in this study were made at ~2 m above the surface. K_S and K_l vary depending upon whether the surface is ice or snow (because of their differing roughnesses) and whether the surface undergoes condensation or evaporation; Table 4.1 lists values used. T, P and δe for each grid cell are calculated using an elevation-dependent lapse rate (Table 4.1) and the relative humidity (RH), which is spatially invariable, justified since RH does not vary substantially over Storglaciären (Hock and Holmgren, 2005).

4.2.1.7. Precipitation

Precipitation measured at the AWS is assumed to fall evenly across Storglaciären's surface, contrasting with the 10% linear increase in precipitation with elevation used by Hock and Noetzli (1997). Given the low altitudinal range (~1130–1730 m a.s.l.), this does not introduce substantial errors. Gauges are known to underestimate precipitation by up to ~25% (Östling and Hooke, 1986; Hock and Noetzli, 1997), and this may be especially true since this environment is windy (Jansson and Näslund, 2009), however this is highly spatio-temporally variable, so no correction is applied.

Precipitation falls as snow for any grid cell where the lapse-rate-corrected air temperature is <1°C; this compares with higher values of 1.5°C used by Hock and Holmgren (2005) and Hock and Noetzli (1997), and 2°C by Oerlemans and Hoogendoorn (1989) and Arnold *et al.* (1996), but the lower 0°C used by Greuell and Oerlemans (1986) and Greuell and Smeets (2001). Section 5.1.2 presents details of sensitivity tests to generate this value. If snow already exists in a cell, new snow is added to the previous depth. If temperature is >1°C, precipitation falls as rain and is inputted to the SROUT model.

4.2.1.8. Accounting

Figure 4.4 details procedures used to determine whether melt is generated or whether the surface warms/cools for each timestep.

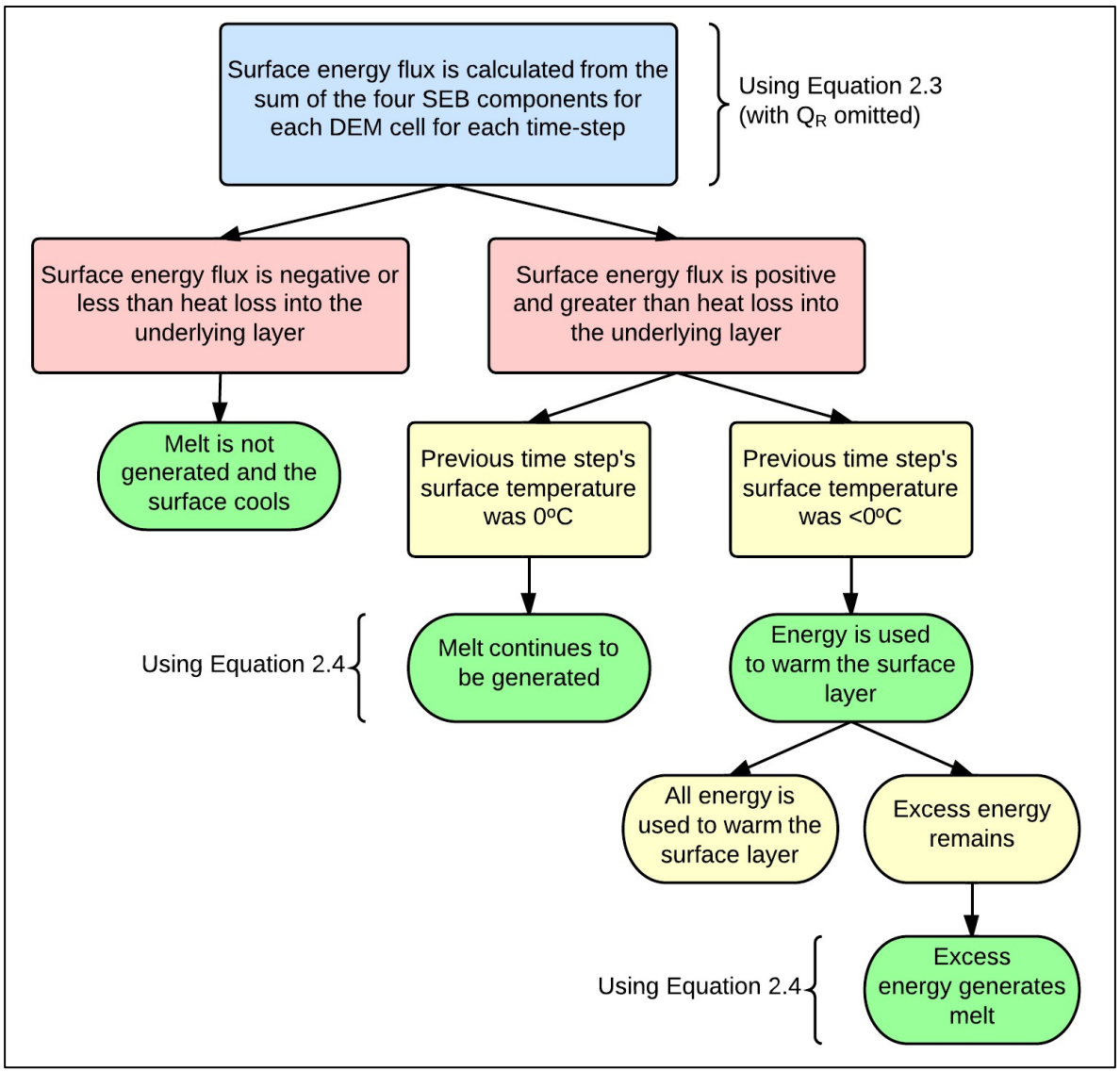

***Figure 4.4**. The method used to determine whether the surface cools/warms and whether melt is generated for each hourly timestep of the SEB model.*

4.2.2. Surface-energy-balance Model Input Data

4.2.2.1. Digital Elevation Models

The model requires DEMs of the glacier surface and surrounding topography to calculate topographic shading, slope angles and aspects, in addition to spatially distributing meteorological data from the AWS using lapse rates.

The glacier-surface DEM (Figure 4.5) is derived using both post-processed differential GPS data and 'Total Station surveys' conducted in mid-late July 2010 (A. Mercer, unpublished). Surveys covered Storglaciären's majority; one benefit of this method is that areas too dangerous to access manually could be surveyed; the overall accuracy is probably <0.1 m (A. Mercer, written communication). The provided DEM was resampled to 20-m resolution (from original 5-m resolution) using a cubic technique to maintain continuity with other input files, exported as an ASCII file and converted using MATLAB to a single-column UNIRAS (1990) file for the model. This method was always adopted when creating single-column files from georeferenced ones.

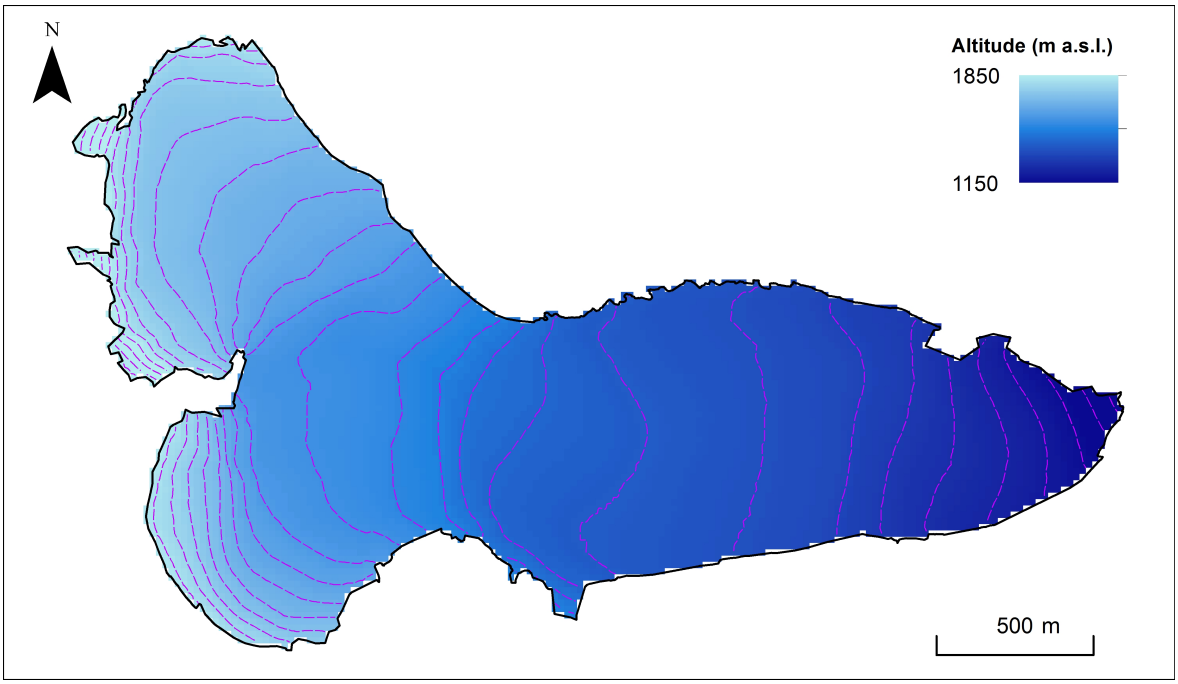

***Figure 4.5**. DEM of Storglaciären's surface topography at 20-m resolution. Contours shown are at 20-m intervals.*

The surrounding-topography DEM (Figure 4.6) is derived from a DEM of the Kebnekaise region, created using photogrammetry; it has 0.05 m horizontal and 0.1 m vertical accuracy (Koblet *et al.*, 2010). It was resampled using a cubic technique and clipped to cover only Storglaciären's immediate surroundings.

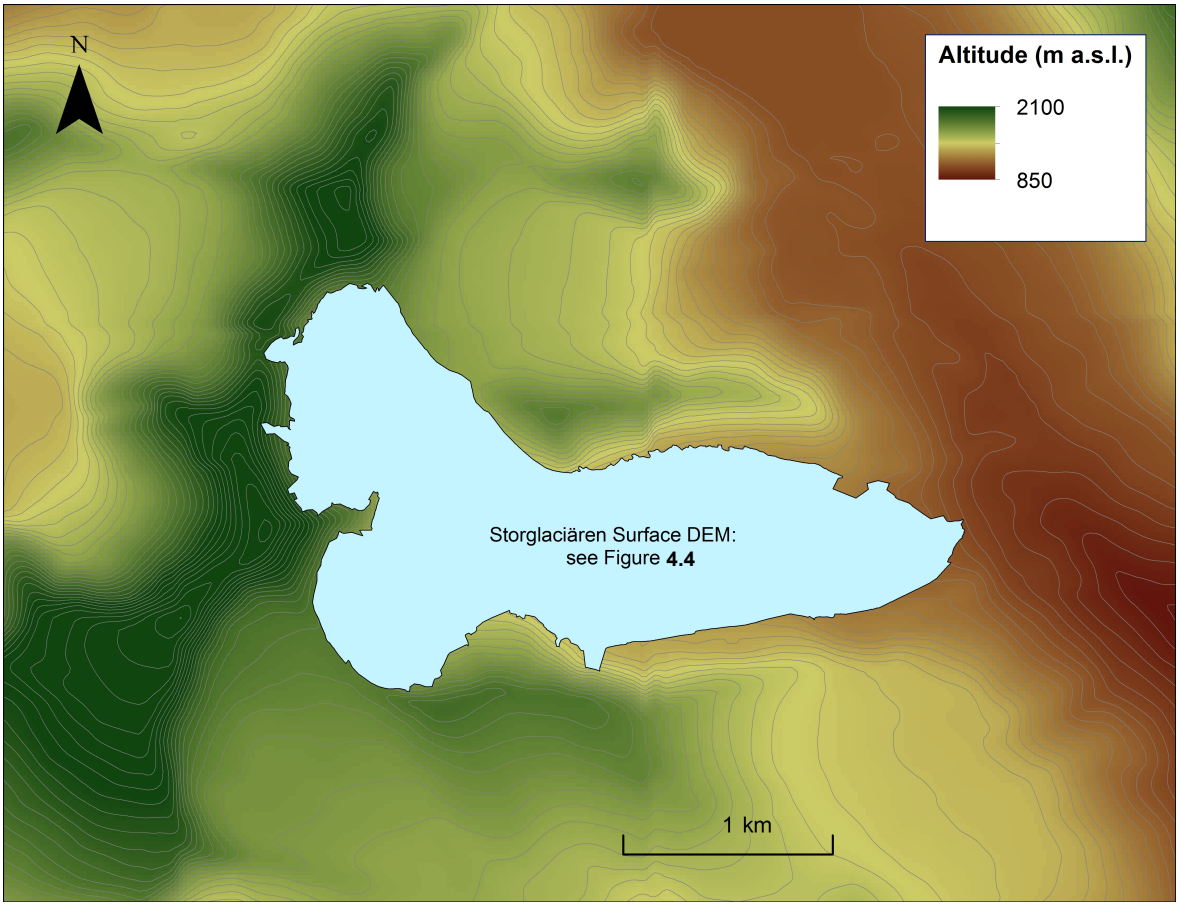

***Figure 4.6**. DEM of the topography surrounding Storglaciären, also of 20-m resolution, with contours shown at 20-m intervals.*

A mask is required to specify the basin's ice-covered areas. This was generated by hand-drawing a polygon (shown in Figure 4.6) around the glacier-surface DEM (Figure 4.5). Locations where ice is present were assigned values of 1 and those where ice absent set to 0.

4.2.2.2. Snow Depths

To determine start-of-season snow depths, snow probing was conducted at 273 points (Figure 4.7), representing ~100 points km^{-2}, in early April 2012 (unpublished data of TRS). Storglaciären's snow distribution is highly sporadic, so extensive coverage is crucial in generating accurate data (Evans *et al.*, 2008). There is some uncertainty over depths in the accumulation area because identifying snow-ice interfaces here is more difficult (e.g., Holmlund and Jansson, 1999). Snow probings are conducted before ablation commences and measurements always occur first at lower elevations to ensure this happens (Holmlund and Jansson, 1999). Sometimes snowfall occurs following initial measurements, however the SEB model accounts for this, so errors are not introduced.

Kriging interpolation was used between these point measurements, with extrapolation to Storglaciären's edge, to form a 20-m resolution raster. No extrapolation was used to the edge of

Storglaciären's watershed, meaning snow on slopes here is omitted from water-flux calculations. However, this is probably only important early melt season (i.e., outside the period of comparison with proglacial-stream discharge).

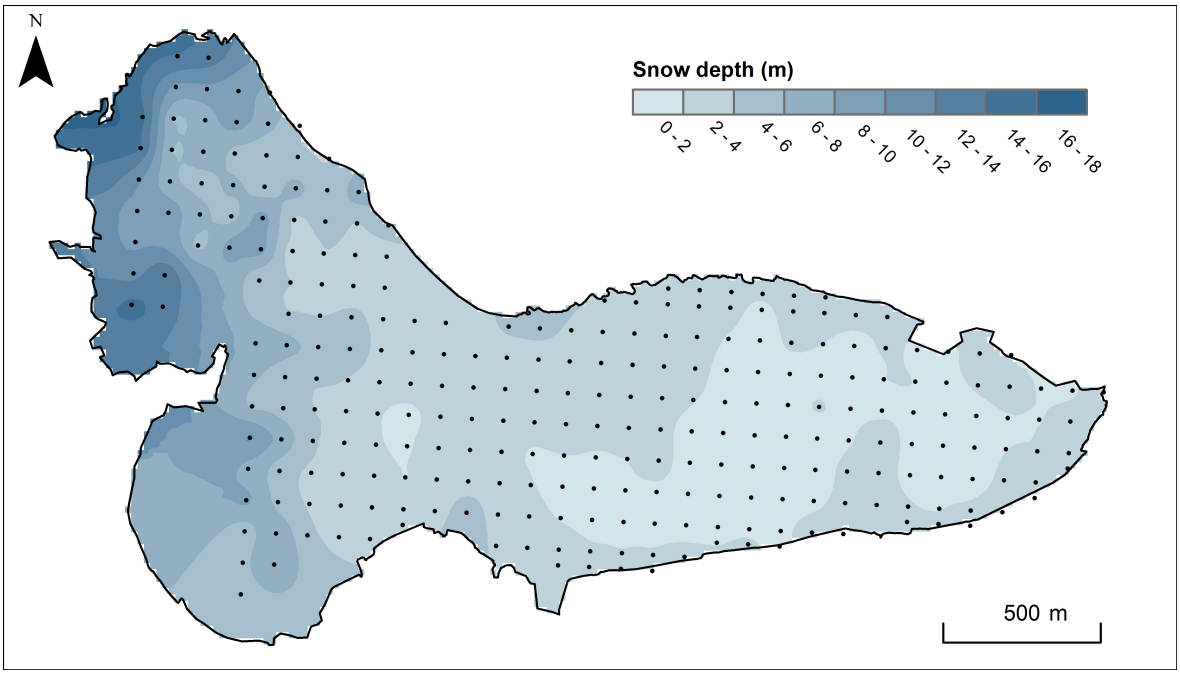

***Figure 4.7**. Storglaciären's start-of-season snow-depth distribution in 2012. Black dots show the locations where snow probing was conducted.*

4.2.2.3. Meteorological Data

The model uses hourly temperatures, SWR, LWR, RH, precipitation, and wind speeds/directions (Figure 4.8).

Most data were derived from the AWS on the glacier surface during 2012 at ~1370 m a.s.l. (Figure 4.16). Owing to problems with this AWS's anemometer, wind data were derived from a second AWS at TRS (Figure 3.1). Given TRS's lower sheltering by surrounding topography, wind speeds may be higher than those on the glacier surface, but no relationship between the two existed, so no correction is applied. Regardless, former studies (e.g., Hock and Holmgren, 2005) showed large scatter in wind speed across Storglaciären, so without numerous AWSs, there is always likely to be unreliability in extrapolating measurements from one location. Model results are also relatively insensitive to wind speeds (N.S. Arnold, personal communication).

Meteorological data were distributed across the surface using a spatio-temporally invariable lapse rate since adjusting the lapse rate would not impact modelled results (Hock and Holmgren, 2005).

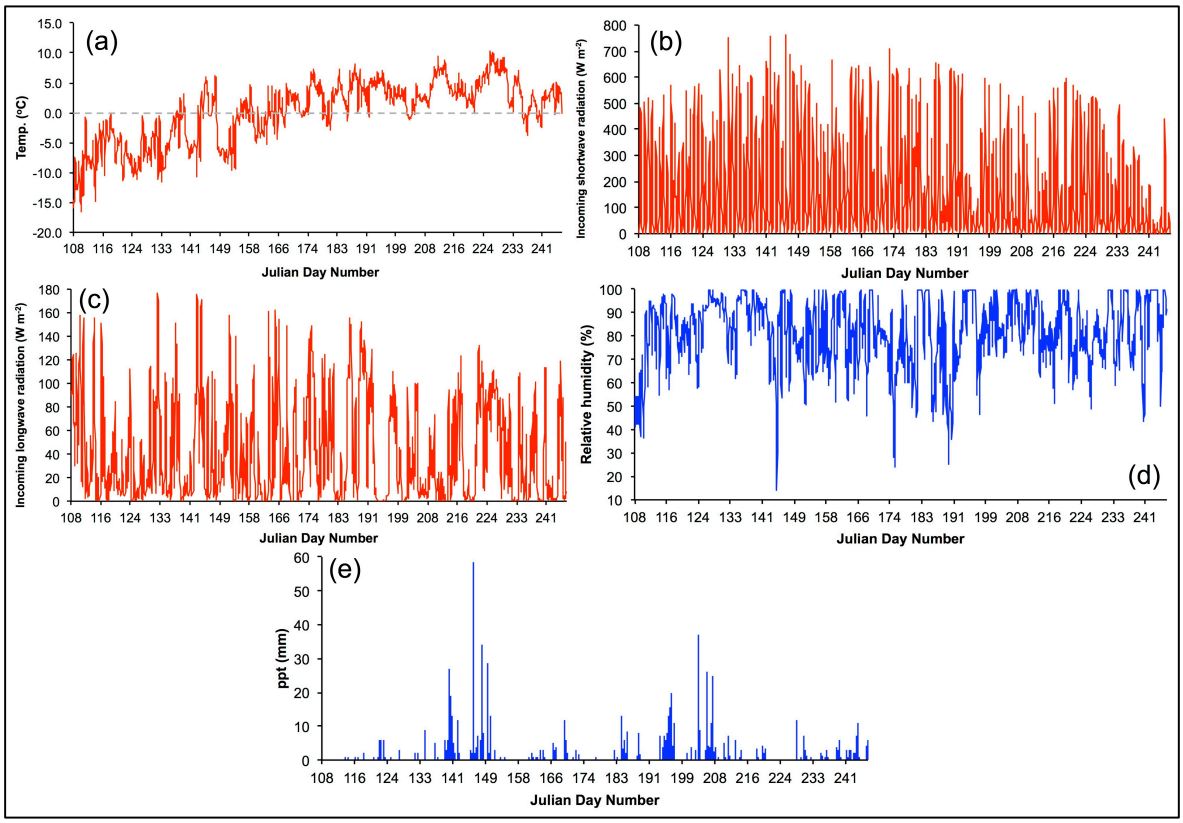

***Figure 4.8**. Meteorological data used by the SEB model: (a) temperature, (b) incoming shortwave radiation, (c) incoming longwave radiation, (d) relative humidity, and (e) precipitation.*

4.3. Supraglacial-routing Model

4.3.1. Model Description

Hourly outputs (of melt/rainfall) from the SEB model are routed supraglacially either to moulins feeding the englacial and ultimately subglacial systems or until they runoff Storglaciären's edges. The SROUT model is that originally developed for HGd'A (Arnold *et al.*, 1998), validated by Willis *et al.* (2002). It was subsequently modified and applied to the GrIS, specifically to include lake filling in supraglacial topographic depressions (Banwell *et al.*, 2012b; Arnold *et al.*, 2013). This increases confidence in the model's ability to perform well.

The model incorporates a flow-delay algorithm (FDA) derived from Arnold *et al.* (1998). From the glacier-surface DEM, moulins' watersheds are calculated, and travel times between the DEM cell where water is present and the moulin into which it drains are calculated using the FDA. It assumes water flows down the steepest hydraulic gradient between cells. Knowledge of snow/ice distribution (from the SEB model) allows calculations of delay times for each DEM cell, which are integrated for individual moulins to generate hourly input hydrographs (Equations 4.9–4.11). Travel times decrease as snow quantities in moulins' catchments decrease over the season. Table 4.2 lists parameters used by the model.

For cells containing snow at a given timestep, vertical and horizontal flow times need calculating. To calculate vertical travel times to the base of the cell's snowpack (D), Colbeck's (1978) equation is used, assuming flow in a Darcian layer:

$$D = \frac{\kappa_e d}{\left(\left(\frac{3\rho_w g}{\mu}\right) w q^2\right)^{1/3}} \tag{4.9}$$

where κ_e is the snowpack's effective porosity, d snowpack depth, ρ_w water density, g gravitational acceleration, μ water viscosity, w snow permeability and q water flux through the snowpack (i.e., melt plus precipitation from the SEB model). Following Arnold *et al.* (1998) and Banwell *et al.* (2012b), k_e and w were kept constant at values for 'medium-grain old dry snow' (Male and Gray, 1981).

To calculate horizontal flow velocities across snow-covered cells (C_s), Colbeck's (1978) equation is used:

$$C_s = \frac{\left(\frac{\rho_w g}{\mu}\right) w \theta}{\kappa} \tag{4.10}$$

where θ is surface slope and κ snow porosity.

To calculate horizontal flow velocities across ice-covered cells (C_i), the Gauckler-Manning-Strickler equation is employed:

$$C_i = \frac{R^{2/3} \theta^{1/2}}{n} \tag{4.11}$$

where R is (spatially constant) hydraulic radius of the supraglacial channel, and n Manning's roughness coefficient. Moulin input hydrographs are insensitive to values for R and n; much greater sensitivity is on the presence of snow within moulins' watersheds (Arnold *et al.*, 1998; Schneider, 1999; Willis *et al.*, 2002; Banwell, 2012)

***Table 4.2**. Values of parameters used in the SROUT model.*

Parameter	Symbol	Value	Units
Hydraulic radius	R	0.035	m
Manning's roughness	n	0.05	$m^{-1/3}$ s
Water density	ρ_w	1000	kg m^{-3}
Ice density	ρ_i	900	kg m^{-3}
Gravitational acceleration	g	9.81	m s^{-2}
Water viscosity	μ	1.8 x 10^{-3}	Pa s
Snow permeability	w	6 x 10^{-9}	m^2
Snow porosity	κ	0.68	–
Snow effective porosity	κ_e	0.63	–

4.3.2. Surface-routing Model Input Data

The model requires four input datasets: glacier-surface topography, moulin locations and their input hydrographs, and snow/ice distributions for each timestep.

4.3.2.1. Surface Topography

The surface DEM (Figure 4.5) was created with the procedure described for the SEB model (Section 4.2.2.1).

However, the SROUT model will not run if depressions exist in the DEM. Thus, these 'sinks' were identified and filled using *ArcGIS*'s *Sink* and *Fill* tools; alternative methods can remove depressions, including allowing them to fill with water, like the model used by Banwell *et al.* (2012b) for the GrIS, but since lakes do not form on Storglaciären's surface, this was inappropriate, so they are instead considered DEM artefacts (Arnold, 2010). To check the surface DEM produced realistic supraglacial flow pathways, and paralleling the procedure used in Section 4.4.2.1, the *Flow Direction* tool determined theoretical flow pathways for the DEM, and the *Flow Accumulation* tool defined the number of upstream-contributing cells. Realistic theoretical flow pathways were produced and they were often intersected by moulins (Figure 4.9).

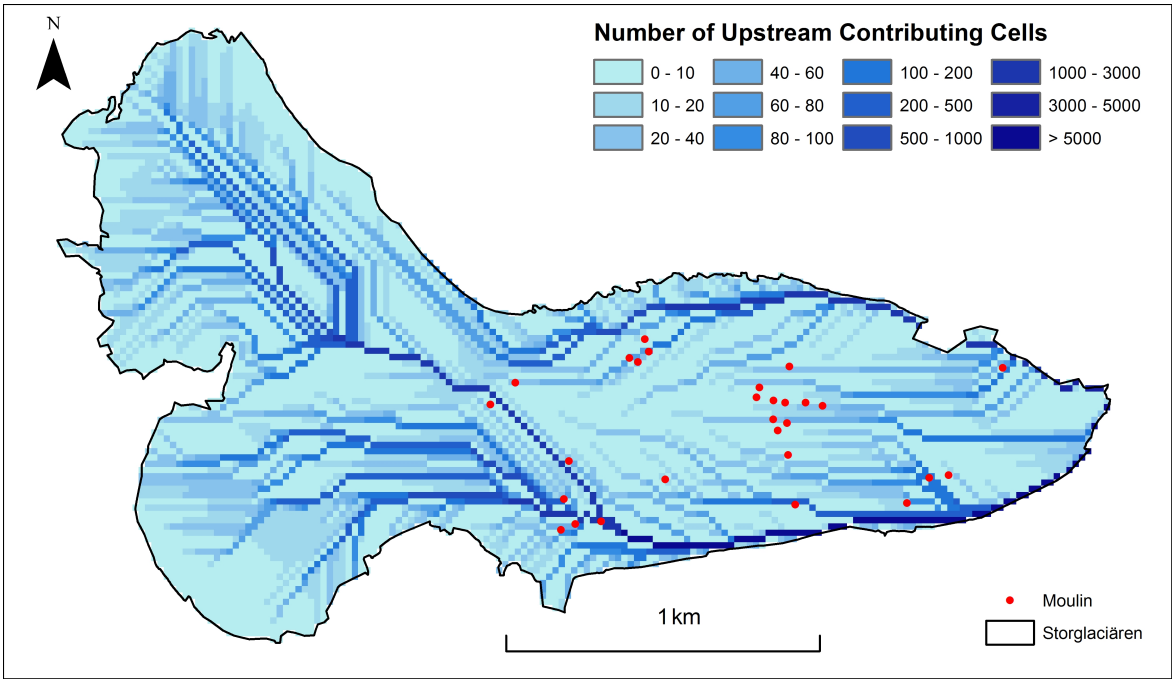

***Figure 4.9**. Flow accumulations over the surface DEM (Figure 4.5) as a check that moulins (red dots) were in locations likely to 'catch' water from theoretical supraglacial flow pathways determined from the surface DEM.*

4.3.2.2. Moulins

Moulin locations (Figure 4.9) used for tracing experiments were recorded using a handheld GPS during 2012 and 2013 (Figure 4.16). Additionally, a more complete list of moulins was provided by TRS, supplementing those used in the field.

The model allows moulin-cell radiuses to be adjusted to account for the fact that occasionally surface meltwater streams predicted by the model flow very close to a moulin's location, but do not intercept it. Field evidence suggests this is unrealistic (e.g., Holmlund, 1988b). For HGd'A, the cell radius had to be set to two/three times the actual cell size to allow water capture (N.S. Arnold, personal communication). Section 5.2 gives full details of sensitivity tests adjusting cell radius.

4.3.2.3. Snow and Ice Distribution

The snow/ice distribution used in the FDA was determined from the modelled snowline retreat.

4.3.2.4. Water Volumes

The SEB model determined meltwater and rainfall volumes.

4.4. Subglacial-hydrology Model

The SUBHYD model is fed with the SROUT model's input hydrographs. There is no englacial-storage component, so water entering moulins is dealt with immediately by the subglacial system, contrasting with other glacier-hydrology models (e.g., Flowers and Clarke, 2002a; Werder *et al.*, 2013). The SUBHYD model uses Arnold *et al.*'s (1998) model applied successfully to HGd'A, the 'Paakitsoq region' of the GrIS (Banwell *et al.*, 2013), and, in simplified form, to Franz Josef Glacier, New Zealand (Anderson *et al.*, in press).

4.4.1. Model Description

The model is derived from the Extended Transport (EXTRAN) block of the US Environmental Protection Agency's Storm Water Management Model (SWMM). EXTRAN is a dynamic model routing inflows from hydrographs in channels, originally developed for urban systems (Roesner *et al.*, 1988). SWMM is a pseudo two-dimensional model because conduits branch and converge at junctions, but only their slopes, lengths and locations relative to other conduits need defining (Banwell *et al.*, 2013). Flow is simulated in 'sewers', fed by 'drains', where water enters (or leaves) the system; for glaciers, 'sewers' are subglacial conduits and 'drains' are moulins receiving inflow (Figure 4.10). 'Junctions' (vertical pipes not receiving surface inputs) connect subglacial conduits.

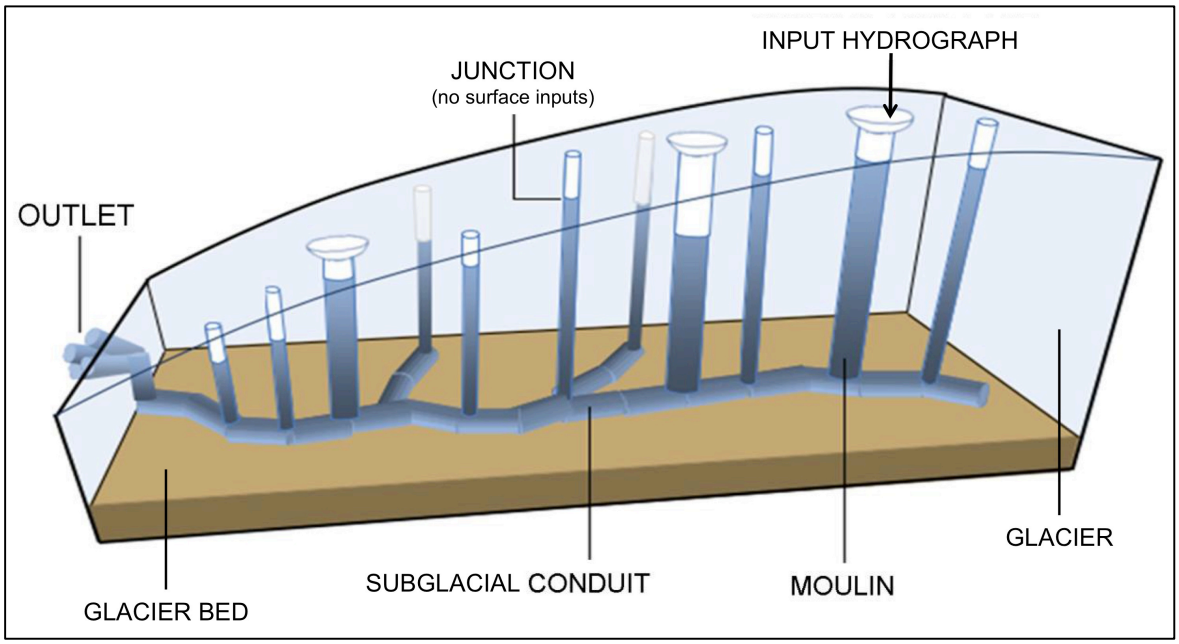

***Figure 4.10**. The configuration of the EXTRAN component of the SUBHYD model. Figure modified from Banwell (2012).*

The SUBHYD model is inherently channelised, routing flow in R-channels (Röthlisberger, 1972). Arnold *et al.* (1998) attempted incorporating distributed drainage into the model, however it performed poorly when the glacier was postulated to be underlain by distributed systems, so no attempt at replicating this behaviour was made for Storglaciären. As further justification for accounting for only

channelised drainage, field evidence from summer 2012 suggested Storglaciären was underlain by channels even with limited early-season water inputs (Williamson, 2013). Hock and Hooke (1993) also present convincing evidence for channelised flow beneath much of Storglaciären. This is likely due to the system being overlain by thin ice, yielding low creep closure. Furthermore, Gulley *et al.* (2012a), based on independent observations of a subglacial system, suggest previous studies using evidence from dye tracing for distributed early-season flow may need revaluation and, instead, conduits may form earlier than previously recognised.

4.4.1.1. Model Formulation and Solution Methods

The model solves the full dynamic equations for gradually varied flow (the 'St. Venant'/'shallow water' equations) with an explicit-solution technique for each time step. In this model, following Banwell *et al.* (2013), a 1-second timestep is employed. Banwell *et al.* (2013) present full numerical details. Table 4.3 lists parameters used in the model. Conduits must have lengths, diameters and Manning's roughnesses assigned at the start of model runs. Junctions and moulins must have their bed and surface elevations specified, including cross-sectional areas (CSAs). Water inputs are specified for specific moulins; the model then calculates discharge and P_w.

4.4.1.2. Model Adaptations

Arnold *et al.* (1998) modified the EXTRAN model to include channel enlargement by flowing meltwater and closure by ice deformation (Röthlisberger, 1972). This follows Spring and Hutter (1981) in assuming conduit wall-melting rate (X), in mass melted per unit length of conduit per unit time, is determined by:

$$X = \frac{\left|(\pi A_c)^{1/2} \rho_w \left(\frac{f_r U^3}{4}\right)\right|}{L_f} \tag{4.12}$$

where A_c is conduit CSA, ρ_w water density, f_r a friction coefficient, U the conduit's water velocity and L_f latent heat of fusion of water.

The rate of conduit closure by ice deformation (C), expressed as change in CSA per unit time is defined as:

$$C = -(P_i - P_w)|P_i - P_w|^{m-1} 2 \left(\frac{1}{mB}\right)^m A_c \quad (4.13)$$

where P_i and P_w are respectively ice-overburden and water pressures, m and B are respectively the exponent and Arrhenius parameter in Glen's (1952) Flow Law, and A_c conduit CSA.

These equations are solved using water velocities and pressures calculated by the model for each conduit; conduit sizes can adjust every timestep.

***Table 4.3**. Values of parameters used in the SUBHYD model.*

Parameter	Symbol	Value	Units
Friction parameter	f_r	0.25	–
Latent heat of fusion of water	L_f	3.34 x 10^5	J kg^{-1}
Arrhenius parameter	B	5.8 x 10^7	N m^{-2} $s^{1/m}$
(SI equivalent)		6.8 x 10^{-15}	s^{-1} kPa^{-3}
Ice flow law exponent	m	3	–

Banwell *et al.* (2013) further modified the model; these modifications are adopted here. They applied two spin-up periods: in the first 24 hours of the run, conduits' initial empty states when overlain by thick ice caused rapid creep closure, so a 24-hour spin-up period was applied when no wall melting/creep closure occurs. A second 24-hour spin-up then follows when Equations 4.12 and 4.13 are linearly introduced to maintain model stability. The model needs a minimum CSA specifying to maintain system connectivity; this was 0.07 m^2 (=0.3 m diameter), contrasting with the higher 0.2 m^2 for HGd'A (Arnold *et al.*, 1998).

4.4.2. Subglacial-hydrology Model Input Data

4.4.2.1. Subglacial Drainage System Structure

Subglacial drainage system structure – its location, alignment and interconnection (Willis *et al.*, 2008) – needs defining. To this end, φ theory (Shreve, 1972) is employed, with water assumed to flow along steepest φ gradients. This requires high-resolution DEMs of the glacier surface and bed for accurate predictions (Sharp *et al.*, 1993; Wright *et al.*, 2008).

Figure 4.5 shows the surface DEM. The bed DEM was generated thus: it initially comprised 818 point measurements derived from radio-echo sounding and ~50 borehole investigations, with densest data in the smooth and easily accessible centre of the glacier (Herzfeld *et al.*, 1993; Eriksson *et al.*, 1993). To form the raster (Figure 4.11), Kriging interpolated between points and extrapolated to Storglaciären's ice mask, selecting 20-m resolution.

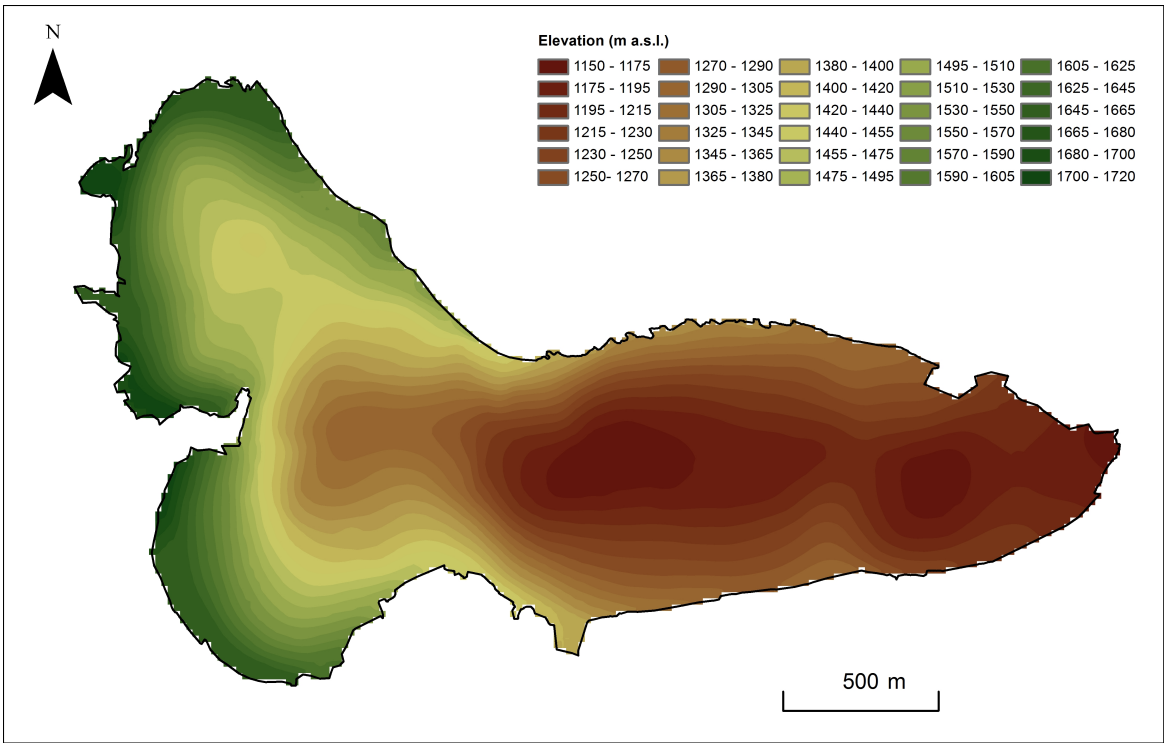

***Figure 4.11**. DEM of the bed topography of Storglaciären, with original data from Eriksson et al. (1993).*

Subglacial φ was determined:

$$\varphi = k\rho_i g(h - z) + \rho_w g z \tag{4.14}$$

where ρ_i is ice density, ρ_w water density, g gravitational acceleration, h and z respective surface and bed elevations, and k the uniform flotation factor, the ratio of P_w to P_i, i.e., P_w/P_i; where $k = 1$ indicates subglacial $P_w = P_i$ and where $k = 0$ represents $P_w = P_a$ (Shreve, 1972; Rippin *et al.*, 2003; Willis *et al.*, 2008, 2012).

Following Willis *et al.* (2012), the theoretical, long-term, steady-state drainage system structures for Storglaciären for 11 k values from $k = 0$ to $k = 1$ at $0.1k$ increments were compared with field observations of proglacial/ice-marginal streams, results from dye-tracing experiments and proglacial discharge data; where $k = 0.7$ best matched field evidence and thus the structure was defined with this value (Williamson, 2013). Better representations of the structure would be produced if localised water inputs were included, and steady state was not assumed, but this is beyond this study's scope (Gulley *et al.*, 2012b). This value indicates 70% ice-overburden is supported by subglacial water in the steady-state configuration, matching previous suggestions for valley glaciers (e.g., Willis *et al.*, 2012), but is lower than the $k = 0.925$ value for the 'Paakitsoq region' of the GrIS, following expectations because of thicker ice here (Banwell *et al.*, 2013). Figure 4.12 shows number of upstream contributing cells where $k = 0.7$.

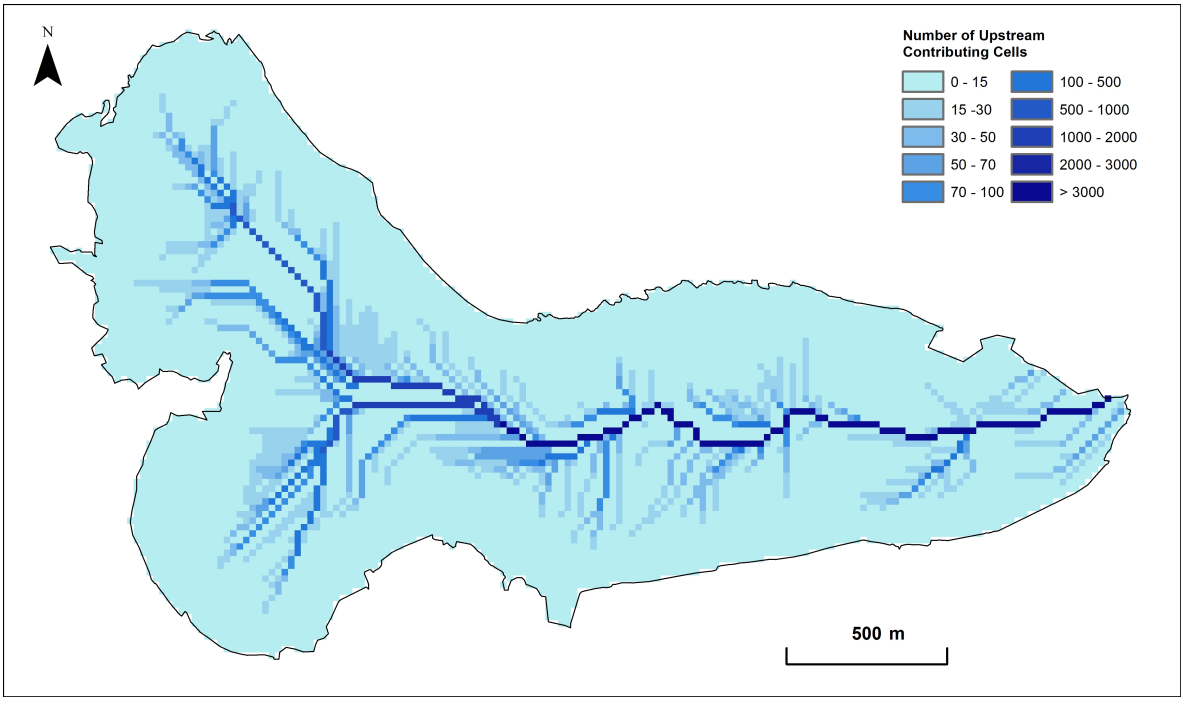

***Figure 4.12**. Flow accumulations (number of upstream contributing cells) of subglacial hydraulic potential where $k = 0.7$.*

The structure for the model was determined by placing subglacial conduits (black lines) along lines of highest φ (Figure 4.13). An extra conduit had to be added beyond the glacier edge to prevent unrealistic discharges at the outflow, resulting from high enlargement rates beneath thin ice close to the terminus. Moulin locations (blue dots) were from field observations and junctions (red dots) were used to connect conduits. The locations of moulins were encouraging since they often lay directly above lines of highest φ, so representing a realistic structure, despite Shreve's (1972) assumptions (Willis *et al.*, 2008; Gulley *et al.*, 2012b). Occasionally, subglacial-conduit locations were adjusted slightly to allow moulins to be incorporated into the structure. Outflows (green dots) were observed outflows from Storglaciären; these correlated well with modelled lines of highest φ, lending further confidence to the drainage-system structure.

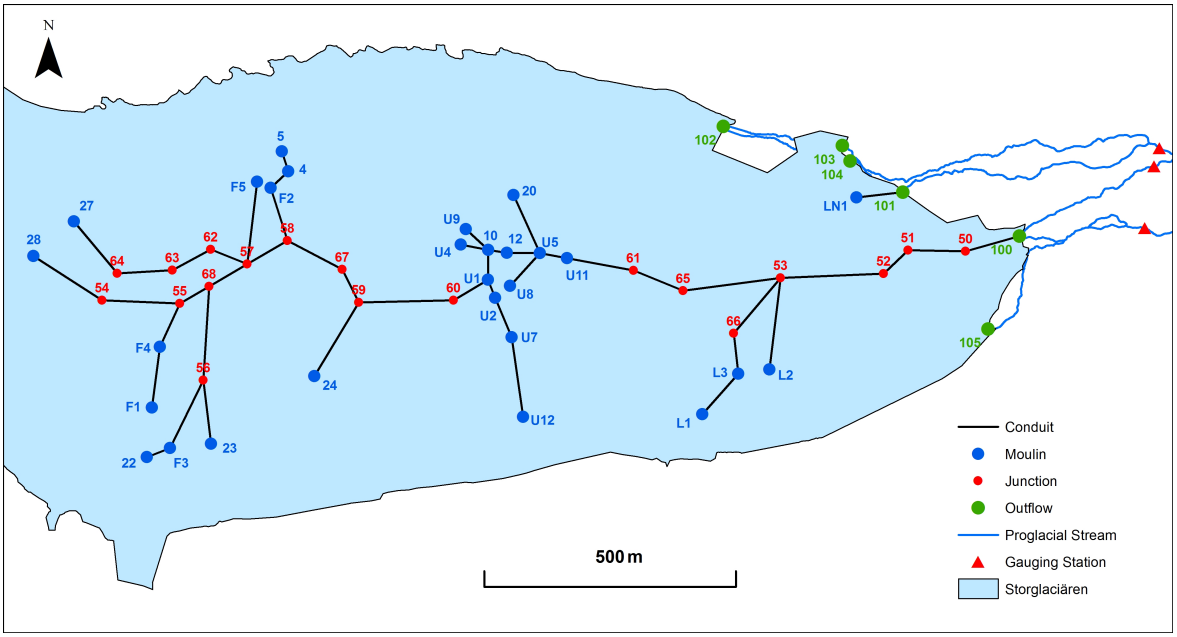

***Figure 4.13**. The inferred drainage system structure for Storglaciären based on accumulating number of upstream contributing cells for the calculation of subglacial hydraulic potential where $k = 0.7$. Black lines correspond to lines of hydraulic potential in Figure 4.12.*

Confidence in this modelled drainage system also arises since a close match was obtained between it and the line of highest φ predicted by Schneider (2001), especially the location where subglacial flow commences (Figure 4.14). Differences between the above modelled structure and Schneider's (2001) likely result from his assumption that $P_w = P_i$, whereas here $P_w = 0.7P_i$.

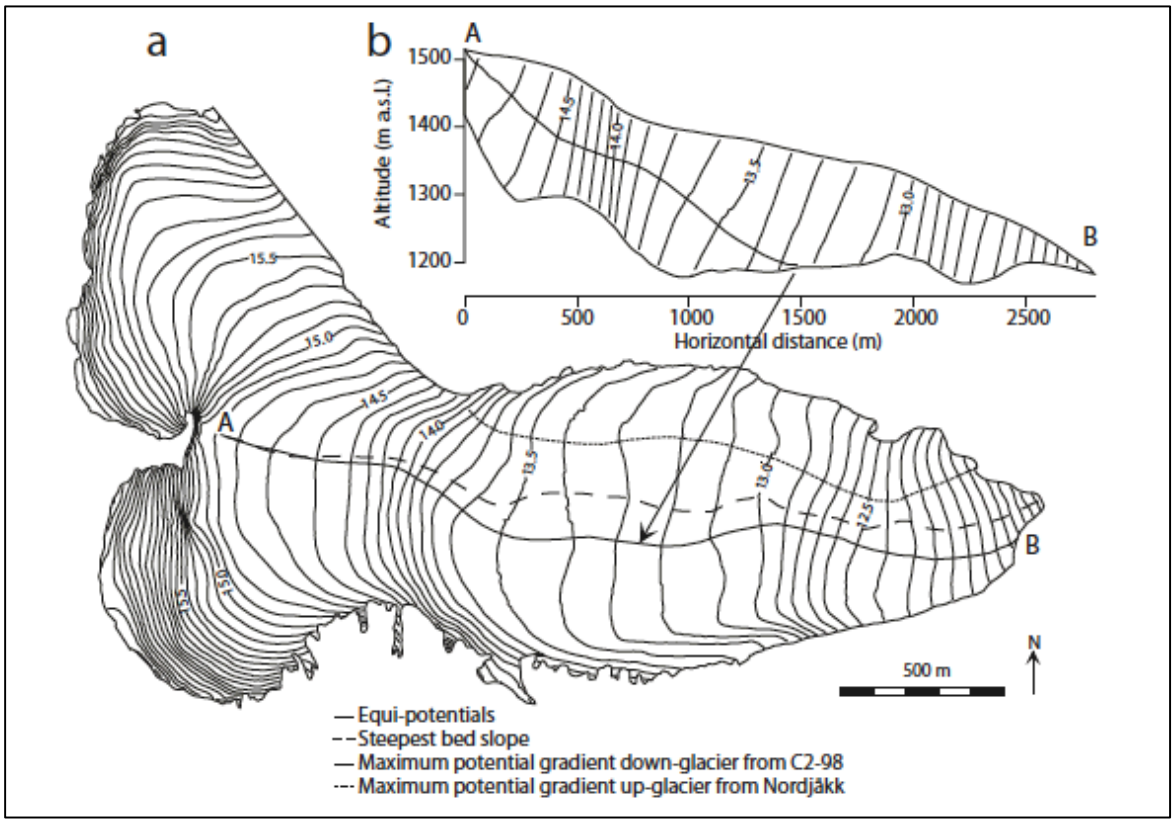

***Figure 4.14**. Schneider's (2001) theoretical flow pathways beneath Storglaciären determined from hydraulic-potential calculations following Shreve (1972). (a) Storglaciären's equipotential fields; water flow will be perpendicular to these lines. Water injected at location A will likely follow the thick line and emerge at B, assuming $P_w = P_i$. If $P_w = P_a$, the water injected at A would follow the dashed line. The modelled structure in this study broadly compares well with these suggestions. (b) A profile along line A–B, showing the location at which water from A would likely reach the glacier bed; again, this compares well (if slightly downglacier) with the modelled structure in this study.*

Conduits' length, including their upstream/downstream connecting junctions, need specifying in the model. Lengths were determined with *ArcGIS*. Moulin and junction surface and 'invert' (bed) elevations were determined using DEMs (Figures 4.5 and 4.11; Appendix I).

4.4.2.2. Subglacial Drainage System Morphology

Conduit morphologies are also required by the model: specifically CSAs, diameters and roughnesses.

To determine CSAs, a procedure similar to that outlined by Willis *et al.* (2012) was followed, using tracing results (Section 4.5.4; Table 5.6). The flow-pathway length between injection site and terminus was derived by summing the lengths of conduits along which tracers travelled (see Figure 4.13 for injection sites and conduits), and this was divided by the time taken from injection to peak breakthrough in proglacial streams to derive a mean throughflow velocity (u_{fp}) for all positive breakthroughs. Where multiple tests were conducted from the same site, the mean of these times was taken. The mean sum of water flowing along the pathway over summer (Q_{fp}) was derived by

weighting the φ grid (Figure 4.12) with 2011 summer mass-balance data, assuming melt reaches the bed *in situ*, and then accumulating discharge along modelled flow pathways; Willis *et al.* (2012) and Williamson (2013) give full details. Mean CSA (CSA_{fp}) of the channel between injection site and terminus was then derived:

$$CSA_{fp} = \frac{Q_{fp}}{u_{fp}} \tag{4.15}$$

Since the aim is deriving start-of-season CSAs, using 2011 mass-balance data to determine mean sums of water flowing along pathways represents a better estimate than using 2012 data. Moreover, 2012 dye-tracing experiments were conducted when moulins had only received water inputs for limited time. This produced CSAs in Appendix I. Conduit diameter (D_{fp}) was determined from:

$$D_{fp} = 2\sqrt{\frac{CSA_{fp}}{\pi}} \tag{4.16}$$

While this method is non-ideal since it assumes uniform CSA between injection sites and terminus (e.g., Hock and Hooke, 1993), it is a fair approximation given the model is more sensitive to roughness than initial CSAs (Banwell, 2012). Roughnesses were not derived from empirical data, but were used as a sensitivity test (Section 5.3.1). This is given debate in the literature surrounding roughnesses (e.g., Gulley *et al.*, 2012a, 2013), and because Willis *et al.* (2012) found roughnesses derived from empirical data were unfeasibly high for R-channels, which are inherently specified in this model.

In addition to conduit morphologies, CSAs of all moulins and junctions must be set. Following Banwell *et al.* (2013), all moulins' CSA is 2.0 m^2. For junctions that are not moulins, CSAs are 0.1 m^2; though low, this prevents high water storage and back-up here.

4.4.2.3. Moulin Input Hydrographs

Moulin input hydrographs are computed by the SROUT model for each hour of the model run.

4.5. Empirical Data for Model Calibration and Evaluation

Several datasets are used for model calibration and evaluation. To validate the SEB model, total summer melt is compared with 2012 mass-balance data, and modelled surface lowering at the AWS is compared with observations. No quantitative data exist to test the SROUT model, so qualitative comparison is made with previous studies' runoff estimates. For the SUBHYD model, two datasets are used: hourly proglacial discharge measurements in summer 2012 and subglacial flow-routing times from 2012 (and several 2013) tracing experiments. Qualitative comparison is made between modelled and observed subglacial P_w from previous studies.

4.5.1. Mass Balance

Total summer (April–September, inclusive) ablation across Storglaciären was derived from 2012 mass-balance data, following Östling and Hooke (1986). Summer balance is measured using a distributed stake network. In 2012, 75 stakes were used, representing ~25 km^{-2}, covering most of Storglaciären, not just its centreline, important for accurate mass-balance estimates (Arnold *et al.*, 2006). Some (e.g., crevassed) areas of Storglaciären are underrepresented with stakes, specifically because of dangers of drilling stakes in heavily crevassed regions, yet these regions may represent areas of considerable loss, adding some unreliability (Holmlund and Jansson, 1999). Overall, however, there is high confidence in Storglaciären's mass balance determined thus (Jansson, 1999); errors are likely ±~2% for each stake, but when accounting for interpolation, total errors amount to ±~4% (Östling and Hooke, 1986), <0.1 m water equivalent (w.e.) (Holmlund *et al.*, 2005). A 10-m resolution summer-balance raster was provided by A. Mercer (unpublished); this was modified to remove points where no melting was observed, thus determining approximate meltwater quantity (Figure 4.15). Each cell's total height change was multiplied by its 10 m^2 size, and summed, generating total summer meltwater production (m^3).

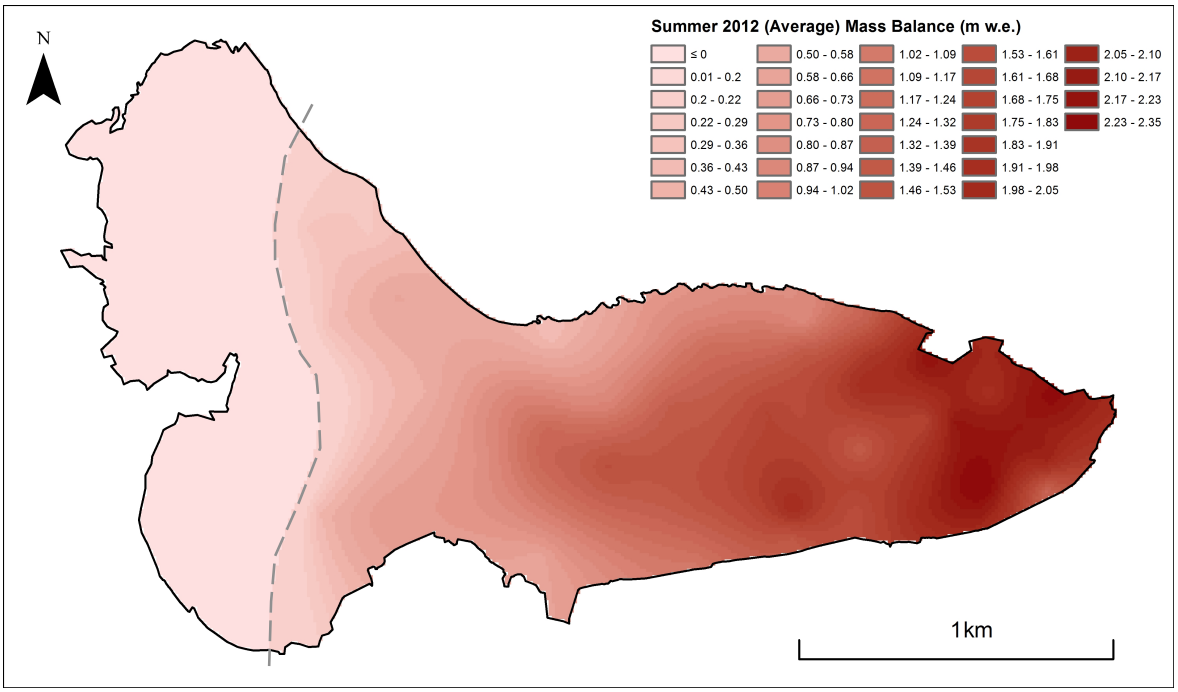

***Figure 4.15**. 2012 summer average mass balance (m w.e.) for Storglaciären. Total summer mass balance for 2012 is then derived by multiplying the net change in each cell by the cell size (10m^2). The dashed line marks the boundary between locations that experienced some melting during the summer with those that experienced no melting overall (i.e., mass balance was <0 m w.e.).*

4.5.2. Surface Lowering

Surface-height change was measured hourly at the AWS (Figure 4.15) over summer.

4.5.3. Proglacial Discharge

Independent discharge measurements were made in proglacial streams in 2012 using the fluorescent slug dye-dilution method (Hubbard and Glasser, 2005). Stage was measured hourly at GSs (Figure 4.16) throughout summer using streambeds; a weir was not used because streambeds are stable in all except the highest flows (Seaberg *et al.*, 1988). GSs were slightly downstream of glacial portals, but flow times to them were less than the model's hourly timestep. Stage data were correlated with independent measurements to generate rating curves, thus deriving hourly discharge for each proglacial stream. Williamson (2013) gives full details.

4.5.4. Subglacial Flow-routing Times

4.5.4.1. 2012 Dye-tracing Experiments

25 dye-tracing experiments using 50–150 ml (20% active ingredient) Rhodamine WT were conducted from 06/08/2012 (JD 219) to 24/08/2012 (JD 237) using 12 injection sites (Figure 4.16). Concentrations were measured in proglacial streams either with automatic fluorometers or manual sampling in the case of fluorometer inoperation. This generated breakthrough curves (BTCs). Flow-routing times were defined as the time taken from injection to peak breakthrough at the GS (Table 5.6). Williamson (2013) details dye-tracing methods.

4.5.4.2. 2013 Tracing Experiments

In addition, this study compares modelled flow-routing times with observations derived from several experiments in 2013 using novel DNA-based tracers. These tracers comprise DNA sequences encapsulated in polylactic microspheres; because DNA strands can be randomly combined, up to 1.61×10^{60} individual tracers can be derived (Sharma *et al.*, 2012). This means multiple sites can be injected simultaneously, representing development from conventional tracers, since only a limited number (~5) are available for simultaneous use. Two simultaneous injections of ten and five tracers were conducted on 05/08/2013 (JD 217) and 09/08/2013 (JD 221), respectively. Six injections showed positive breakthroughs and were used to derive 2013 subglacial flow-routing times (Table 5.6).

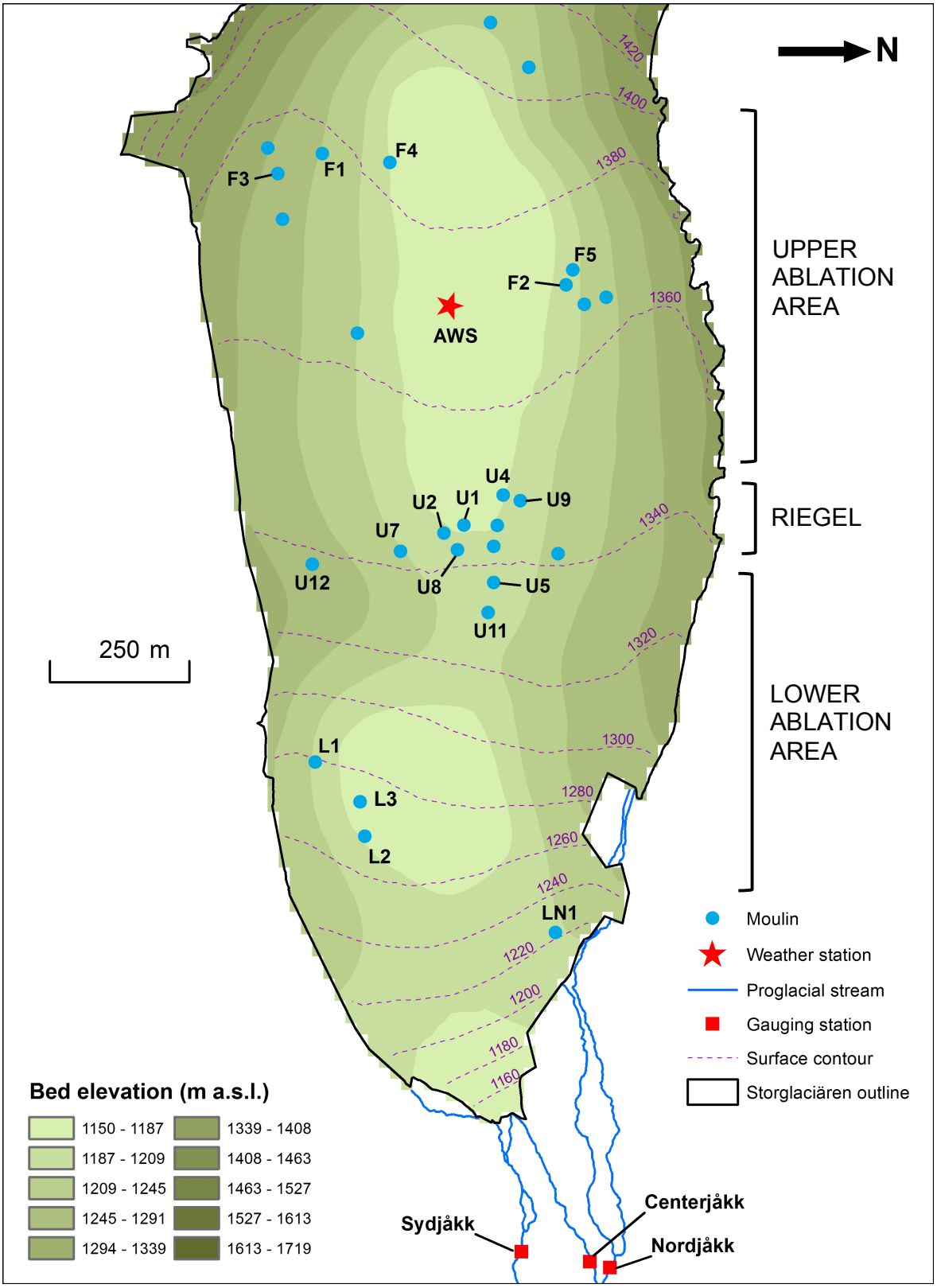

***Figure 4.16**. Locations used for tracing experiments in 2012 and 2013, superimposed on bed topography, with the locations of proglacial streams and their gauging stations also shown. Note that moulins labeled here are the same as those in Figure 4.13. Those labelled here represent those moulins that were used for tracing experiments (cf. Table 5.6) (though not necessarily producing positive returns); unlabelled moulins were not used.*

4.6. Experimental Design

First, the SEB and SROUT models are run in isolation of the SUBHYD model and validated using mass-balance and surface-lowering data (Table 4.4). Several runs are conducted to test for sensitivity to the threshold for solid precipitation, snow density, and moulin radius. Once matches between observed and modelled data are optimised, moulin input hydrographs are fed into the SUBHYD model. This is run using differing conduit roughnesses; outputs are compared with proglacial discharge and tracing data. Borehole P_w data are presented for the run producing best matches between modelled and observed data.

***Table 4.4**. Summary of stages of testing used to validate this study's models.*

Test Stage	Model Tested	Parameter Tested	Range of Values Tested	Empirical Data for Validation
1	SEB	Snow density	100–500 kg m^{-3}	Mass balance
2	SEB	Threshold for solid precipitation	1.5–0.9°C	Surface lowering at AWS & mass balance
3	SROUT	Moulin cell radius	1–3	Runoff at glacier edges
4	SUBHYD	Subglacial conduit roughness	0.150–0.050 $m^{-1/3}$ s	Proglacial discharge & subglacial water-flow routing times

Where possible, models are evaluated statistically using R^2 values, the Nash-Sutcliffe Model Efficiency Coefficient, and the Root Mean Square Error (RMSE). The Nash-Sutcliffe value (Y) is defined as (Nash and Sutcliffe, 1970):

$$Y = 1 - \frac{\sum_{t=1}^{T}(V_o^t - V_m^t)^2}{\sum_{t=1}^{T}(V_o^t - \overline{V_o})^2} \quad (4.17)$$

where V_o is the mean of the observed values over the time period, V_m modelled value, and V_o^t observed value at time t. Y ranges from 1 to $-\infty$;1 represents perfect match between observed and modelled values; 0 indicates that the model predicts values as accurately as the mean of observations; values <0 indicate the observed mean is a better predictor than the model. While traditionally used for hydrological models, the Nash-Sutcliffe value can be used to define other models' efficiency (Krause *et al.*, 2005). To avoid cancelling errors of opposite signs, the square of results is used; this means emphasis is placed on larger errors, with smaller ones neglected (Legates and McCabe, 1999; Krause *et al.*, 2005). Furthermore, this indicates improvements to model efficiency occur at peak values (flows) rather than low values (flows), so higher Nash-Sutcliffe values represent better model replication of peak values (flows) (Krause *et al.*, 2005). Yet, it remains justified for measuring model efficiency (e.g., Coffey *et al.*, 2004; McCuen *et al.*, 2006).

Other measures are advised in conjunction with Nash-Sutcliffe values (Jain and Sudheer, 2008). The $RMSE$ is also used, determined from:

$$RMSE = \sqrt{\frac{\sum(V_o - V_m)^2}{G}} \tag{4.18}$$

where G is degrees of freedom.

5. Results

5.1. Surface-Energy-Balance Model Sensitivity and Outputs

SEB outputs are distributed hourly melt, and surface lowering at the AWS. Since net all-wave radiation measurements at the AWS were used as model input and no further measurements from 2012 elsewhere on Storglaciären are available, these cannot be used to validate the model. Furthermore, measured snow albedo at the AWS cannot be used for model evaluation as these data were used to derive the snow-albedo relation. Unfortunately, 2012 snowline retreat measurements are unavailable. However, comparison with two empirical datasets still allows model validation and the key is generating distributed melt rather than comprehensively evaluating various energy fluxes' contribution to ablation.

5.1.1. Sensitivity to Snow Density

Two parameters were changed to test sensitivity. The first was snow density; the model cannot account for spatial snow-density variations; instead, a uniform value needs prescribing. The model was insensitive to this, varied from 100–500 kg m^{-3}. This led to total ablation variations of <18,000 m^3 over summer, seeming initially high, but being <1% observed summer ablation. Thus, the value of 331 kg m^{-3} was retained from Arnold *et al.* (1996, 2006), comparing favourably with snow-density measurements on Storglaciären (Schytt, 1973).

5.1.2. Sensitivity to the Threshold for Solid Precipitation

The model was more sensitive to the threshold for solid precipitation. If precipitation is recorded, whether it falls as snow/rain is determined based on cells' temperatures for each model timestep. With a higher threshold, more precipitation falls as snow than with a lower threshold. Three thresholds (1.5–0.9°C) were tested to determine impact on total melt and surface lowering.

5.1.2.1. Comparison with Surface Lowering

Surface-lowering measurements were made at the glacier-surface AWS (Figure 4.16) over summer. Raw data show large variation, often with wildly positive and negative values for surface-height change, not correlating well with snowfall events. This may be due to water vapour refreezing on the surface (Willis *et al.*, 2002; Arnold *et al.*, 2006) and because the uppermost ice layers are likely to have 'weathering crusts' (Müller and Keeler, 1969; Hock and Holmgren, 1996). The aim is to calibrate the model, rather than examine these processes. Thus, to remove data noise, comparison with lowering data is only conducted when reliable data existed from JDs 199–227. Empirical data are smoothed using a 13-point moving average, following Arnold *et al.* (2006). Modelled data are

corrected for snow/ice densities. The model was run with each threshold and data were cumulated over the period to determine total surface lowering (Figure 5.1).

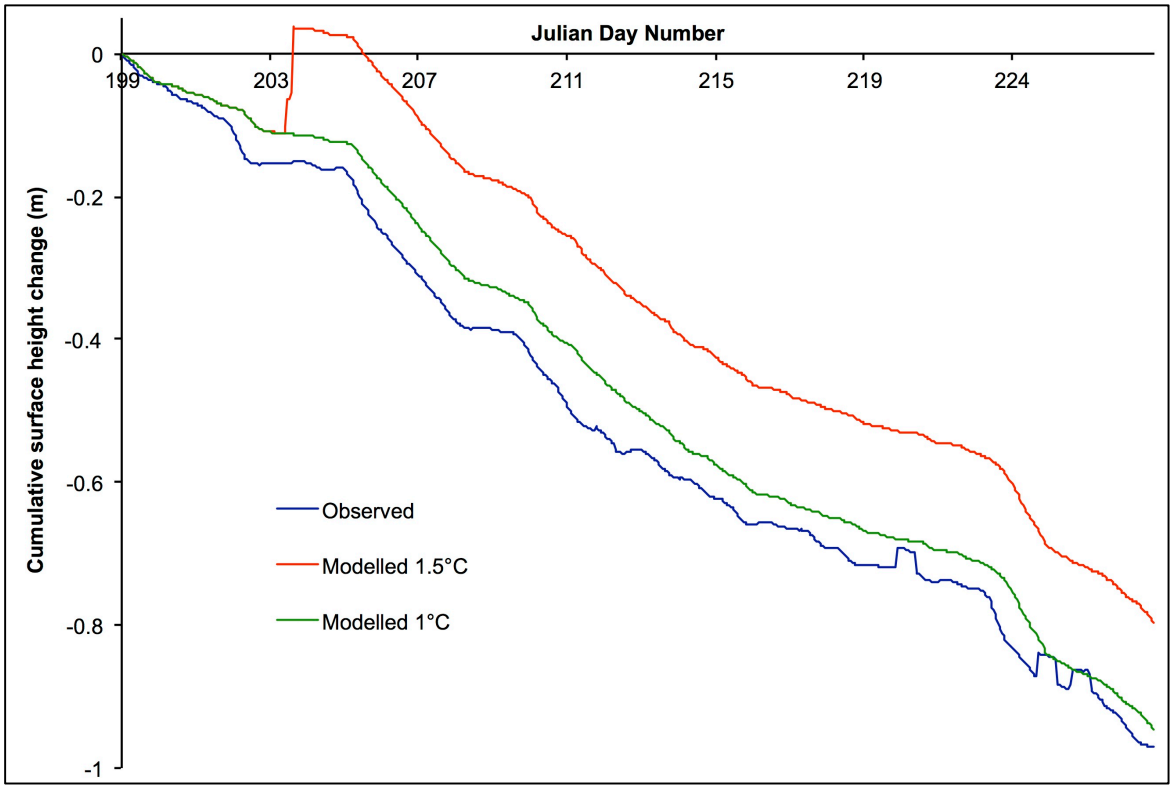

***Figure 5.1**. Modelled and observed cumulative surface lowering at the AWS over the period of reliable measurements. The modelled lowering for the 0.9°C is not shown because it exactly matched the 1.0°C curve.*

For all thresholds, data show initially good agreement, however partway through JD 203, the 1.5°C threshold predicts snowfall, increasing surface height. Following this, the modelled outputs run largely parallel with observations. For the 1.0°C (and 0.9°C) threshold, this snowfall is not predicted (precipitation instead falls as rain), meaning modelled data better resemble observations. For all thresholds, there are small snowfalls (like on JD 220) unpredicted by the model, but recorded in observations, though the 1.0°C line does slightly rise here. The alternative explanation would be that these small rises represent similar events to those generating the early-season noise, albeit of smaller magnitude. Even for the 1.0°C threshold, surface-height lowering (and thus ablation) is slightly underpredicted.

Table 5.1 shows statistical performance of the runs. Performance for 0.9°C is the same as 1.0°C, suggesting model insensitivity to values <1.0°C. The Nash-Sutcliffe and R^2 values for the 1.0°C threshold are very high, likely because there is very close match following small deviations at the beginning of the model run. Total underestimation of surface lowering for this threshold over the period is 2.39 cm (9.56 m^3 melt), equivalent to 0.034 mm (0.0137 m^3 melt) h^{-1}.

***Table 5.1**. Statistical performance of the SEB model compared with surface lowering for differing thresholds for solid precipitation.*

Modelled Snow Threshold (°C)	Nash-Sutcliffe Coefficient	R^2	RMSE (m)	Modelled Minus Observed Surface Lowering (m)
0.9	0.966	0.994	0.051	0.0239
1.0	0.966	0.994	0.051	0.0239
1.5	0.551	0.947	0.185	0.1745

5.1.2.2. Comparison with Mass Balance

In addition to comparing with surface lowering for different thresholds for solid precipitation, modelled mass balance was compared with observed 2012 summer mass balance. Empirical mass-balance measurements do not account for rainfall. Moreover, total modelled water balance accounts only for ablation, not rainfall, but does account for extra melt potentially occurring if new snow falls. Snow also impacts albedo, so there are two competing effects: one which increases the mass loss (because total water balance accounts for snow melt, but not rainfall) and another which decreases it due to reduced SWR available for melting with higher albedos. Figure 5.2 presents total predicted and observed ablation for different thresholds.

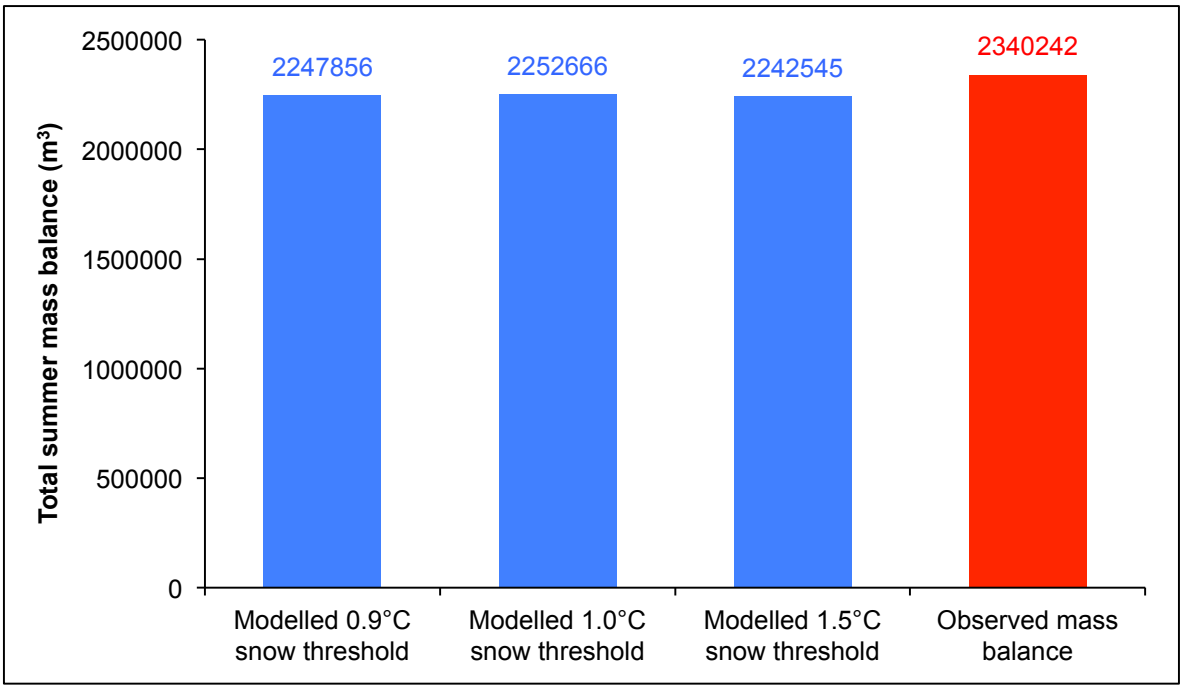

***Figure 5.2**. Modelled (blue bars) versus observed (red bar) 2012 summer mass balance (i.e., melting in m^3) for three differing snow thresholds tested in the model. Each bar's value is shown above.*

These data indicate that best match (~4% difference) is found with the 1.0°C threshold, however there remains overall underestimated ablation compared with observed mass balance. Section 6.2.1 gives possible reasons for this discrepancy. When the threshold is set at 0.9°C, while there would be more

snow across Storglaciären available to melt, this clearly acts to reduce melting (due to its effect on albedo) more than for the 1.0°C scenario.

5.1.3. Total Modelled Melt

From this, the 1.0°C threshold for solid precipitation was adopted in all runs. Hourly melt across Storglaciären is totalled (Figure 5.3). Towards the beginning of the melt season, little ablation occurs until JD 145, when a melt event lasts until JD 149. Unsurprisingly, this mirrors high temperatures recorded at the AWS (Figure 4.8). Melting then reduces until JD 160, when fairly consistent (daytime) ablation begins until the conclusion of the model run. Melt peaks correlate with temperature peaks. High-amplitude diurnal fluctuations are observed in data throughout the season, representing lack of radiation available for melting during the night.

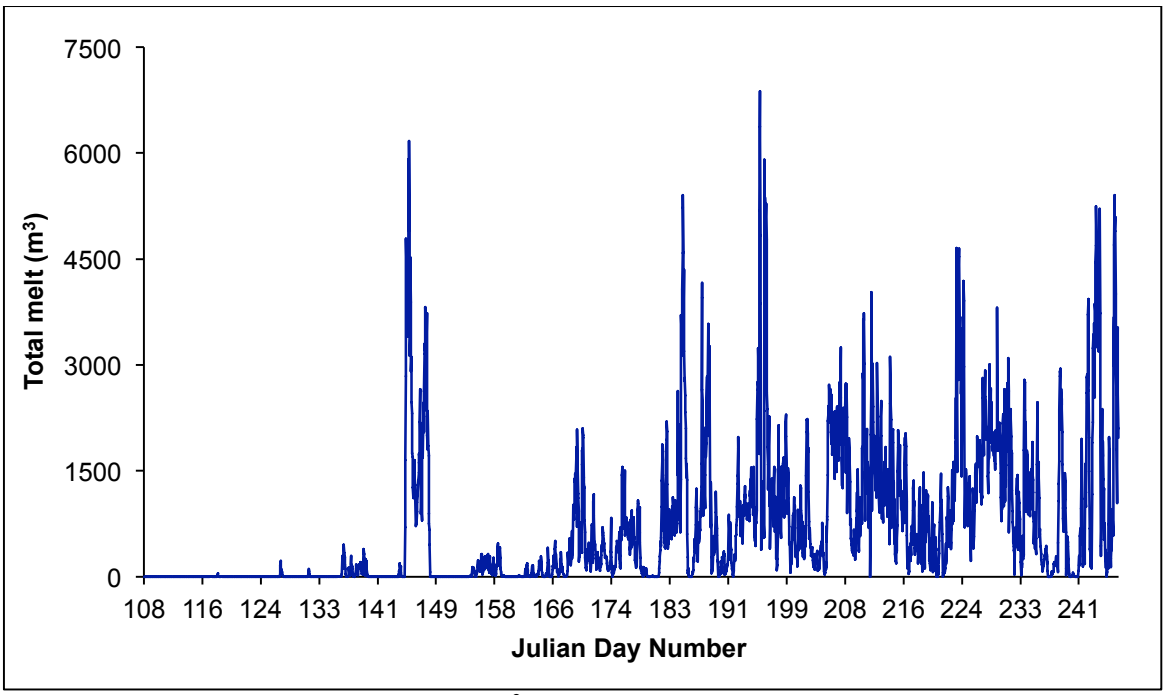

***Figure 5.3**. Total meltwater production (m^3) over the entire glacier surface predicted by the SEB model.*

5.2. Surface-Routing Model Sensitivity and Outputs

In addition to meltwater (Figure 5.3), the SROUT model also deals with rainfall arriving on Storglaciären (Figure 4.8). This model produces moulin input hydrographs. Unfortunately, there was lacking empirical data for extensive sensitivity tests varying, for example, snow density and snow porosity, like in Willis *et al.* (2002). Thus, only qualitative comparisons can be made against former suggestions that 15% water likely runs directly off at the terminus (e.g., Seaberg *et al.*, 1988; Kohler, 1992).

5.2.1. Sensitivity to Moulin Radius

In the model used for HGd'A (Arnold *et al.*, 1998), the SROUT model occasionally required moulin radiuses adjusting to allow accurate representations of water capture by moulins, since sometimes supraglacial streams would flow directly past moulins instead of being captured by them, as happens in reality (N.S. Arnold, personal communication). This largely results from surface-DEM resolution, preventing recognition of subtle topographic changes altering flow direction near moulins. Moulin radius is initially set at 1, meaning each moulin occupies an entire $20m^2$ grid cell. If a greater radius is used, cell size is multiplied by the number; the model was only tested using three cell radiuses (1, 2 and 3) since radiuses >3 grossly misrepresent reality. The aim was investigating the impact this has on total water capture by moulins versus runoff.

It was found there was little impact on the water quantity captured by the vast majority of moulins (Table 5.2). Most moulins gain more (~15–50%) water with moulin-radius increases. Largest changes are for moulins 5, U12 and L1. These mainly lie towards Storglaciären's edges (5 to the north, U12 and L1 to the south; cf. Figure 4.13). Decreased capture by moulin L1 is compensated for by increased capture by U12, since a stream that for lower radiuses would have flowed past moulin U12 downglacier to L1 is captured by U12's higher radius. This parallels field observations and previous research indicating more water flowing into moulins above the riegel than further downglacier. Increased capture by moulin 5 (Figure 5.4) was believed to be more realistic since this moulin captures water that would otherwise have flowed off Storglaciären's edge, yet no major ice-marginal stream is observed here (cf. Figure 3.1).

Table 5.2. *Water quantity (values in $m^3 s^{-1}$) captured by moulins on the glacier surface for differing moulin radiuses (see Figure 4.13 for locations on the glacier surface).*

	Moulin number	LN1	F5	F2	4	5	U11	U5	U9	U4	10	U1	12	U8	U2	U7
Cell radius	1 (20m)	45.26	24.94	8.11	1.45	3.36	2.60	2.86	0.87	6.10	10.08	5.83	2.31	1.75	9.58	19.55
	2 (40m)	57.71	15.89	9.66	2.53	7.39	5.38	4.00	1.47	14.67	1.47	5.83	3.99	3.43	15.55	22.00
	3 (60m)	75.34	26.13	15.75	3.63	111.1	6.50	5.40	3.10	18.13	1.47	10.10	3.99	4.81	12.35	27.43

	Moulin number	U12	L1	L3	L2	20	F3	22	23	24	F4	F1	27	28	Runoff
Cell radius	1 (20m)	3.14	156.77	12.01	45.01	19.05	8.22	5.87	2.52	33.88	22.28	332.92	425.41	44.79	542.11
	2 (40m)	52.10	93.02	43.59	28.70	21.50	5.18	16.39	12.89	35.62	27.62	324.33	436.71	57.76	472.73
	3 (60m)	100.29	27.34	33.14	35.98	30.93	4.95	21.80	17.38	43.65	29.21	317.63	439.04	66.91	306.02

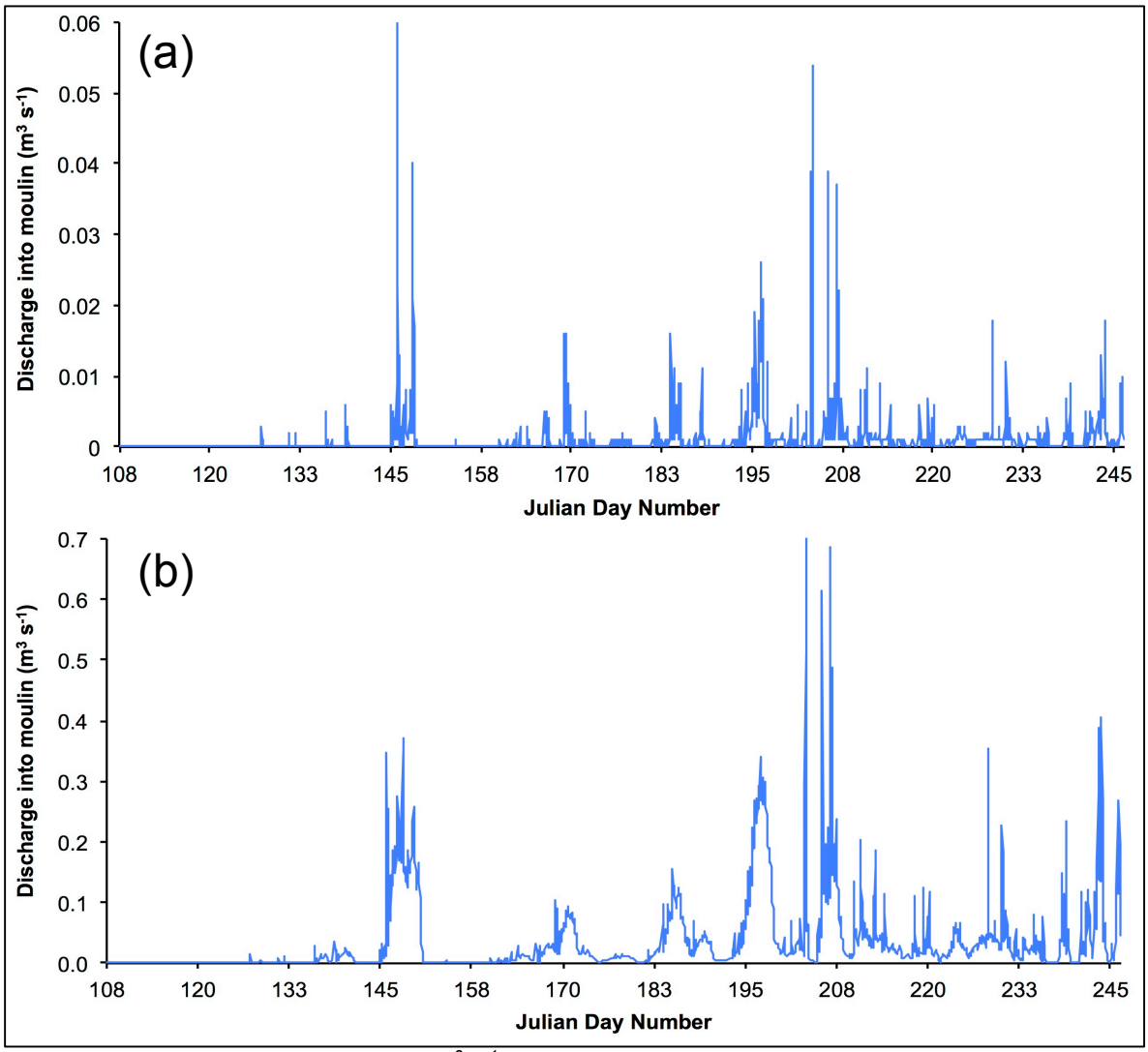

***Figure 5.4**. Comparison of discharge (m^3 s^{-1}) into moulin 5 (cf. Figure 4.13) over the entire model run when cell radius was set to 1 (a) and 3 (b). Note the differing y-axis scales.*

The net effect of increasing moulin radius to 3 was to decrease total runoff at Storglaciären's edges. Again, this is believed to represent best observations in 2012 and prior summers: previous research (e.g., Seaberg *et al.*, 1988; Kohler, 1992) suggested runoff as ~15% of total water flowing across Storglaciären's surface; best match for this is reproduced using moulin radius of 3 (Figure 5.5); only 2% difference existed between modelled runoff and this value.

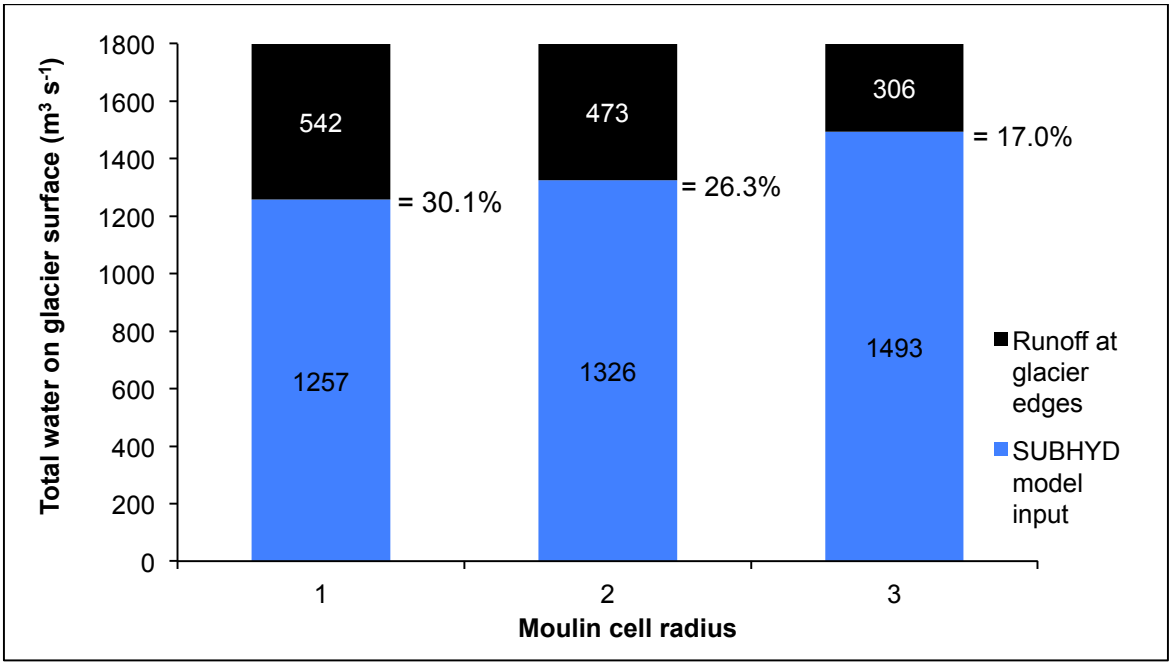

***Figure 5.5**. Comparison of total water fed into the SUBHYD model (i.e., being fed into moulins) compared with runoff at the glacier edges for differing moulin cell radiuses. Numbers within bars are the value they represent and percentages indicate percentage runoff at edges compared to the total water volume.*

5.2.2. Modelled Moulin Input Hydrographs

Using a moulin radius of 3, hourly input hydrographs are produced for every moulin for the model run. Figure 5.6 shows sample input hydrographs for moulins progressively further downglacier. Hydrographs depend upon total water within moulins' watersheds, the watersheds' size and the presence of snow, delaying travel times. Understandably, little water is initially fed into moulins because of low temperatures/precipitation. Strong correlation exists between discharges for different moulins, with inflow peaks corresponding well, due to similar melt across Storglaciären. Towards the end of the melt season, moulins still display diurnal variation in inputs, with higher daytime inputs, but some inflow still occurs at night. Moulin 27 displays consistently high input discharges, reflecting snow's presence here for the model run's duration; this delays runoff, with discharge fed into the moulin at nighttime. The effect of a moulin's catchment size on discharge is seen when examining hydrographs for moulins LN1 (Figure 5.6(f)) and 27 (Figure 5.6(a)): with large catchments, they receive much higher water quantities than moulins with smaller catchments, such as U4 (Figure 5.6(c)), above the riegel, and L3 (Figure 5.6(e)), since much of their melt is intercepted by moulins further upglacier.

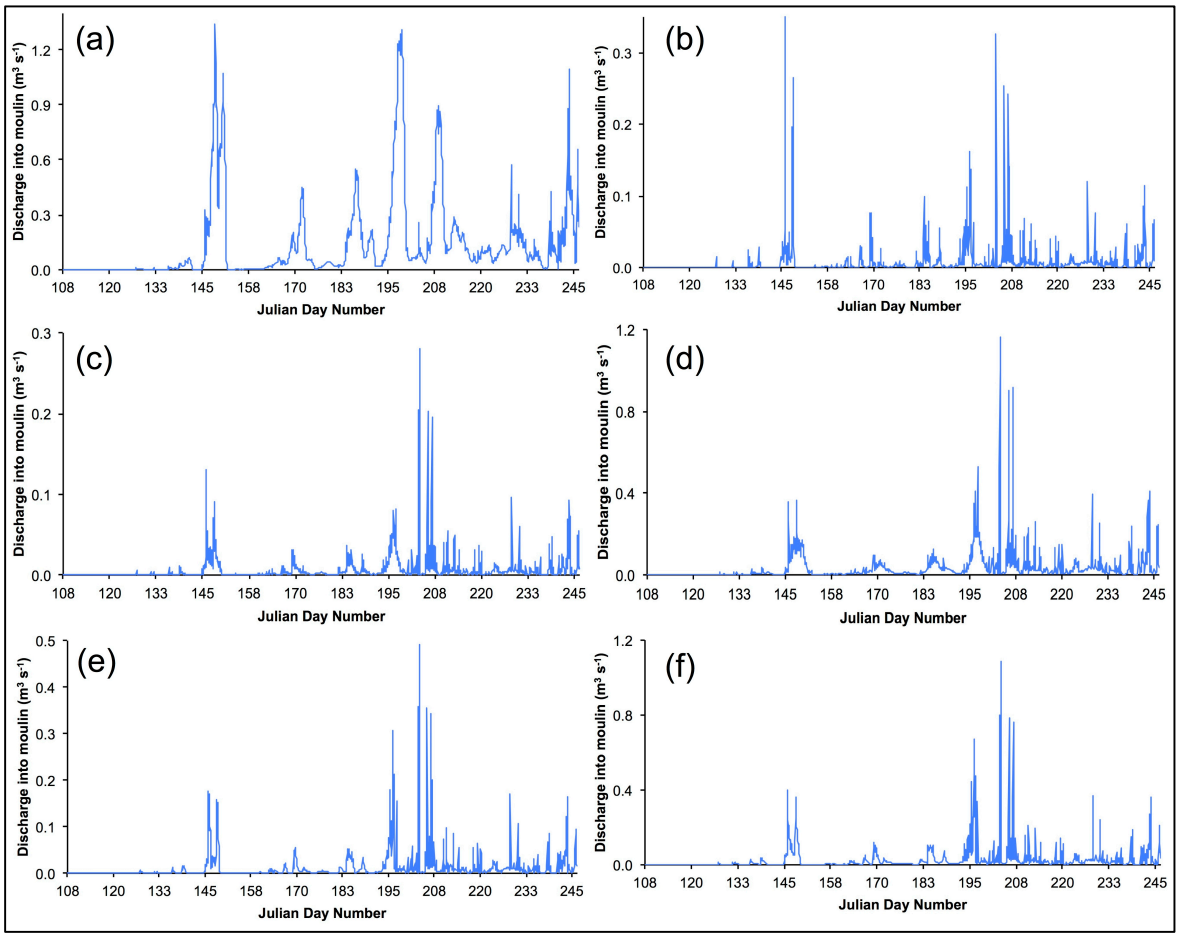

Figure 5.6. *Moulin input hydrographs for the entire model run for moulins progressively further downglacier: (a) moulin 27, towards the upper end of the overdeepening, (b) moulin 22, south of the overdeepening, (c) moulin U4, above the riegel, (d) moulin U12, on the southern side of the riegel, (e) moulin L3, downglacier of the riegel, on the southern side and (f) moulin LN1, close to the terminus on the northern side. For moulin locations on the glacier, see Figure 4.13.*

5.3. Subglacial-Hydrology Model Sensitivity and Outputs

Hydrographs are fed to the SUBHYD model. Given CSAs were derived from tracing results (Section 4.4.2.2), only one model parameter could be used as a sensitivity test: conduit roughness (n). There is much debate over roughness in glaciology (e.g., Gulley *et al.*, 2012a, 2013) and various values were used in previous models (Arnold *et al.*, 1998; Banwell *et al.*, 2013). In this study, several values were tested and compared with proglacial discharge and water flow-routing times from tracing experiments to determine best representation of Storglaciären's conduit roughness. Section 5.3.2 presents modelled subglacial P_w for the run with roughness best matching observations.

5.3.1. Sensitivity to Conduit Roughness

5.3.1.1. Modelled Proglacial Discharge: Sydjåkk and Centerjåkk

Five tests were conducted using five roughnesses: in the first four, uniform conduit roughness was adopted, and in the fifth, conduit roughness was linearly related to conduit CSA, following Arnold *et al.* (1998). Given only one conduit supplies Nordjåkk's outflow (cf. Figure 4.13), this conduit's roughness was tested independently of others; Section 5.3.1.2 presents these results.

Figure 5.7 presents modelled and observed discharges where $n = 0.150$ for all conduits, Figure 5.8 where $n = 0.125$, Figure 5.9 where $n = 0.100$, Figure 5.10 where $n = 0.050$ and Figure 5.11 where n was linearly related to CSA. n values > 0.150 and < 0.050 were believed to unrealistically represent conduit roughness (Banwell, 2012). Table 5.3 compares modelled results with observations.

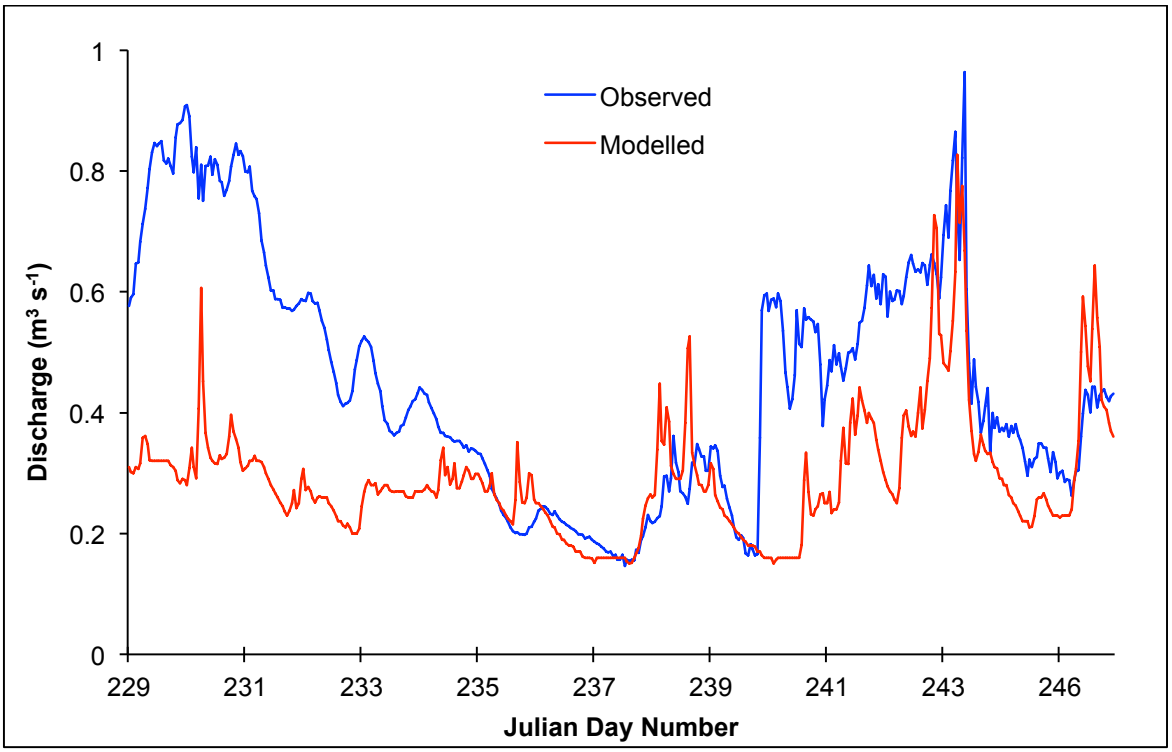

***Figure 5.7**. A comparison of modelled versus observed discharge for Sydjåkk and Centerjåkk where $n = 0.150$ for all conduits.*

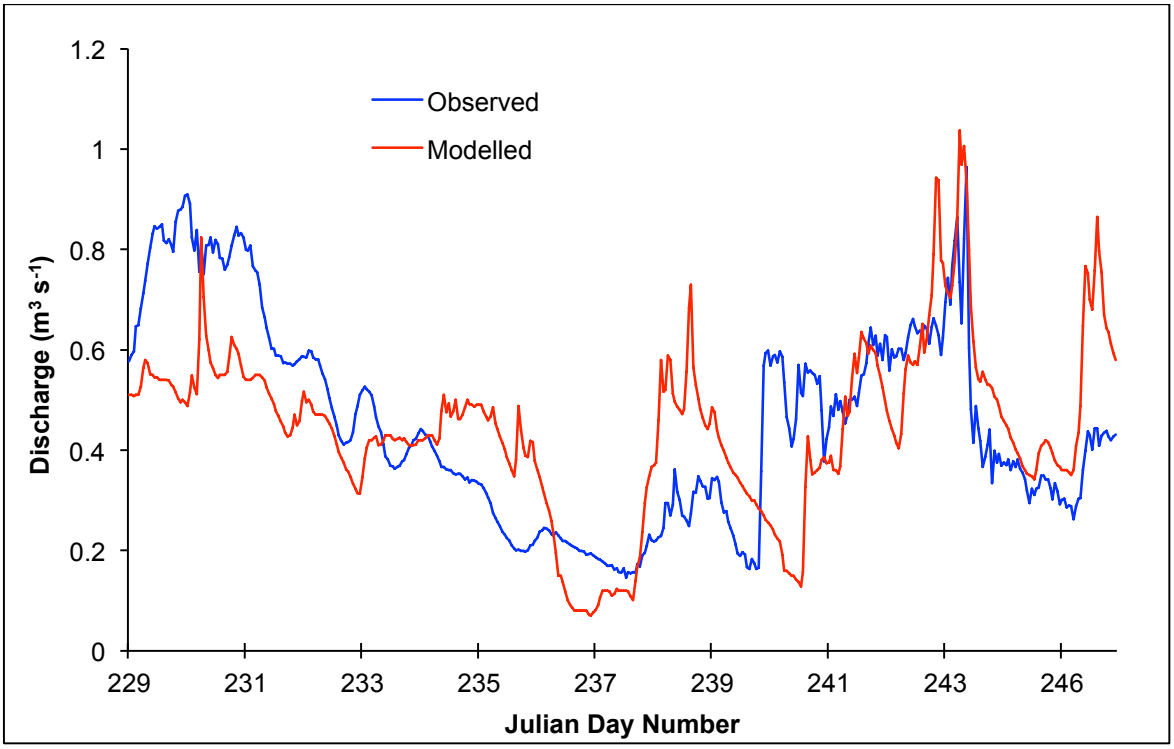

***Figure 5.8**. A comparison of modelled versus observed discharge for Sydjåkk and Centerjåkk where $n = 0.125$ for all conduits.*

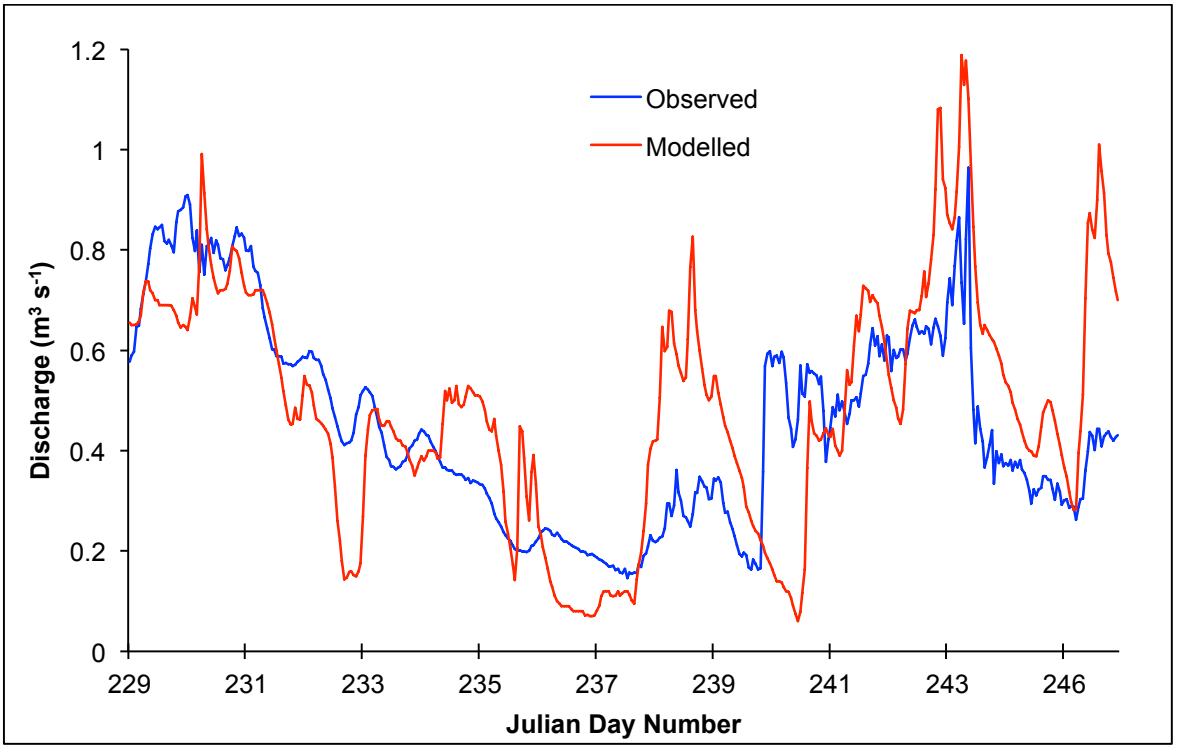

***Figure 5.9**. A comparison of modelled versus observed discharge for Sydjåkk and Centerjåkk where $n = 0.100$ for all conduits.*

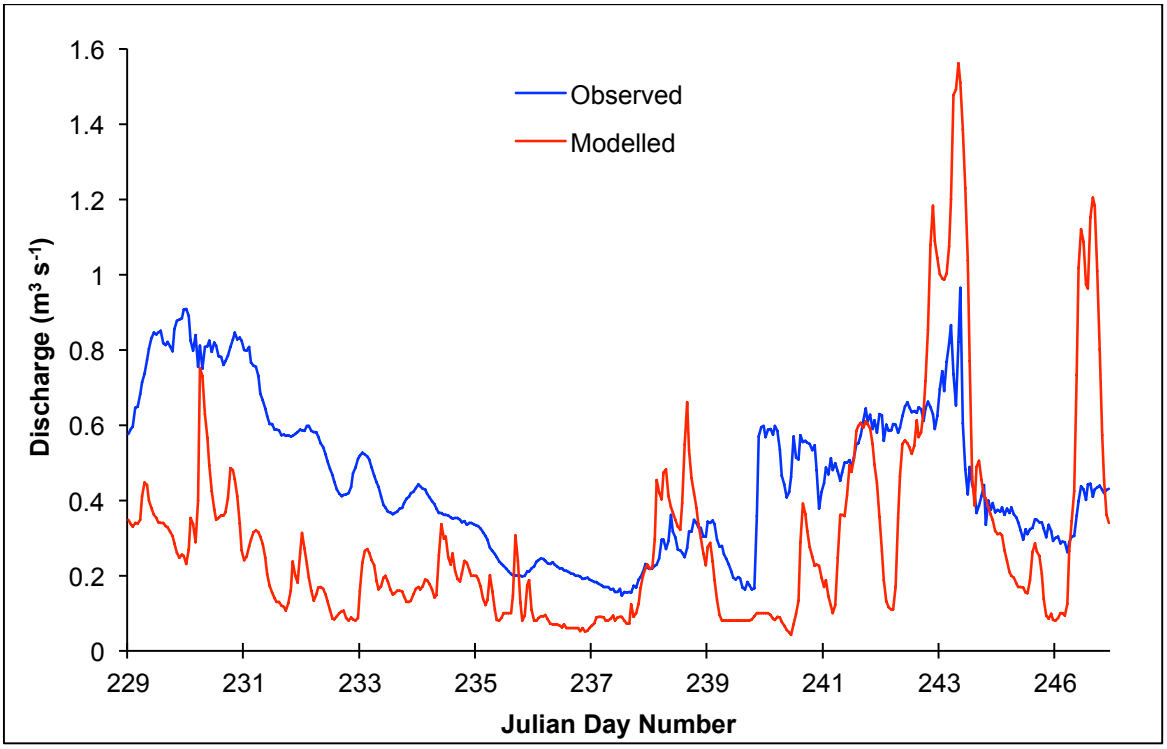

***Figure 5.10**. A comparison of modelled versus observed discharge for Sydjåkk and Centerjåkk where $n = 0.050$ for all conduits.*

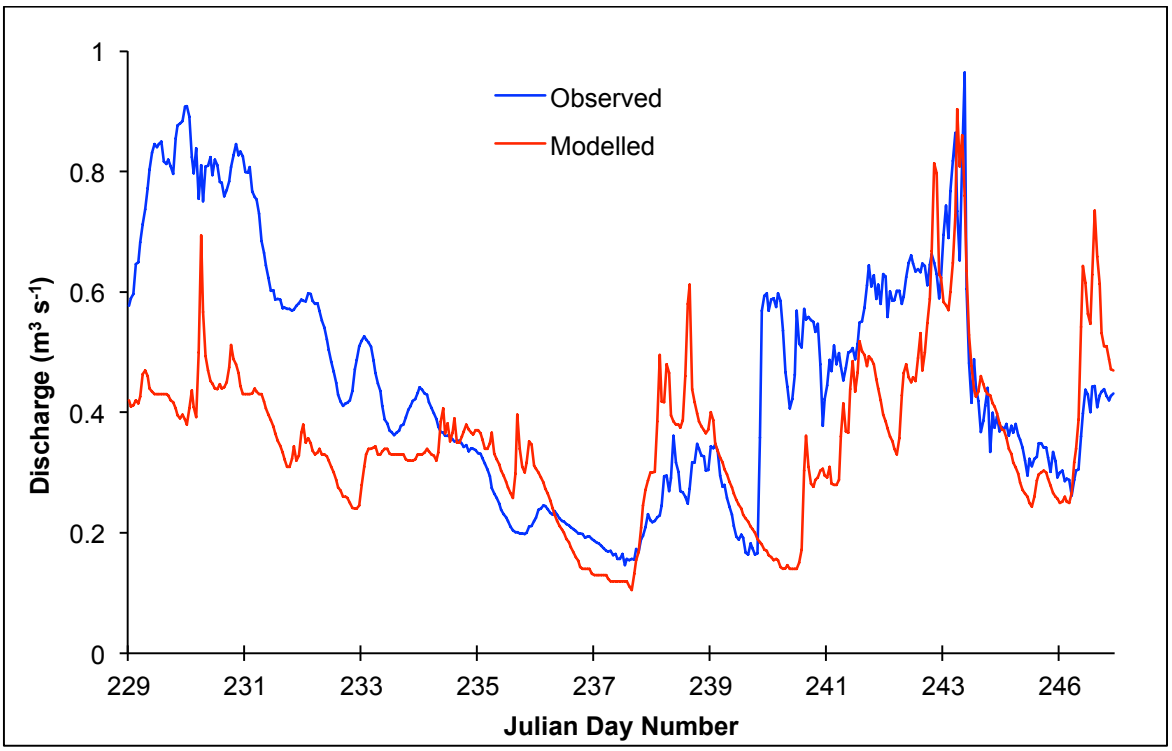

***Figure 5.11**. A comparison of modelled versus observed discharge for Sydjåkk and Centerjåkk where n was linearly related to conduit cross-sectional area.*

***Table 5.3**. Summary of statistical performance for model runs using different values of n for the conduits ultimately producing outflow at Sydjåkk and Centerjåkk.*

Value of conduit roughness (n)	Nash-Sutcliffe Coefficient	R^2	RMSE ($m^3 s^{-1}$)	Modelled Minus Observed Proglacial Discharge ($m^3 s^{-1}$)
0.050	-1.300	0.182	0.304	-65.751
0.100	0.107	0.417	0.189	13.212
0.125	0.265	0.337	0.172	-7.594
0.150	-0.440	0.211	0.241	-70.263
Linear relation to CSA	0.060	0.312	0.195	-44.396

The empirical data show Centerjåkk/Sydjåkk respond to precipitation peaks (including on JDs 230, 238, 240 and 243), with short lags since events, suggesting rapid water routing through the system.

Table 5.3 indicates that best performance of observed versus modelled data was for uniform roughnesses of $n = 0.125$: highest Nash-Sutcliffe value, lowest RMSE, and lowest discrepancy between modelled and observed discharge were obtained here. R^2 was also second highest. $n = 0.100$ provided second best performance, and had the highest R^2, with linear relation of n to CSA only slightly underperforming. Poorest performance was where $n = 0.050$.

Where $n = 0.150$ (Figure 5.7), modelled discharges underestimate observations; this is especially true for the start of the observations, where modelled values are ~0.5 $m^3 s^{-1}$ lower than observations. There are two likely explanations for this: first, during this time, inflow into the subglacial drainage system was too rapid for conduits to evacuate water, so water backed up in the system, was lost onto the glacier surface (from overflowing moulins) and thus from the SUBHYD model; second, a large water quantity was not lost from the system, but instead it was routed through the system too slowly, arriving later. This is possible, especially since there is better match between observed and modelled data later: the water arriving later masked lower modelled flows then. Best match between modelled and observed discharges was for JDs 238 and 243–245.

Where $n = 0.125$, there is better match between modelled and observed discharges, however, overall insufficient discharge arrives at the GS; this could be for the same reasons as outlined for $n = 0.150$. The magnitude of the difference between modelled outputs and observations is less pronounced, however, suggesting lower overflow of moulins from inability of the drainage system to evacuate melt quickly enough. Similar patterns are seen for $n = 0.100$, however, high flows are overpredicted (by up to 0.5 $m^3 s^{-1}$) and low flows underpredicted (by 0.1–0.4 $m^3 s^{-1}$), such as on JD 233; this helps explain why this model run performs more poorly than where $n = 0.125$, even though R^2 is higher.

Where $n = 0.050$, peak (low) flows are overestimated (underestimated). This is likely because of too rapid runoff during high water inputs (due to faster flow with lower roughness). This water then does not arrive during lower flows, explaining their underestimation in modelled data. There is marked

underestimated discharge (by ~0.2–0.25 m^3 s^{-1}) early season. This could be because modelled discharge was routed too quickly prior to the beginning of the plotted discharge values shown here.

For all runs, modelled peaks on JD 230 are absent from observations. It is unclear whether these are due to high precipitation/temperatures. This could be due to inability of empirical measurements to record accurately high stream discharges, especially if not using a stream weir, true in this study (Seaberg *et al.*, 1988; Hock and Noetzli, 1997), so may not represent problems with modelling.

5.3.1.2. Modelled Proglacial Discharge: Nordjåkk

Sensitivity tests were conducted using four subglacial conduit roughnesses. Figure 5.12 presents results where $n = 0.125$, Figure 5.13 where $n = 0.100$, Figure 5.14 where $n = 0.075$ and Figure 5.15 where $n = 0.050$. Table 5.4 presents statistical performance.

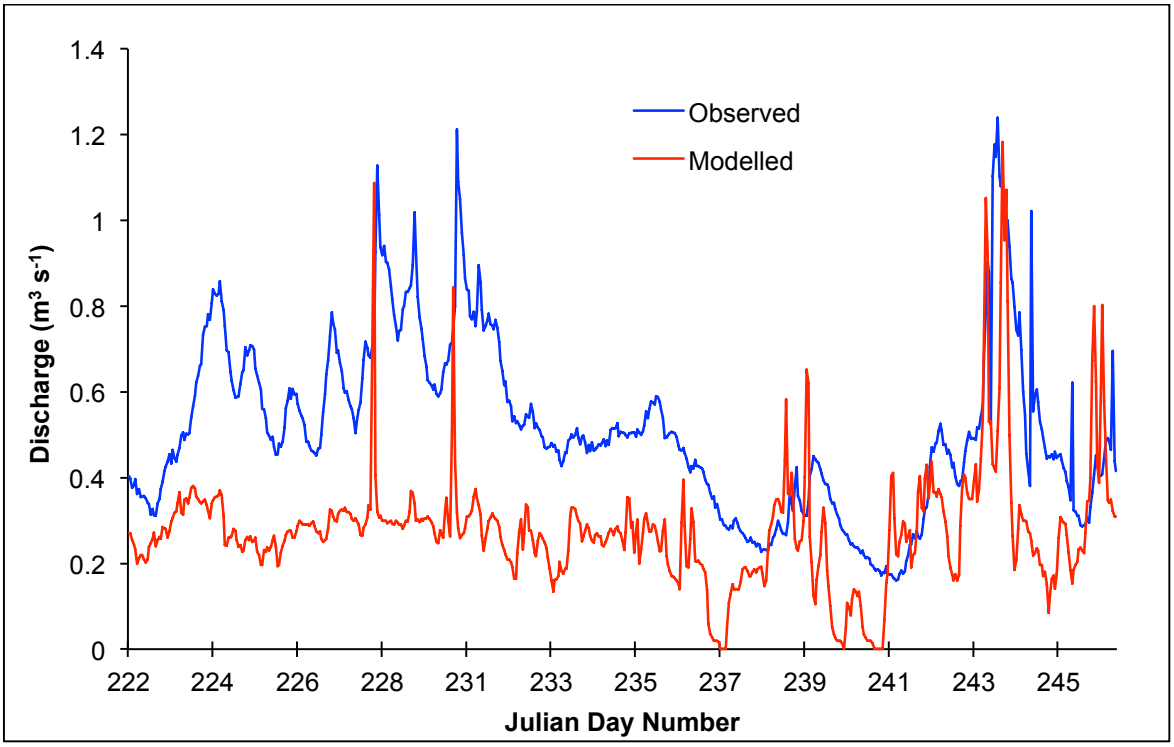

***Figure 5.12**. A comparison of modelled versus observed discharge for Nordjåkk where $n = 0.125$.*

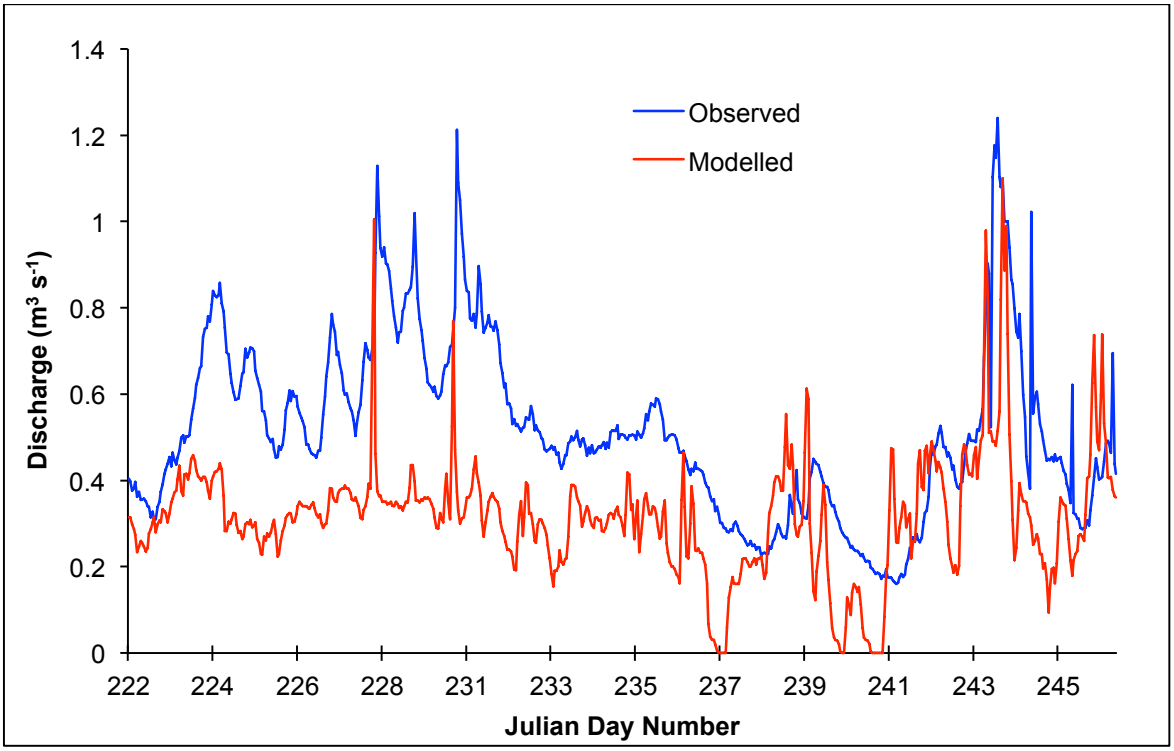

***Figure 5.13**. A comparison of modelled versus observed discharge for Nordjåkk where $n = 0.100$.*

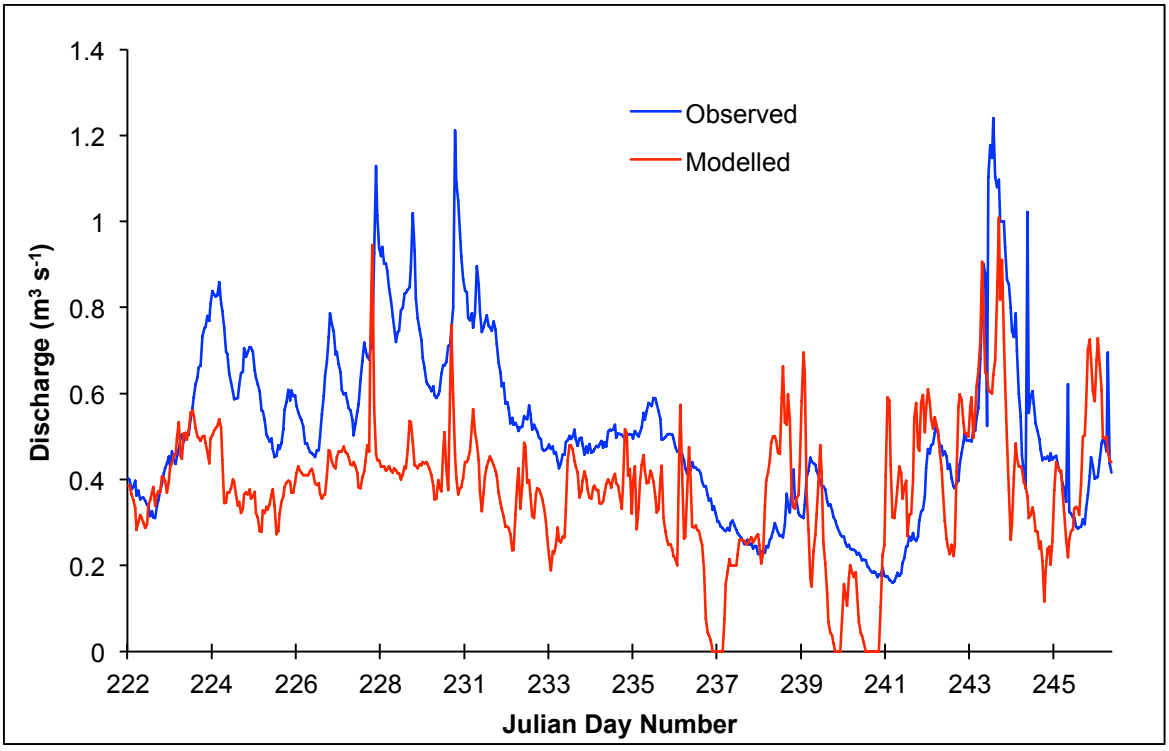

***Figure 5.14**. A comparison of modelled versus observed discharge for Nordjåkk where $n = 0.075$.*

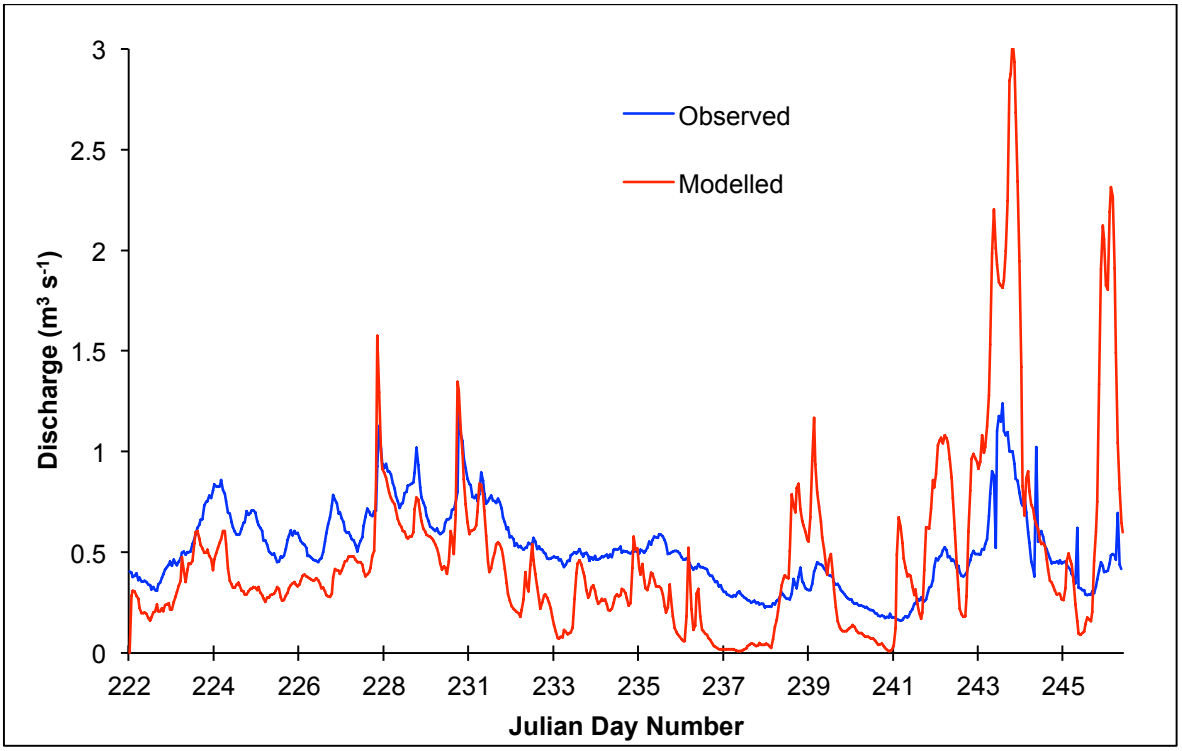

***Figure 5.15**. A comparison of modelled versus observed discharge for Nordjåkk where $n = 0.050$.*

***Table 5.4**. Summary of statistical performance for model runs using different values of n for the conduit producing outflow at Nordjåkk.*

Value of conduit roughness (n)	Nash-Sutcliffe Coefficient	R^2	RMSE ($m^3 s^{-1}$)	Modelled Minus Observed Proglacial Discharge ($m^3 s^{-1}$)
0.050	-2.929	0.265	0.402	-19.047
0.075	-0.277	0.231	0.230	-78.347
0.100	-0.780	0.223	0.271	-116.427
0.125	-1.235	0.199	0.304	-139.15

Nordjåkk discharge responds strongly to peaks in precipitation: for example, precipitation events on JDs 228, 230 and 244 produce pronounced peaks in observed discharge.

Table 5.4 indicates all model runs underestimated discharge. Best matches between observed and modelled data were where $n = 0.075$: this value generated the highest Nash-Sutcliffe value (though this was still slightly negative, indicating the mean of observed discharges is a better predictor than the model) and only a slightly poorer R^2 value than $n = 0.050$. $n = 0.075$ produced the lowest RMSE, however the discrepancy between observed and modelled discharge was better for $n = 0.050$ than for $n = 0.075$, but this is offset by the much lower Nash-Sutcliffe value. This likely results because where $n = 0.050$, two overpredicted peak flows on JDs 244 and 246 compensated for model underprediction elsewhere; these peaks are not as prominent where $n = 0.075$. This is reflected in the Nash-Sutcliffe value's tendency to be more influenced by peak flows rather than low ones (Krause *et al.*, 2005).

There are occasions when modelled data predict no flow whatsoever (JDs 237 and 241 in all runs), when observations suggested flow throughout nights; this may be because the model does not account for englacial storage.

Broadly, as n decreases, more modelled water arrives at the GS, not being lost from the SUBHYD model, which occurs with higher roughness values, explained in Section 5.3.1.1. There is also generally greater diurnal range in modelled discharge as n decreases: again, this is likely because, with higher values, some of the water during the day is lost onto the glacier surface and thus diurnal variations masked.

Even though the model run where $n = 0.075$ displayed best match for observed data, there is still some discrepancy. Towards the start of the model run, discharge is underestimated by ~0.1–0.15 $m^3 s^{-1}$. Section 6.2.2.1 outlines possible reasons behind this.

5.3.1.3. Modelled Subglacial Flow-routing Times

Modelled subglacial water-flow (moulin-to-terminus) routing times are compared with observed water-routing times from summer 2012 (supplemented with several 2013 observations). Observed travel times are times taken from injection to peak breakthrough; these are derived for all injections producing positive breakthroughs. For breakthroughs in both Centerjåkk and Sydjåkk, mean travel time was taken; there was close agreement between breakthrough times, so this was a fair approximation. For full details on dye-tracing experiments, see Williamson (2013). Sample BTCs from 2012 and 2013 are presented in Appendix II. To calculate modelled flow-routing times, the mean flow velocity for each conduit along which the tracer passed was calculated for the test duration (approximated with observed travel times); conduit lengths were used to generate travel times for each individual conduit; these were integrated to produce each test's total travel time. Given conduit flow velocities were not modelled for 2013 since the model was only run for 2012, modelled 2013 times were derived using mean flow velocities for each conduit over all of August 2012. Table 5.6 compares observed and modelled travel times for differing conduit roughnesses; Figure 5.16 graphs these data. Table 5.5 presents statistical performance for differing roughnesses.

Best matches between observed and modelled travel times were where $n = 0.125$ and poorest matches where $n = 0.050$, though Nash-Sutcliffe values are always negative and RMSE always high (>500 minutes). For most tests, modelled travel times are greater than observed travel times. Generally, higher conduit roughnesses increase travel times, since velocity in rough channels is reduced, true in any hydrological system. It may then be expected that values where $n = 0.050$ would best represent the system since the aim would be producing more rapid routing, aligning observed and modelled times. However, this is offset by the fact that for numerous tests where $n = 0.125$, there was very close match between modelled and observed data (e.g., tests 2012-14 and 2012-17) and $n = 0.125$ was the only run producing *some* underestimated modelled times (e.g., tests 2012-3 and

2012-16). Thus, it seems that $n = 0.125$ best represents subglacial conduit roughness based on water flow-routing times.

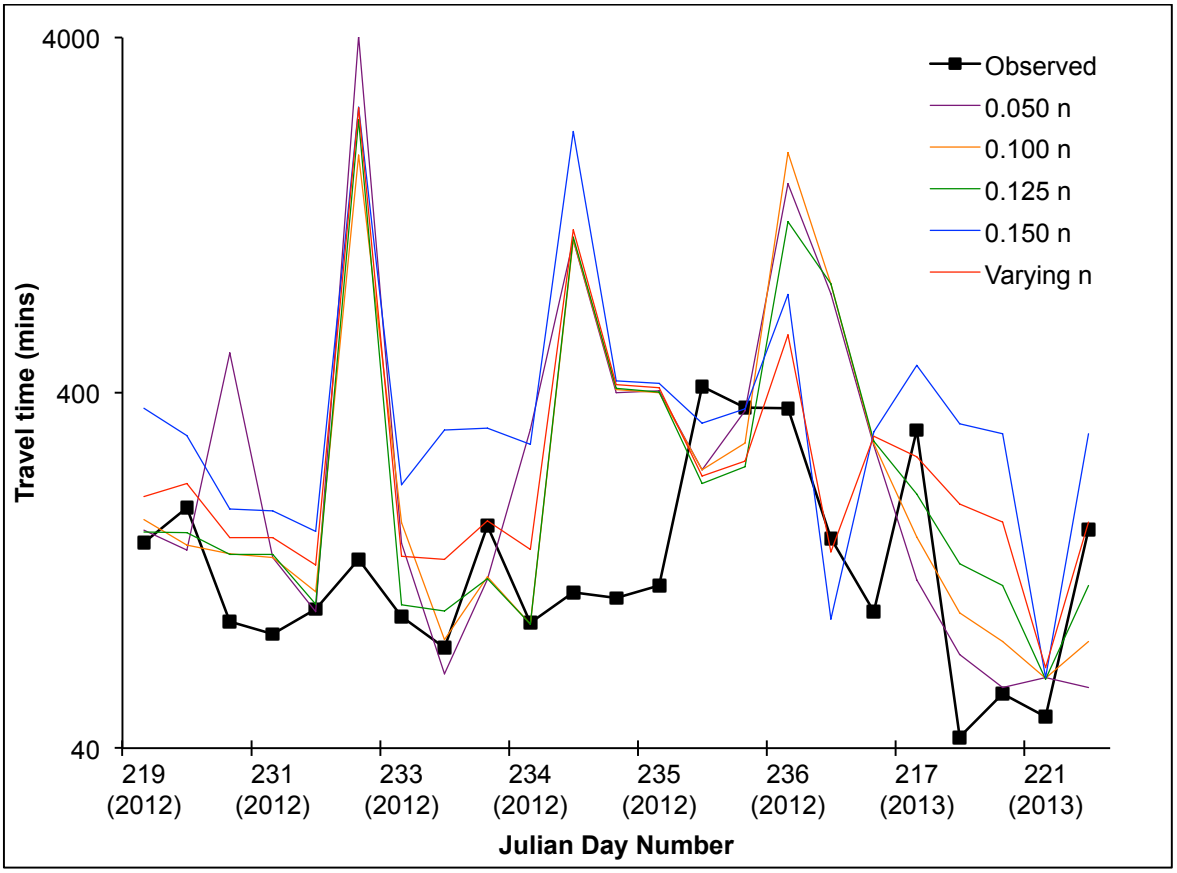

***Figure 5.16**. Comparison of flow-routing times for different values of conduit roughness used in model runs (from Table 5.6) with observed travel times. Black squares on the observed flow routing show the specific times of individual tracing experiments. Note that the y-axis is logarithmic to account for the high variation in travel times recorded in these data.*

***Table 5.5**. Summary of the statistical performance of differing conduit roughnesses when compared with subglacial flow routing times derived from tracing experiments.*

Conduit roughness (n)	RMSE (min)
0.050	895.66
0.100	551.78
0.125	564.30
0.150	688.00
Linear relation to CSA	560.00

The fact that comparison with both these data and proglacial-discharge data yielded $n = 0.125$ as the most-likely subglacial conduit roughness adds confidence to this conclusion.

***Table 5.6**. Summary of observed versus modelled tracing results. For injection site locations, see Figure 4.16. In the emergence column, C = Centerjåkk, N = Nordjåkk, S = Sydjåkk. Tracer RWT = Rhodamine WT dye.*

Test ID	Julian Day Number	Injection Time	Injection Site	Tracer	Emergence	Observed travel time (min)	Modelled travel time (min) with conduit roughness (n):				
							0.050	0.100	0.125	0.150	Linear relation to CSA
2012-1	219	11:40	U2	RWT	C & S	152	164	176	162	363	205
2012-3	222	12:30	U2	RWT	C & S	190	144	149	161	304	222
2012-9	231	11:22	U4	RWT	C & S	91	518	141	140	188	156
2012-10	231	14:56	U4	RWT	C & S	84	138	138	140	186	157
2012-11	232	12:36	U7	RWT	C & S	99	97	110	102	163	131
2012-13	233	10:29	L1	RWT	C & S	136	4034	1864	2348	2542	2532
2012-14	233	14:20	U4	RWT	C & S	94	151	172	101	221	139
2012-15	233	15:58	U8	RWT	C & S	77	65	81	97	315	136
2012-16	234	11:20	U2	RWT	C & S	169	119	122	120	318	174
2012-17	234	15:43	U4	RWT	C & S	90	315	89	89	287	145
2012-18	235	10:34	U9	RWT	C & S	110	1077	1078	1097	2177	1149
2012-19	235	13:13	L1	RWT	C & S	106	400	409	412	432	422
2012-20	235	16:30	L2	RWT	C & S	115	405	400	402	425	413
2012-21	236	11:10	U7	RWT	C & S	417	243	243	222	329	233
2012-22	236	13:53	U7	RWT	C & S	364	356	289	247	360	257
2012-23	236	20:40	U7	RWT	C & S	361	1553	1896	1214	757	582
2012-25	237	14:15	L3	RWT	C & S	156	759	810	810	92	143
2013-1	217	11:23	L3	T3(M)	S	97	284	288	292	311	302
2013-2	217	11:25	F2	RWT	C & S	315	119	157	208	478	264
2013-3	217	11:07	U2	T11(free)	C & S	43	73	96	132	328	195
2013-4	217	10:58	U1	Uranine	C & S	57	59	80	115	307	173
2013-5	221	10:36	LN1	T3(free)	N	49	63	63	63	63	67
2013-6	221	10:05	U1	T4(free)	C & S	145	59	80	115	307	173

5.3.2. Modelled Subglacial Water Pressure

5.3.2.1. Data for the Entire Model Run

Since best matches between modelled and observed (proglacial discharge and water flow-routing) data were achieved where $n = 0.125$, and given lack of direct borehole P_w data to compare against modelled results, P_w results where $n = 0.125$ are presented. Analysis of all runs' borehole P_w data indicated where $n < 0.100$, predicted P_w was lower than expected from previous studies (Section 3.4.2).

P_w data are divided fourfold:

- P_w close to the 'lower moulins' (Figure 5.17),
- P_w close to the riegel separating the lower and upper ablation areas, above which lies the main moulin field (Figure 5.18),
- P_w close to the terminus (Figure 5.19), and
- P_w within the overdeepening (Figures 5.20 and 5.21).

To compare P_w beneath differing ice thicknesses, P_w is expressed as a fraction of P_i.

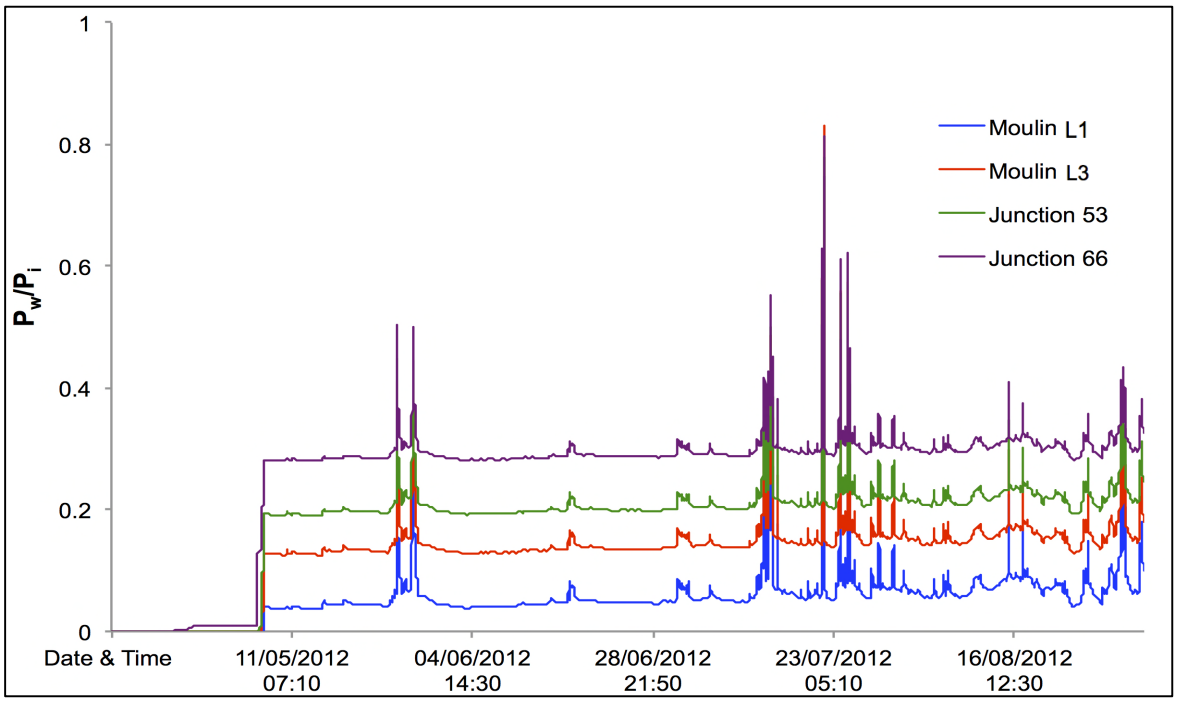

***Figure 5.17**. Subglacial water pressures for junctions and moulins close to the lower moulins.*

Figure 5.17 shows low subglacial P_w, never reaching P_i. This is unsurprising given the moulins feeding this branch of the drainage system receive low overall inflow (Table 5.2). Expectedly, the P_w increases progressively further downstream this branch of the drainage system, as the system becomes more filled with water and ice thickness increases towards the centreline (cf. Figures 3.2 and 4.13). There

are several P_w peaks, especially close to the start of the model run and ~23/07/2012 (JD 205). That these peaks were observed simultaneously adds confidence. There appears to be only low-amplitude diurnal fluctuations, with P_w instead remaining relatively consistent, probably because conduits beneath thin ice (Figure 3.2) were rarely water-filled.

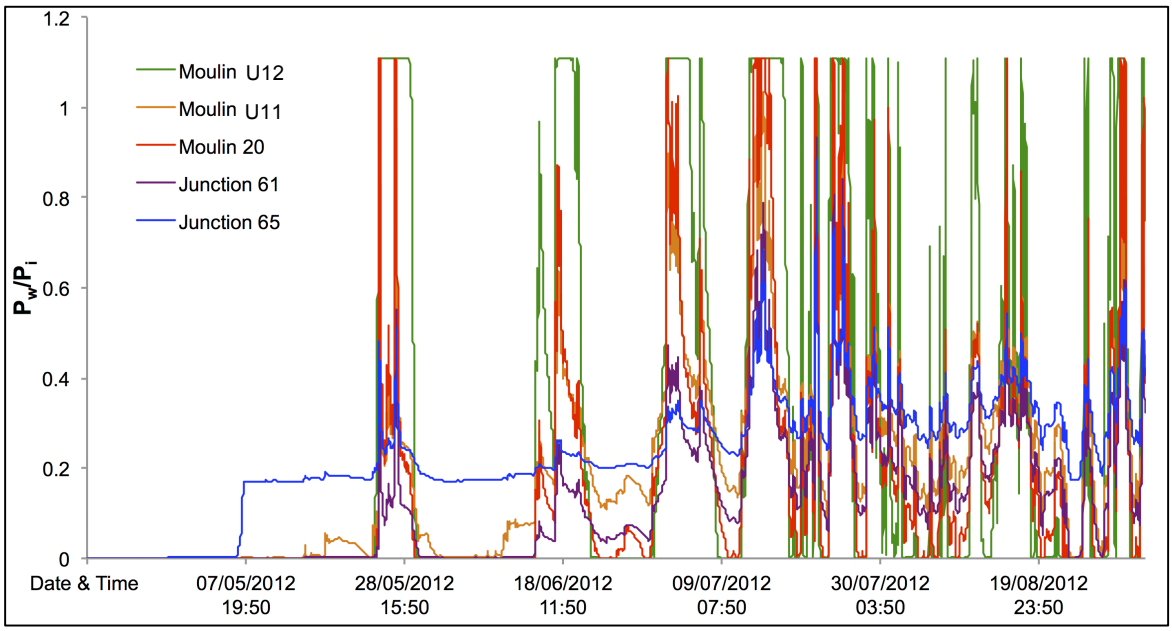

***Figure 5.18**. Subglacial water pressures for junctions and moulins close to the riegel.*

P_w close to the riegel displays much higher-amplitude diurnal fluctuation than for the lower moulins. Junctions 65 and 61 display unusual patterns since they experience P_w nearly always 20–40% P_i, with several minor spikes in early/mid-July. This is likely because these junctions lie beneath comparatively thinner ice than the other moulins displayed here (cf. Figure 3.2). Other moulins' P_w display striking resemblance: initially low P_w since there was no water within channels (due to no melt; cf. Figure 5.3), followed by 'spikes' at the end of May, with greater diurnal variations from P_w at $\sim P_a$ to P_i from ~10/07/2012, a response to diurnally varying water in well established channels.

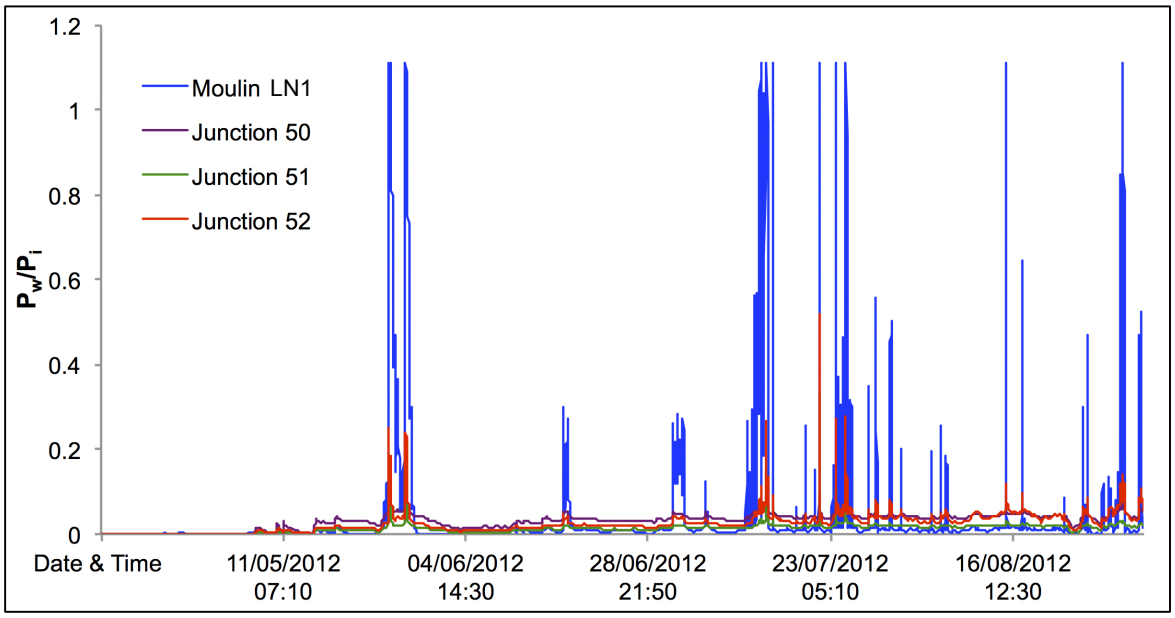

***Figure 5.19**. Subglacial water pressures for junctions and moulins close to the terminus.*

P_w close to the terminus is much lower, likely since conduits here can expand rapidly due to large water quantities flowing through the system, thus enlarging conduits, and also due to overlay by thin ice (cf. Figure 3.2), presenting low creep closure. Normally, P_w is not >~10% P_i. The exception is moulin LN1, experiencing numerous P_w 'spikes', likely due to extreme melting/rainfall events (e.g., Vieli *et al.*, 2004) and because the conduit here cannot cope with such water volumes (due to high melting within the moulin's catchment), so water is lost onto the glacier surface when $P_w > P_i$.

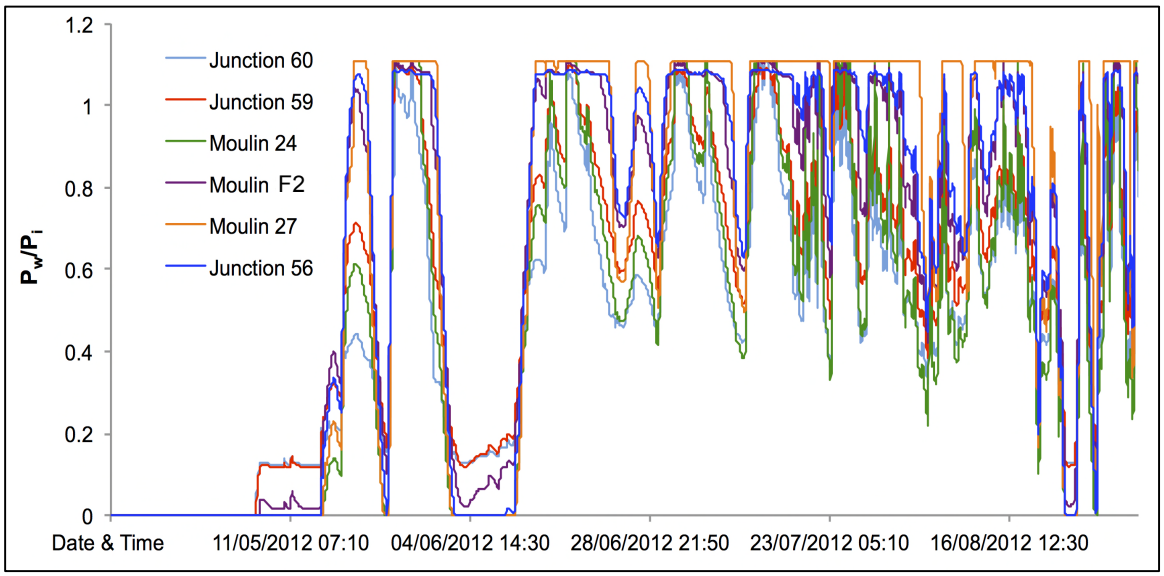

***Figure 5.20**. Subglacial water pressures for junctions and moulins within the overdeepened area.*

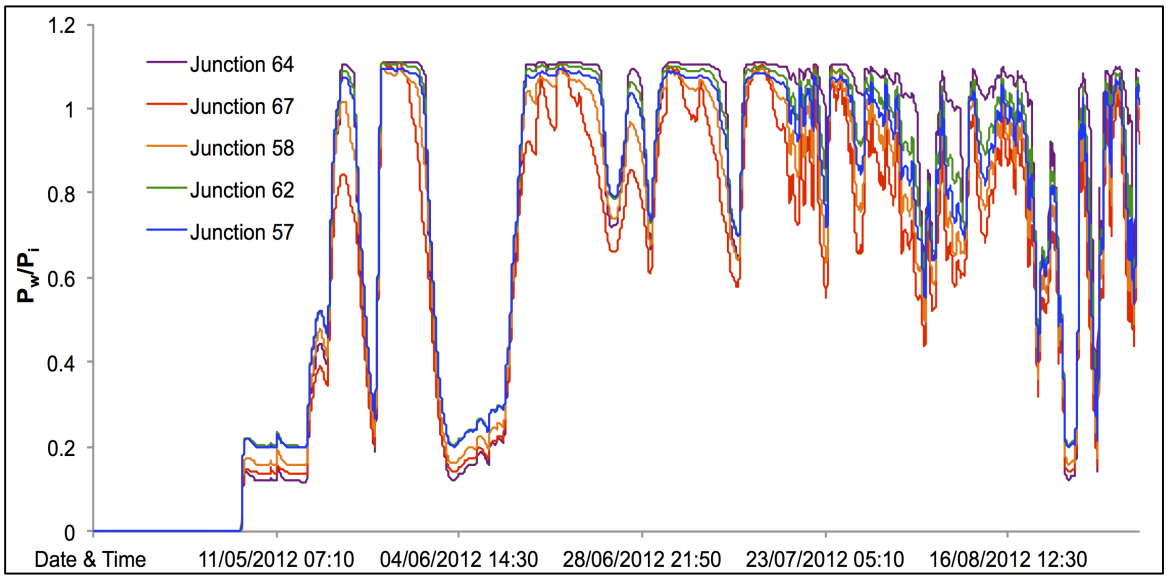

***Figure 5.21**. Subglacial water pressures for junctions and moulins within the overdeepened area.*

Within the overdeepening, P_w is consistently high, except for the beginning of the model run, when there was no water input to channels. P_w is often consistently $> P_i$, with some low-amplitude fluctuations at ~60–110% P_i. Moulin 27 displays consistently high P_w for the majority of the melt season. This follows expectations since the overdeepening is overlain by thick ice, causing high creep closure, with the system unable to expand quickly enough from enlargement by flowing meltwater. This means water is often lost from the SUBHYD model onto Storglaciären's surface. There are periods in early June and mid-August when P_w is lower than other periods; these follow episodes of consistently high water inputs. The likely explanation is that conduits enlarged with these meltwater inputs; it then took a short while for the system to readjust when meltwater input was lower, so overall P_w declined.

5.3.2.2. Seasonal Evolution

Figures 5.22 and 5.23 display mean P_w over summer and from the onset of continuous melting, overlain onto ice-thickness maps. Both Figures show expected intra-glacier variation: P_w is highest beneath thick ice; there is striking resemblance of P_w to ice thickness: even within very similar areas and branches of the system, P_w is always higher where ice is thicker. Mean summer P_w is lower than P_w from the period of continuous melting (note different scales on Figures). This likely results from much higher water inputs during the later period, with the system generally unable to expand quickly enough.

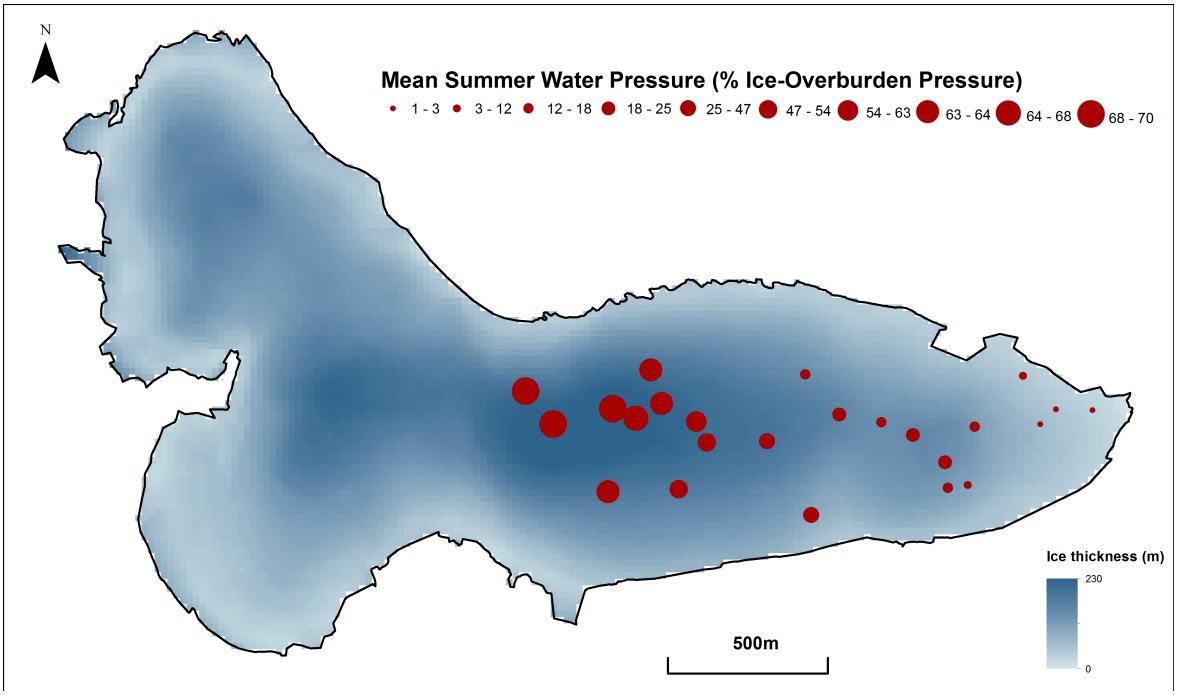

***Figure 5.22**. Mean summer subglacial water pressure (as a % of ice-overburden pressure) overlain onto a map of ice thickness.*

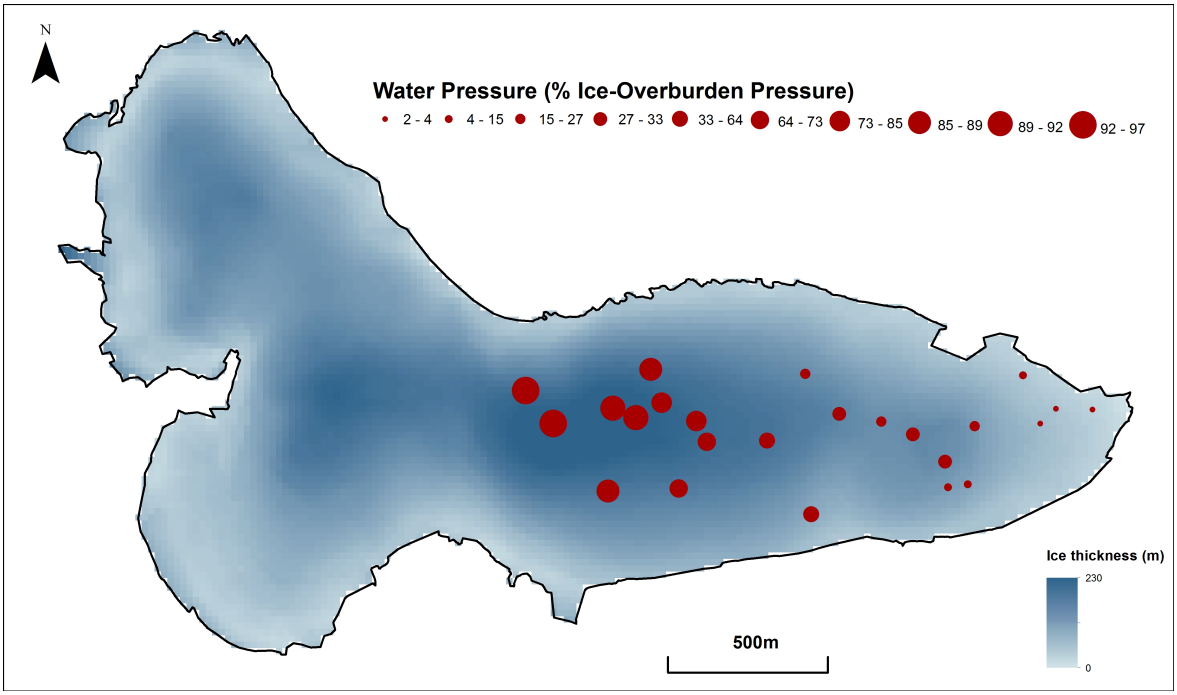

***Figure 5.23**. Late-season (from JD 180 to the end of the model run) subglacial water pressure (as a % of ice-overburden pressure) overlain onto a map of ice thickness.*

6. Discussion

6.1. Overall Model Performance

Broadly, models successfully replicated empirical observations. Several inferences about glacier hydrology are possible from the results.

6.1.1. Surface-energy-balance Model

The SEB model replicated well the observed surface lowering at the AWS (underestimated by 0.0137 $m^3\ h^{-1}$) and total ablation (~4% difference) with the 1.0°C threshold for solid precipitation. Yet, it underpredicted total ablation, similar to previous studies, where ~10% underestimation was seen (e.g., Hock and Holmgren, 2005). The model was especially sensitive to the threshold for solid precipitation, less so to snow-density variations. It was important to model accurately whether precipitation falls as snow/rain since precipitation is fundamental for proglacial streams' discharge (Gravelle, 2013). Performance was as good as other melt models applied here (e.g., Hock and Holmgren, 1996, 2005; Hock, 2005), capturing seasonal and diurnal melt variations, though previous models were tested against more data (including snowline retreat).

6.1.2. Surface-routing Model

With empirical data unavailable to test the model, crude comparison was made with studies suggesting direct runoff over Storglaciären (i.e., that not routed into the englacial/subglacial system) is ~15% the total; this expectation was replicated (with ~2% difference) with moulin cell radiuses of 3. The model produced realistic moulin input hydrographs. Specifically, the importance of moulins' catchment sizes for their hydrographs was determined and the importance of snow in delaying runoff highlighted.

6.1.3. Subglacial-hydrology Model

The SUBHYD model was comprehensively evaluated using hourly proglacial discharge and ~25 tracing experiments. This study advances Arnold *et al.*'s (1998) since in their study, modelled flow-routing times were compared with those from a different year (Nienow *et al.*, 1996); this study compared modelled and observed values for the same season. The model performed best with high conduit roughness ($n = 0.125$) for the system feeding Centerjåkk/Sydjåkk and $n = 0.075$ for the conduit feeding Nordjåkk. These roughnesses may initially seem large, especially compared with $n = 0.050$ used for the 'Paakitsoq region' of the GrIS (Banwell *et al.*, 2013). Yet, the need for high n, roughly in line with a 'boulder-strewn subglacial bed' (Cuffey and Paterson, 2010), probably indicates subglacial drainage is braided, likely in broad, low H-channels (Hooke *et al.*, 1990; Hock and Hooke,

1993). The SUBHYD model does not allow specification of this conduit morphology, instead prescribing R-channels. Thus, it would seem to offset the model's inability to account specifically for flow in H-channels, this must be compensated for with high roughnesses. The overall effect is the same: to delay runoff. In this regard, there is therefore high confidence that the model required high roughnesses to replicate empirical data.

There is still some discrepancy between modelled and observed data, especially for some of the tracing experiments, and modelled Sydjåkk/Centerjåkk discharge tended to be underestimated early in the season, then later modelling tended to underestimate low flows and overestimate peak flows. This matches underprediction found by Arnold *et al.* (1998). For Nordjåkk, there was tendency to underpredict discharge. Several reasons help explain discrepancies (Section 6.2.2.1). Also evident is the system probably never exists in steady state over summer, likely due to highly variable meltwater/rainfall.

6.1.3.1. Comparison with Alternative Glacier-hydrology Models

The fact that Storglaciären has seen such intensive research means it provides ideal opportunity for comparing simpler linear-reservoir glacier-hydrology models with this physically based model. This is, surprisingly, the first direct comparison of the two model types for the same glacier.

This study obtained R^2 values of 0.337 for Centerjåkk/Sydjåkk's discharge and 0.231 for Nordjåkk's using physically based modelling. Overall, this performance is less favourable than linear-reservoir models formerly applied here (Hock and Noetzli, 1997; Hock and Holmgren, 2005; Gravelle, 2013). Hock and Noetzli (1997) obtained R^2 values of 0.82 and 0.88 for 1993 and 1994, respectively, and Hock and Holmgren (2005) achieved high Nash-Sutcliffe values of 0.83 and 0.86, when comparing modelled with observed proglacial discharge. While Gravelle's (2013) study also used linear-reservoir modelling, there was 'tuning' to fit modelled to observed discharges and 'implied input' was used instead of modelled melt, so direct comparison with this model is unwarranted.

This model's lower statistical performance does not, however, render application here useless. It should be borne in mind that linear-reservoir models have temporally invariable storage constants, adjusted to provide best matches between observed and modelled data. Furthermore, they yield much lower information on complex interactions within a glacier's system. Even though the physically based model's performance was lower, the strengths of it must be highlighted: specifically, it predicted hourly basal P_w for every moulin and junction specified in the model. Such high-resolution data have never before been generated for Storglaciären, yet having reliable basal P_w estimates is crucial to informing our knowledge of GIC's response to climate change due to P_w's crucial control on dynamics (e.g., Iken and Bindschadler, 1986; Boulton and Hindmarsh, 1987). Thus, further research should apply other (more advanced) physically based models here and this study's could be forced with future climate projections.

6.2. Explaining Discrepancies between Modelling and Observations

6.2.1. Surface-energy-balance Model

First, several potential reasons explain the SEB model's underestimation of total mass balance. Most obvious is that summer mass balance runs from the beginning of April to the end of September, yet the model was only run until 02/09/2012 (JD 246) due to unavailable meteorological data beyond then. Given ablation at the model run's conclusion was still high (cf. Figure 5.3), if the model continued to run, additional melt would be added, aligning more closely modelled and observed data. It is therefore, in a sense, encouraging that the SEB model under rather than overpredicted total melt. To approximate this, average daily melt for the final four days of the model run (JDs 243–246) was extrapolated beyond the model run's end, but linearly decreased such that for the final day in September, no melting was observed, but midway through the remaining 28 days, half the total daily mean melt from JDs 243–246 was experienced. This added 746748 m^3 melt, bringing total predicted melt (now 2999414 m^3) ~28% above the observed 2340242 m^3. Clearly, this is an oversimplification since melt would almost certainly not linearly decrease thus but, as a first-order approximation, is encouraging, especially since direct mass-balance measurements may underpredict ablation (e.g., Krimmel, 1999).

There is still suggestion that melt was slightly underestimated by the SEB model (as shown by comparison with AWS surface lowering). Several model inadequacies potentially explain this. Firstly, only a simple albedo parameterisation was used for snow and ice; detailed changes across the surface were unaccounted for, yet previous research (e.g., Jonsell *et al.*, 2003) showed complex spatio-temporal variation exists. More complex relations could be incorporated, which would modify snow albedo as a function of time since snowfall, air temperature and cloudiness (Hock and Holmgren, 2005); incorporating these effects was beyond this study's scope. Yet, this model is better than others prescribing spatio-temporally invariable albedos for one/both of ice/snow (e.g., Banwell *et al.*, 2012a). Furthermore, the turbulent-flux scheme was simple, yet Hock and Holmgren (2005) showed highly spatio-temporally variable roughnesses on Storglaciären; to model melt accurately, further work estimating roughness lengths is needed since turbulent fluxes play more important roles in SEB than some studies indicate. Thirdly, sub-surface refreezing (e.g., Rye *et al.*, 2010; Banwell *et al.*, 2012a) was not included, yet firnification and storage in a firn aquifer is important on Storglaciären (Schneider, 2001; Jansson *et al.*, 2003; Reijmer and Hock, 2008).

Despite this, the key objective of generating accurate melt across Storglaciären's surface was achieved successfully.

6.2.2. Subglacial-hydrology Model

Because Storglaciären's drainage system is complex (e.g., Hock and Jansson, 2005), there are several potential reasons explaining discrepancies between modelled and observed data. Some of these are due to inherent model oversimplification, but processes operating in the internal hydrological system may aid explanation.

6.2.2.1. Modelled versus Observed Proglacial Discharge

Field evidence, including dye tracing (e.g., Hooke *et al.*, 1988) and boreholes (e.g., Pohjola, 1994), suggests Storglaciären has an extensive englacial network, supposedly draining to Nordjåkk. This study in no way accounted for storage/displacement by the englacial system. Instead, it assumed all modelled water either reaches the bed through moulins or runs off Storglaciären's edges. There is to date no glacier-hydrology model developed, save for Shreve's (1972) theoretical work with many simplifying assumptions, explicitly accounting for englacial-flow routing. Models incorporate englacial *storage* (e.g., Flowers and Clarke, 2002a), but no model explicitly considers englacial *routing*, which can considerably alter the position of entry to the internal system with the point where water reaches the bed, if it ever does. It is believed for Storglaciären that most of the firn and upper ablation areas are drained in this manner and little is known about when these presumed englacial conduits reach the bed, if they ever do; it is possible englacial flow occurs all the way from here to Nordjåkk with no subglacial transport. The SUBHYD model cannot account for this; instead, water entering moulins upglacier of the riegel is routed to Storglaciären's bed *in situ* with no englacial displacement, then routed through the system leading to outflow at Centerjåkk/Sydjåkk, not Nordjåkk (cf. Figure 4.13). Nordjåkk's discharge in this model is instead accounted for by limited subglacial flow from water entering moulin L1, with this fed principally by meltwater from Storglaciären's northern half (cf. Figures 4.12 and 4.15).

The expectation may then be that large discrepancies would exist between modelled and observed discharges at these outflows, especially since moulins above the overdeepening have large catchments, therefore receiving relatively high water inputs over the season's duration (cf. Figure 5.6 and Table 5.2). While some discrepancies exist in data, there is broadly close match between modelled and observed discharges for Centerjåkk/Sydjåkk and Nordjåkk. This raises the question of whether Storglaciären's drainage system has been formerly accurately interpreted, specifically whether the englacial network feeds Nordjåkk, with no flow to Centerjåkk/Sydjåkk.

In reality, there is only very limited support for the conclusion that all flow from the upper ablation and firn areas reaches Nordjåkk: most authors cite one tracer experiment conducted by Hooke *et al.* (1988) producing breakthrough in Nordjåkk, but little further evidence for this conclusion exists. A reevaluation of the drainage system may suggest there is indeed an extensive englacial network here (indicated by borehole investigations), but that instead of water routing to Nordjåkk, it is routed to Sydjåkk/Centerjåkk. Further confidence in this conclusion arises because dye injected at F2 (test

2013-2; Figure 4.16) above the overdeepening produced returns in Sydjåkk/Centerjåkk, not Nordjåkk. Modelling evidence presented here suggests Nordjåkk may instead be fed by large volumes of supraglacial water (not contradicting the observation that it is normally clear). This could be supplemented by some englacial flow, with englacial flow perhaps explaining the small discrepancy between observed and modelled discharges, or some other supraglacial runoff contributing to Nordjåkk's other branch (cf. Figure 4.13). Furthermore, that Nordjåkk responds quickly to peaks in precipitation suggests rapid precipitation routing into the stream, rather than delays imposed by transfer through the internal drainage system, as would occur if its discharge were mainly supplied englacially. It is plausible that since the injection by Hooke *et al.* (1988), there has been reorganisation of the drainage system in a warming climate: as water inputs have increased at progressively higher elevations on Storglaciären (with a retreating ELA), this resulted in preferential water routing towards the bed, away from the englacial network. This could only be confirmed with further study: more injections, perhaps with novel DNA-based tracers (Sharma *et al.*, 2012), covering a more expansive time period would help validate these conclusions, since although extensive tracer experiments were recently conducted (Williamson, 2013), they were in the lower ablation area. Other 2013 injections above the overdeepening did not produce returns, but this may be due to low proglacial-sampling resolution, due to tracer storage in the system, or because the tracer cloud became so dispersed that it was essentially undetectable (e.g., Seaberg *et al.*, 1988). These negative tracer returns parallel Hock *et al.*'s (1999) for Aletschgletscher, Switzerland. There remains high uncertainty over the overdeepening's drainage: specifically, whether subglacial drainage exists and, if it does, its morphology.

The model also did not account for discharge arriving at GSs from other branches of proglacial streams: specifically for Sydjåkk and Nordjåkk (cf. Figure 4.13). Observations suggested these branches supply much lower discharge. Moreover, Sydjåkk's southern branch is likely supplied mainly supraglacially or from snow melt on valley sides. However, these branches of streams were not accounted for in the model, so may explain some discrepancies. Finally, losses from the SUBHYD model by moulin overflow when $P_w > P_i$ need accounting for; these may mask that some water is temporarily englacially stored.

6.2.2.2. Modelled versus Observed Subglacial Flow-routing Times

While modelled flow-routing times compared best with observed times from tracing where $n = 0.125$, discrepancies exist between datasets.

To generate modelled flow-routing times, flow velocities for each individual conduit between injection site and terminus are calculated; this means if one conduit's velocity is especially low (~0.0 m s^{-1}), it disproportionately affects overall modelled times. This could result from poor representation of conduit geometry in the model, or the amount of water flowing through the conduit being too low, thereby decreasing velocity from higher contact with the bed and thus friction. This highlights need for

accurate representations of water input to the subglacial system, suggested by Hock and Jansson (2005); errors either in melt modelling or surface routing therefore influence modelled flow velocities. The small (~10–20% over/underestimation, with overestimation more common) discrepancies for most tests are likely explained by small errors in meltwater input or representations of surface topography, impacting routing. It is encouraging that travel times tend to be overpredicted by the model compared with observations given it has already been highlighted that melt is slightly underestimated by the SEB model (Section 6.1.1).

Largest discrepancies between modelled and observed times were for tests 2012-13, 2012-18, 2012-19, 2012-23 and 2012-25. For tests 2012-13 and 2012-18, modelled times are overestimated by more than an order of magnitude compared with observations. Detailed analysis revealed for tests 2012-23 and 2012-25 (JDs 236 and 237), this was due to underpredicted flow velocities for *all* conduits in the model. Given the uniform pattern for all conduits, this is most likely because of underestimated water inputs to the system then (probably due to issues in melt modelling). Indeed, proglacial-discharge hydrographs indicate underpredicted modelled discharges for these two days. Contrastingly, for tests 2012-13, 2012-18 and 2012-19, modelled travel times were likely much higher than observations because the time for water flow through one conduit was overpredicted. For these tests, conduits with extremely low velocity were immediately downstream of injection sites: in tests 2012-13 and 2012-19, this was the conduit linking moulin L1 with L3, and for test 2012-18, this was the conduit linking moulin U9 with moulin 10 (Figure 4.13). Exceptionally low velocities are likely produced because the water volume fed into these two moulins was predicted much too low by the model, likely because water was not captured by these moulins. This could be due to unreliable representations of surface topography (so supraglacial streams do not cascade into moulins) or due to capture by a nearby moulin at the expense of the moulin used for injection. That such low velocities were predicted for both tests using L1 suggests there is a topographic-representation problem. Injection site U9 was only used once for injection; thus, further tests would be needed to confirm topography used by the model was the cause of the problem, rather than another factor. If topography is an issue, using a higher-resolution surface DEM to reproduce more accurately supraglacial routing may improve results. To quantify the impact of extreme results on model statistical performance, they were removed from data and statistical measures recalculated (Table 6.1). Encouragingly, performance is now much better, though overestimation of travel times still apparent, likely because of underestimated melt, as formerly discussed. Best performance is now for $n = 0.100$, but the difference between this and $n = 0.125$ is trivial.

***Table 6.1**. Recalculated RMSE for differing conduit roughnesses, but with tests 2012-13, 2012-18, 2012-19, 2012-23 and 2012-25 removed, to examine their overall impact on model performance.*

Conduit roughness (n)	RMSE (min)
0.050	157.26
0.100	106.83
0.125	107.31
0.150	175.65
Linear relation to CSA	115.19

6.3. Subglacial Water-pressure Predictions

The strength of physically based approaches is their modelling of physical systems' internal states as well as their outputs. Here, subglacial P_w is modelled, which could ultimately inform ice-flow models. Predicted subglacial P_w largely mirrors previous studies' suggestions (e.g., Jansson, 1996; Jansson and Näslund, 2009; Schoof, 2010). The model's inability to represent 'distributed' drainage means start-of-season P_w is probably lower than it should be, highlighting some model inaccuracy.

Mean summer subglacial P_w shows striking correlation with ice thickness (Figure 5.22), suggesting ice thickness is crucial for the drainage system's adaptation to fluctuating water inputs. This is most true within the overdeepened area, where P_w is consistently high (~60–110% P_i). P_w here displays excellent matches with suggestions from borehole studies (e.g., Hooke and Pohjola, 1994; Jansson, 1995; Jansson and Näslund, 2009). While there is uncertainty about the drainage-system morphology here, it seems that with R-channels (inherent in this model), the empirical P_w observations are reproduced, suggesting this drainage morphology may be possible here. R-channels within overdeepenings are not necessarily unrealistic representations of drainage since broad, low H-channels are less likely due to constantly flooded (full) channels, meaning wall melting is concentrated not just on channels' edges but on their entire diameter (Cook and Swift, 2012). This makes viscous energy dissipation less effective (Creyts and Clarke, 2010), limiting enlargement, and thus the system's ability to transmit rapidly meltwater (Cook and Swift, 2012); this appears well represented in modelled P_w (Figure 6.1). Storglaciären's overdeepening appears to show behaviour closer to curve (ii) on Figure 6.1(b) since P_w remains consistently high over the season, suggesting the system cannot evolve here. Future research should model differing drainage-system morphologies here and integrate predictions of P_w for them (and thus velocity) to determine which morphology best matches observations, contributing to our presently low understanding of processes within overdeepenings (Cook and Swift, 2012).

The model captures some seasonal P_w evolution. It appears the 'Spring Event', indicated by high early-season P_w (and thus velocities) was captured towards the end of May, and is observed in all junctions/moulins, but is more pronounced for those further upglacier and beneath thicker ice, where

the system cannot expand quickly enough in response to high meltwater inputs, following expectations. Two notable effects appear as summer progresses: an overall (though, not pronounced) P_w decline from channel enlargement by flowing meltwater and fewer 'spikes' in P_w, caused by more rapid water evacuation; this is especially true further downglacier, following expectations from research on many GIC (e.g., Willis, 1995; Mair *et al.*, 2002) and the GrIS (e.g., Schoof, 2010; Banwell *et al.*, 2013; Chandler *et al.*, 2013). Figure 6.1 shows expected P_w with melt-season progression; there is some resemblance to this, however, decline in P_w for Storglaciären late-season is less pronounced than that suggested by Figure 6.1.

There appears high correlation between subglacial P_w and major forcings like temperature/rainfall, suggested by Holmlund and Hooke (1983). The model also captures Jansson and Näslund's (2009) remark that some moulins (such as moulin U11, close to the riegel) were insensitive to these forcings. This is likely because they are poorly connected to the system compared with others, so water does not back-up here.

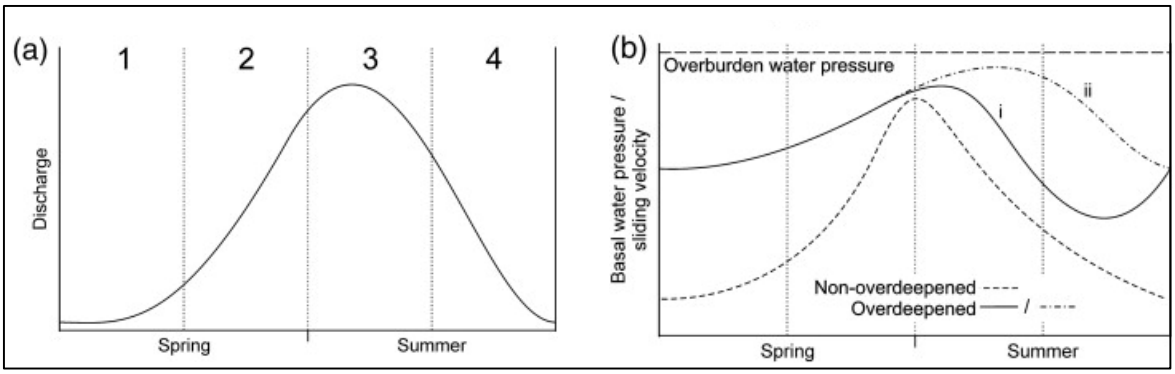

Figure 6.1. *(a) Typical progression in discharge, supplied by surface meltwater and basal melting, over the course of a melt season for a valley glacier; (b) expected water pressure (and thus sliding velocity) for the same time periods as in (a) for non-overdeepened and overdeepened beds (adapted from Cook and Swift, 2012, p.360). For the non-overdeepened areas of the glacier, sliding should peak at the 'Spring Event' (i.e., slightly within section 3), when the change occurs from 'distributed' to 'channelised' drainage and then decline as the season progresses due to channel enlargement by flowing meltwater. For the overdeepened bed, water pressure is consistently high, but there may be some drainage system evolution either from switching to more efficient channels or by transfer to englacial flow pathways, as in curve (i) or any evolution may be severely limited, as in curve (ii). Curve (ii) matches behaviour within Storglaciären's overdeepening best.*

7. Conclusions

7.1. Overview

This study was the first to apply a time-dependent physically based glacier-hydrology model (comprising SEB, SROUT and SUBHYD submodels) to Storglaciären, Sweden, integrating modelled outputs with numerous empirical datasets: mass balance, surface lowering, surface runoff, proglacial discharge, and tracing experiments. It is one of surprisingly few glacier-hydrology studies comparing modelled data with more than one empirical dataset, thus permitting more detailed evaluation of models' ability to represent glaciers' complex drainage systems. Studies like this are crucial for informing GIC's response to climate change and thus their impact on societies like the Sami population dependent on glacial runoff downstream of Storglaciären.

7.2. Synthesis

The research objectives in Chapter 1 were fulfilled. Once properly calibrated, the models broadly performed well at replicating observations, though some discrepancies existed between modelled and observed data, possibly due to inherent model oversimplifications. In contrast to previous linear-reservoir models applied here, which performed overall better, this physically based approach could model subglacial P_w, thus making it more valuable due to the crucial dependence of ice flow on basal processes; this is the first study that has provided continuous summer P_w data for Storglaciären and its response to major glaciological/meteorological factors. P_w compared well with suggestions in previous research, with strong dependence on ice thickness, including capturing high P_w during times of likely speed-up (such as the 'Spring Event'), corroborating research both on Storglaciären and for other valley glaciers (e.g., Mair *et al.*, 2003; Anderson *et al.*, in press). Unfortunately, lacking empirical borehole data did not allow P_w to constrain the model, which was crucial in calibrating Arnold *et al.*'s (1998) model.

A thesis is intended to further our scientific understanding, either by adding evidence for or contradicting previous theories. This thesis contributes in two main ways. A reassessment of the internal drainage system was presented, with modelling evidence suggesting that Nordjåkk may not be fed by the englacial network in the upper ablation and firn areas, but instead may be fed by supraglacial discharge, with limited subglacial flow. The englacial network likely feeds the outlet supplying Sydjåkk/Centerjåkk. This study also informed our understanding of processes in overdeepenings, which represents a fundamental research agenda in glaciology. Specifically, it predicted P_w comparing favourably with expectations from empirical studies, suggesting if subglacial drainage does exist here, R-channels (inherent to the model) could represent the system's morphology.

7.3. Future Research Directions

Future research could help either overcome this study's limitations or build upon its findings.

The SEB model could be verified using more *in situ* measurements if these existed, including snowline retreat, and albedo and surface lowering at other locations on Storglaciären. It could also incorporate more complex energy-flux calculations. The SROUT model could use a higher-resolution (~2-m) surface DEM. One inherent problem with the SUBHYD model is when $P_w > 1.1P_i$, water is lost from the model onto the glacier surface, but no account is taken of what then happens to this water. Further research could account for the magnitude of this loss, feeding this water back into the SROUT model and determining whether it ultimately runs off the glacier or enters a different moulin. Furthermore, the SUBHYD model assumes no change in roughness or locations of subglacial conduits over the season. As research on conduit roughness continues (e.g., Gulley *et al.*, 2013), more accurate estimates could be incorporated in future modelling. Moreover, it specified an inherently channelised system, an oversimplification, likely to be most crucial early season, though attempts were made with this model at incorporating 'distributed' drainage, but were unsuccessful (Arnold *et al.*, 1998). Proglacial discharge could be measured using alternative methods, especially during peak flows, since this could explain discrepancies between observed and modelled results, rather than model problems. Englacial storage or, preferably, routing needs accounting for in modelling, but the latter has not been achieved by any approach to date.

Storglaciären presents an almost unique research possibility because it has been so extensively researched, because it is very accessible, and because much is already known about many aspects of its glaciology. It would thus be wise to take advantage of this existing breadth of research, but to supplement it with new, focused studies. Most valuable would be at least one intensive field season where all of the following would be measured, supplementing the continuing mass-balance measurements: generation of a new bed DEM using radio-echo sounding or mass conservation, detailed albedo measurements across the glacier surface, measurements of supraglacial runoff either into moulins or at glacier edges, comprehensive discharge measurements in the three proglacial streams and further downstream (a GS existed here, but was destroyed during a 2012 flood), measurements of snowline retreat, more tracing experiments (especially further upglacier), perhaps employing DNA-based tracers to allow for higher injection-site concentration, continuous borehole P_w measurements across the glacier and, crucially, ice-velocity measurements. Such measurements could allow for perhaps the most extensive understanding of a glacier's hydrological system ever generated, since although many studies have suggested a need for detailed measurements over field seasons, nobody has conducted such work. Measurements could then be used to extensively verify and test melt and hydrology models, and coupling between P_w and velocity would inform ice-flow models (Schoof and Hewitt, 2013; de Fleurian *et al.*, 2013). Comparing various models of glacier hydrology (including Werder *et al.*'s [2013] recent two-dimensional approach) would be valuable since direct inter-model comparisons cannot currently be made as models have been run using differing input data and for different years; they have also used differing approaches to generate melt; thus, it

is impossible to constrain whether model performance is limited due to issues in melt computation or due to specific hydrological-model issues. The fact that Storglaciären has an overdeepening makes it an especially valuable site for testing Werder *et al.*'s (2013) model since this model's major intended future application is to ice sheets, which often flow through overdeepened troughs.

Comprehensively evaluating glacier-hydrology models, including coupling to ice-flow models, in this valley-glacier setting would bring greater confidence in glacier-hydrology models, thus making their applications to ice sheets more justified. This would permit better forecasts of runoff and ultimately SLR from the cryosphere, both now and into the future, thereby informing important societal decisions.

Appendix I: Subglacial Network Configuration

Conduits (cf. Figure 4.13)

Upstream Junction	Downstream Junction	Length (m)	Diameter (m)	Cross-sectional Area (m^2)
53	52	205.07	1.126	0.996
65	53	195.46	1.126	0.996
59	60	188.43	1.516	1.805
56	68	186.81	1.126	0.996
L2	53	183.35	1.513	1.799
24	59	171.15	1.516	1.805
F5	57	164.65	0.933	0.683
28	54	162.09	0.933	0.683
U12	U7	159.67	1.126	0.996
54	55	154.65	0.933	0.683
F3	56	150.13	1.126	0.996
66	53	144.34	1.513	1.799
U11	61	134.46	1.126	0.996
27	64	134.42	0.933	0.683
23	56	127.22	1.126	0.996
20	U5	126.54	1.126	0.996
58	67	123.03	1.516	1.805
F1	F4	122.05	0.933	0.683
51	50	114.32	1.126	0.996
50	Outflow	111.28	1.126	0.996
F2	58	110.10	1.516	1.805
64	63	109.72	0.933	0.683
L1	L3	107.48	1.513	1.799
61	65	106.26	1.126	0.996
F4	55	94.83	0.933	0.683
LN1	Outflow	93.08	0.536	0.226
57	58	92.32	0.933	0.683
U8	U5	87.78	1.126	0.996
68	57	87.76	0.933	0.683
63	62	86.66	0.933	0.683
U7	U2	84.69	1.126	0.996
L3	66	80.97	1.513	1.799
60	U1	79.52	1.516	1.805
62	57	78.40	0.933	0.683
67	59	73.32	1.516	1.805
55	68	67.50	0.933	0.683
52	51	67.37	1.126	0.996
12	U5	65.34	1.126	0.996
U9	10	60.82	1.126	0.996
U1	10	59.47	1.126	0.996
U4	10	55.44	1.126	0.996
U5	U11	54.92	1.126	0.996
22	F3	49.43	1.126	0.996
4	F2	47.78	1.516	1.805
5	4	41.41	1.516	1.805
U2	U1	38.63	1.126	0.996
10	12	37.70	1.126	0.996

Junctions (cf. Figure 4.13)

Junction Number	Surface Elevation (m a.s.l.)	Bed Elevation (m a.s.l.)	Receives Supraglacial Inputs?	Used for Tracing Experiment(s)? (Table 5.6)
LN1	1224.93	1200.00	Yes	Yes
F5	1369.82	1205.08	Yes	Yes
F2	1367.93	1196.00	Yes	Yes
4	1364.90	1213.89	Yes	No
5	1363.79	1235.12	Yes	No
U11	1333.50	1198.63	Yes	Yes
U5	1338.50	1191.47	Yes	Yes
U9	1348.94	1192.80	Yes	Yes
U4	1349.57	1188.54	Yes	Yes
10	1346.50	1188.20	Yes	No
U1	1346.50	1186.10	Yes	Yes
12	1343.50	1189.01	Yes	No
U8	1344.06	1189.74	Yes	Yes
U2	1344.94	1189.30	Yes	Yes
U7	1342.36	1214.19	Yes	Yes
U12	1338.00	1262.35	Yes	Yes
L1	1279.32	1204.86	Yes	Yes
L3	1275.25	1179.17	Yes	Yes
L2	1269.25	1187.40	Yes	Yes
20	1342.06	1221.16	Yes	No
F3	1373.97	1277.92	Yes	Yes
22	1376.93	1300.72	Yes	No
23	1372.07	1260.14	Yes	No
24	1365.79	1213.82	Yes	No
F4	1381.90	1191.51	Yes	Yes
F1	1377.79	1247.60	Yes	Yes
27	1407.00	1228.00	Yes	No
28	1409.18	1214.36	Yes	No
54	1394.25	1177.21	No	N/A
55	1384.78	1162.30	No	N/A
56	1377.00	1216.04	No	N/A
57	1377.22	1160.00	No	N/A
58	1371.18	1170.13	No	N/A
59	1364.07	1179.18	No	N/A
60	1350.50	1179.57	No	N/A
61	1315.54	1196.36	No	N/A
53	1270.47	1173.45	No	N/A
52	1229.50	1190.00	No	N/A
51	1216.21	1190.00	No	N/A
50	1184.50	1179.05	No	N/A
62	1381.07	1158.15	No	N/A
63	1387.07	1158.44	No	N/A
64	1396.00	1175.06	No	N/A
65	1297.32	1170.73	No	N/A
66	1279.25	1160.00	No	N/A
67	1364.90	1174.90	No	N/A
68	1381.50	1160.25	No	N/A

Appendix II: Tracing Breakthrough Curves

Sample BTCs from tracing experiments in summers 2012 and 2013 are shown below.

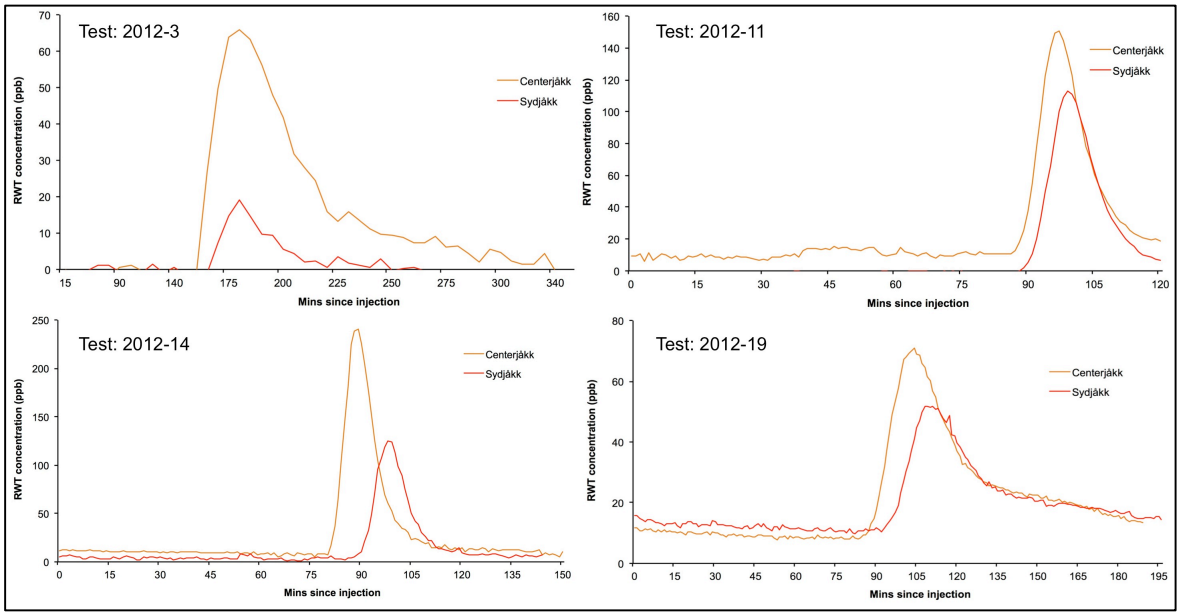

Sample 2012 BTCs; test numbers refer to those listed in Table 5.6. Note differing x- and y-axis scales.

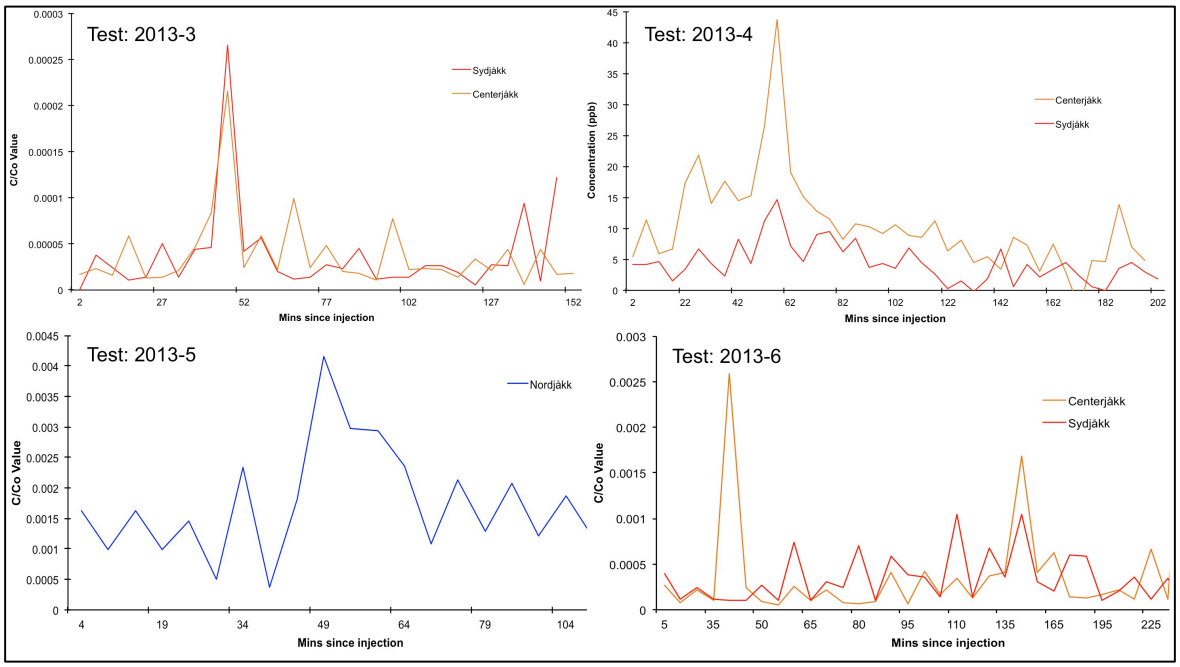

Sample 2013 BTCs; test numbers refer to those listed in Table 5.6. Note differing y- and x-axis units and scales. For details on calculating C/Co values (for DNA-based tracers), see Sharma et al. *(2012).*

References

Alley, R.B., Cuffey, K.M., Evenson, E.B., Strasser, J.C., Lawson, D.E. and Larson, G.J., 1997. How glaciers entrain and transport basal sediment: physical constraints. *Quaternary Science Reviews*, **16**, 1017–1038.

Ambach, W. 1986. Nomographs for the determination of meltwater from snow- and ice surfaces. *Berichte des Naturwissenschaftlich-Medizinischen Vereins in Innsbruck*, **73**, 7–15.

Anderson, B., Willis, I., Goodsell, B., Banwell, A., Owens, I., Mackintosh, A. and Lawson, W., in press. Annual to daily ice velocity and water pressure variation on Ka Rolmata o Hlne Hukatere / Franz Josef Glacier, New Zealand. *Arctic, Antarctic and Alpine Research*.

Andréasson, P.G and Gee, D.G., 1989. Bedrock geology and morphology of the Tarfala area, Kebnekaise Mts., Swedish Caledonides. *Geografiska Annaler*, **71A**(3–4), 235–239.

Arendt, A., 1999. Approaches to modelling the surface albedo of a high Arctic glacier. *Geografiska Annaler*, **81A**(4), 477–488.

Arnold, N., 2005. Investigating the sensitivity of glacier mass balance/ elevation profiles to changing meteorological conditions: model experiments for Haut Glacier d'Arolla, Valais, Switzerland. *Arctic, Antarctic and Alpine Research*, **37**(2), 139–145.

Arnold, N.S., 2010. A new approach for dealing with depressions in Digital Elevation Models when calculating flow accumulation values. *Progress in Physical Geography*, **34**(6), 781–809.

Arnold, N.S. and Rees, W.G., 2009. Effects of digital elevation model spatial resolution on distributed calculations of solar radiation in a high arctic glacierised catchment. *Journal of Glaciology*, **55**(194), 973–984.

Arnold, N., Willis, I.C., Sharp, M.J., Richards, K.S. and Lawson, W.J., 1996. A distributed surface energy balance model for a small valley glacier: 1. Development and testing for Haut Glacier d'Arolla, Valais, Switzerland. *Journal of Glaciology,* **42**, 77–89.

Arnold, N., Richards, K.S., Willis, I.C. and Sharp, M.J., 1998. Initial results from a physically-based, distributed model of glacier hydrology. *Hydrological Processes,* **12**, 191–219.

Arnold, N.S., Rees, W.G., Hodson. A.J. and Kohler, J., 2006. Topographic controls on the surface energy balance of a high Arctic glacier. *Journal of Geophysical Research*, **111**, F01011, doi:10.1029/2005JF000426.

Arnold, N.S., Banwell, A.F. and Willis, I.C., 2013. High-resolution modelling of the seasonal evolution of surface water storage on the Greenland Ice Sheet. *The Cryosphere Discuss*, **7**, 6143–6170.

Bahr, D.B. and Radić, V., 2012. Significant contribution to total mass from very small glaciers. *The Cryosphere*, **6**, 763–770.

Bahr, D.B., Dyurgerov, M. and Meier, F., 2009. Sea-level rise from glaciers and ice caps: a lower bound. *Geophysical Research Letters*, **36**(4), L03501.

Baker, D., Escher-Vetter, H., Moser, H., Oerter, H. and Reinwarth, O., 1982. A glacier discharge model based on results from field studies of energy balance, water storage and flow. *Internal Association of Hydrological Sciences Publication* 138 (Symposium at Exeter 1982 – *Hydrological Aspects of Alpine and High Mountain Areas),* 103–112.

Bamber, J.L. and Payne, A.J. (Eds.), 2004. *Mass Balance of the Cryosphere: Observations and Modelling of Contemporary and Future Changes.* Cambridge: Cambridge University Press.

Bamber, J.L. and Aspinall, W.O., 2013. An expert judgement assessment of future sea-level rise from the ice sheets. *Nature Climate Change*, **3**, 424–427.

Banwell, A.F., 2012. *Modelling the hydrology of the Greenland Ice Sheet*. Unpublished Ph.D. Thesis, University of Cambridge, Cambridge, UK.

Banwell, A.F., Willis, I., Arnold, N., Messerli, A., Rye, C. and Ahlstrom, A., 2012a. Calibration and validation of a high resolution surface mass balance model for Paakitsoq, west Greenland. *Journal of Glaciology*, **58**(212), 1047–1062.

Banwell, A.F., Arnold, N.S., Willis, I.C., Tedesco, M. and Ahlstrøm, A.P., 2012b. Modeling supraglacial water routing and lake filling on the Greenland Ice Sheet. *Journal of Geophysical Research: Earth Surface*, **117**(F4), F04012.

Banwell, A.F., Willis, I. and Arnold, N., 2013. Modeling subglacial water routing at Paakitsoq, West Greenland. *Journal of Geophysical Research: Earth Surface*, **118**, 1282–1295.

Baraer, M., Mark, B.G., Mckenzie, J.M., Condom, T., Bury, J., Huh, K-I., Portocarrero, C. Gómez, J. and Rathay, S., 2012. Glacier recession and water resources in Peru's Cordillera Blanca. *Journal of Glaciology*, **58**(207), 134–150.

Barnett, T.P., Adam, J.C. and Lettenmaier, D.P., 2005. Potential impacts of a warming climate on water availability in snow-dominated regions. *Nature*, **438**(7066), 303–309.

Bartholomaus, T.C., Anderson, R.S. and Anderson, S.P., 2008. Response of glacier basal motion to transient water storage. *Nature Geoscience*, **1**, 33–37.

Bartholomew, I., Nienow, P., Mair, D., Hubbard, A., King, M.A. and Sole, A., 2010. Seasonal evolution of subglacial drainage and acceleration in a Greenland outlet glacier. *Nature Geoscience*, **3**, 408–411.

Bartholomew, I.D., Nienow, P., Sole, A., Mair, D., Cowton, T., King, M.A. and Palmer, S., 2011a. Seasonal variations in Greenland Ice Sheet motion: Inland extent and behaviour at higher elevations. *Earth and Planetary Science Letters*, **307**(3–4), 271–278.

Bartholomew, I.D., Nienow, P., Sole, A., Mair, D., Cowton, T., Palmer, S. and Wadham, J., 2011b. Supraglacial forcing of subglacial drainage in the ablation zone of the Greenland Ice Sheet. *Geophysical Research Letters*, **38**(8), L08502.

Bartholomew, I., Nienow, P., Sole, A., Mair, D., Cowton, T. and King, M.A., 2012. Short-term variability in Greenland Ice Sheet motion forced by time-varying meltwater drainage: Implications for the relationship between subglacial drainage system behaviour and ice velocity. *Journal of Geophysical Research*, **117**, F03002, doi:10.1029/2011JF002220.

Benn, D.I. and Evans, D.J.A., 2010. *Glaciers and Glaciation*. 2nd Edition. London: Hodder Education.

Bindschadler, R.A., 1983. The importance of pressurized subglacial water in separation and sliding at the glacier bed. *Journal of Glaciology*, **29**, 3–19.

Bingham, R.G., Nienow, P.W. and Sharp, M.J., 2003. Intra-annual and intra-seasonal flow dynamics of a High Arctic polythermal valley glacier. *Annals of Glaciology*, **37**(1), 181–188.

Björnsson, H., 1981. Radio-echo sounding maps of Storglaciären, Isfallsglaciären and Rabots Glacier, northern Sweden. *Geografiska Annaler,* **63A**(3–4), 225–231.

Bolch, T., Kulkarni, A., Kääb, A., Huggel, C., Paul, F., Cogley, J.G., Frey, H., Kargel, J.S., Fujita, K., Scheel, M., Bajracharya, S. and Stoffel, M., 2012. The state and fate of Himalayan glaciers. *Science*, **366**(6079), 310–314.

Boulton, G.S. and Hindmarsh, R.C.A., 1987. Sediment deformation beneath glaciers: rheology and geological consequences. *Journal of Geophysical Research*, **92**(B9), 9059–9082.

Brand, G., Pohjola, V. and Hooke, R.LeB., 1987. Evidence for a till layer beneath Storglaciären, Sweden, based on electrical resistivity measurements. *Journal of Glaciology*, **33**(115), 311–314.

Brock, B., **Willis, I. and Sharp, M.J.**, 2000. Measurement and parameterization of albedo variations at Haut Glacier d'Arolla, Switzerland. *Journal of Glaciology*, **46**(155), 675–688.

Brock, B., Willis, I.C., Sharp, M.J. and Arnold, N.S., 2002. Modelling seasonal and spatial variations in the surface energy balance of Haut Glacier d'Arolla, Switzerland. *Annals of Glaciology*, **31**, 53–62.

Bronge, C., 1996. The excavation of the Storglaciären trough during the Quaternary. *Geografiska Annaler*, **78A**(2–3), 163–169.

Brugger, K.A., 1996. Predicted response of Storglaciären, Sweden, to climatic warming. *Annals of Glaciology*, **24**, 217–222.

Brugger, K.A., 2007. The non-synchronous response of Rabots Glaciär and Storglaciären, northern Sweden, to recent climate change: a comparative study. *Annals of Glaciology*, **46**(1), 275–282.

Brugger, K.A., Refsnider, K.A. and Whitehill, M.F., 2005. Variation in glacier length and ice volume of Rabots Glaciär, Sweden, in response to climate change, 1910–2003. *Annals of Glaciology*, **42**, 180–188.

Campbell, F.M.A., Nienow, P.W. and Purves, R.S., 2006. Role of the supraglacial snowpack in mediating meltwater delivery to the glacier system as inferred from dye tracer investigations. *Hydrological Processes*, **20**(4), 969–985.

Chandler, D.M., Wadham, J.L., Lis, G.P., Cowton, T., Sole, A., Bartholomew, I., Telling, J., Nienow, P., Bagshaw, E.B., Mair, D., Vinen, S. and Hubbard, A., 2013. Evolution of the subglacial drainage system beneath the Greenland Ice Sheet revealed by tracers. *Nature Geoscience*, **6**, 195–198.

Chow, V., Maidment, D.R. and Mays, L.W., 1988. *Applied Hydrology*. Civil Engineering Series. McGraw-Hill International Editions: New York. 572pp.

Church, J.A. and White, N.J., 2006. A 20th century acceleration in sea-level rise. *Geophysical Research Letters*, **33**, GL024826.

Church, J.A., White, N.J., Aarup, T., Wilson, W.S., Woodworth, P.L., Domingues, C.M., Hunter, J.R. and Lambeck, K., 2008. Understanding global sea levels: past, present and future. *Sustainability Science*, **3**, 9–22.

Clarke, G.K.C., 1996. Lumped-element analysis of subglacial hydraulic circuits. *Journal of Geophysical Research*, **101**, 17547–17599.

Coffey, M.E., Workman, S.R., Taraba, J.L. and Fogle, A.W., 2004. Statistical procedures for evaluating daily and monthly hydrologic model predictions. *Transactions of the ASAE*, **47**(1), 59–68.

Cogley, J.G. and Adams, W.P., 1998. Mass balance of glaciers other than ice sheets. *Journal of Glaciology,* **44**(147), 315–325.

Colbeck, S.C., 1978. The physical aspects of water flow through snow. In: **Chow, V.T. (Ed.),** 1978. *Advances in Hydroscience.* **11**, 165–206. New York: Academic Press.

Colgan, W., Rajaram, H., Anderson. R.S., Steffen, K., Zwally, J., Phillips, T. and Adbalati, W., 2012. The annual glaciohydrology cycle in the ablation zone of the Greenland ice sheet: Part 2: Observed and modeled ice flow. *Journal of Glaciology*, **58**(207), 51–64.

Cook, S.J. and Swift, D.A., 2012. Subglacial basins: Their origin and importance in glacial systems and landscapes. *Earth-Science Reviews*, **115**(4), 332–372.

Copland, L. and Sharp, M., 2001. Mapping thermal and hydrological conditions beneath a polythermal glacier with radio-echo sounding. *Journal of Glaciology*, **47**(157), 232–242.

Copland, L., Harbor, J., Gordon, S. and Sharp, M., 1997. The use of borehole video in investigating the hydrology of a temperate glacier. *Hydrological Processes*, **11**(2), 211–224.

Covington, M.D., Banwell, A.F., Gulley, J., Saar, M.O., Willis, I. and Wicks, C.M., 2012. Quantifying the effects of glacier conduit geometry and recharge on proglacial hydrograph form. *Journal of Hydrology*, **414**, 59–71.

Creyts, T.T. and Schoof, C.G., 2009. Drainage through subglacial water sheets. *Journal of Geophysical Research*, **114**, F04008, doi:10.1029/2008JF001215.

Creyts, T.T. and Clarke, G.K.C., 2010. Hydraulics of subglacial supercooling: theory and simulations for clear water flows. *Journal of Geophysical Research: Earth Surface*, **115**, F03021.

Cuffey, K. M. and Paterson, W.S.B., 2010. *The Physics of Glaciers*. 4th Edition. Oxford: Butterworth-Heinemann.

Cutler, P., 1998. Modelling the evolution of subglacial channels due to varying water input. *Journal of Glaciology*, **44**(148), 485–497.

Dahlke, H.E., Lyon, S.W., Stedinger, J.R., Rosqvist, G. and Jansson, P., 2012. Contrasting trends in floods for two sub-arctic catchments in northern Sweden – does glacier presence matter? *Hydrology and Earth System Sciences*, **16**, 2123–2141.

Das, S.B., Joughin, I., Behn, M.D., Howat, I.M., King, M.A., Lizarralde, D. and Bhatia, M.P., 2008. Fracture propagation to the base of the Greenland Ice Sheet during supraglacial lake drainage. *Science*, **320**, 778–781.

de Fleurian, B., **Gagliardini, O., Zwinger, T., Durand, G., Le Meur, E., Mair, D. and Råback, P.**, 2013. A subglacial hydrological model dedicated to glacier sliding. *The Cryosphere Discuss,* **7**(4), 3449–3496.

Dowdeswell, J.A., Hagen, J.O., Björnsson, H., Glazovsky, A.F., Harrison, W.D., Holmlund, P., Jania, J., Koerner, R.M., Lefauconnier, B., Ommanney, C.S.L. and Thomas, R.H., 1997. The mass balance of circum-Arctic glaciers and recent climate change. *Quaternary Research*, **48**(1), 1–14.

Dyurgerov, M.B. and Meier, M.F., 1997. Year-to-year fluctuations of global mass balance of small glaciers and their contribution to sea-level change. *Arctic and Alpine Research*, **29**, 392–402.

Ensminger, S.L., Evenson, E.B., Larson. G.J., Lawson, D.E., Alley, R.B. and Strasser, J.C., 1999. Preliminary study of laminated, silt-rich debris bands: Matanuska Glacier, Alaska, USA. *Annals of Glaciology*, **28**, 261–266.

Eriksson, M.G., Björnsson, H., Herzfeld, U.C. and Holmlund, P., 1993. *The bottom topography of Storglaciären: a new map based on old and new ice depth measurements, analyzed with geostatistical methods*. Forskningsrapportserien STOU–NG 95.

Escher-Vetter, H., 1985. Energy balance calculations for the ablation period 1982 at Vernagtferner, Oetzal Alps. *Annals of Glaciology*, **6**, 158–160.

Evans, E., Essery, R. and Lucas, R., 2008. Changing snow cover and the net mass balance of Storglaciären, northern Sweden. *Annals of Glaciology*, **49**(1), 199–204.

Fischer, U.H., Braun, A., Bauder, A. and Flowers, G.E., 2005. Changes in geometry and subglacial drainage derived from digital elevation models: Unteraargletscher, Switzerland, 1927**–**1997. *Annals of Glaciology*, **40**, 20–24.

Flowers, G.E., 2008. Subglacial modulation of the hydrograph from glacierized basins. *Hydrological Processes,* **22**(19), 3903–3918.

Flowers, G.E. and Clarke, G.K.C., 1999. Surface and bed topography of Trapridge Glacier, Yukon Territory, Canada: digital elevation models and derived hydraulic geometry. *Journal of Glaciology*, **45**(149), 165–174.

Flowers, G.E. and Clarke, G.K.C., 2002a. A multicomponent coupled model of glacier hydrology 1. Theory and synthetic examples. *Journal of Geophysical Research: Solid Earth*, **107**(B11), ECV9-1–ECV9-17.

Flowers, G.E. and Clarke, G.K.C., 2002b. A multicomponent coupled model of glacier hydrology 2. Application to Trapridge Glacier, Yukon, Canada. *Journal of Geophysical Research: Solid Earth*, **107**(B11), ECV10-1–ECV10-16.

Fountain, A.G., 1992. Subglacial water flow inferred from stream measurements at South Cascade Glacier, Washington, U.S.A. *Journal of Glaciology*, **38**(128), 51–64.

Fountain, A.G. and Walder, J.S., 1998. Water flow through temperate glaciers. *Reviews of Geophysics*, **36**, 299–328.

Fountain, A.G., Jacobel, R.W., Schlichting, R. and Jansson, P., 2005. Fractures as the main pathways of water flow in temperate glaciers. *Nature*, **433**, 618–621.

Fudge, T.J., Harper, J.T., Humphrey, N.F. and Pfeffer, W.T., 2009. Rapid glacier sliding, reverse ice motion and subglacial water pressure during an autumn rainstorm. *Annals of Glaciology*, **50**(52), 101–108, doi: 10.3189/172756409789624247.

Fyffe, C.L., Reid, T.D., Brock, B.W., Kirkbridge, M.P., Diolaiuti, G., Smiraglia, C. and Diotri, F., 2014. A distributed energy-balance melt model of an alpine debris-covered glacier. *Journal of Glaciology*, **60**(221), 587–602.

Gardner, A.S., Moholdt, G., Cogley, J.G. Wouters, B., Arendt, A.A., Wahr, J., Berthier, E., Hock, R., Pfeffer, W.T., Kaser, G., Ligtenberg, S.R.M., Bolch, T., Sharp, M.J., Hagen, J.O., van den Broeke, M.R. and Paul, F., 2013. A reconciled estimate of glacier contributions to sea level rise: 2003 to 2009. *Science*, **340**(6134), 852–857.

Glen, J.W., 1952. Experiments on the deformation of ice. *Journal of Glaciology*, **2**(12), 111–114.

Gordon, S., Sharp, M., Hubbard, B., Smart, C., Ketterling, B. and Willis, I., 1998. Seasonal reorganization of subglacial drainage inferred from measurements in boreholes. *Hydrological Processes*, **12**(1), 105–133.

Gordon, S., Sharp, M., Hubbard, B., Willis, I., Smart, C., Copland, L., Harbor, J. and Ketterling, B., 2001. Borehole drainage and its implications for the investigation of glacier hydrology: experiences from Haut Glacier d'Arolla, Switzerland. *Hydrological Processes*, **15**(5), 797–813.

Gravelle, R.D., 2013. Temporal variability of meltwater and sediment transfer dynamics at an Arctic glacier, Storglaciären, northern Sweden. Unpublished Ph.D. Thesis, University of Loughborough, Loughborough, UK.

Greuell, W. and Oerlemans, J., 1986. Sensitivity studies with a mass balance model including temperature profile calculations inside the glacier. *Z. Gletscherkd. Glazialgeol.*, **22**(2), 101–124.

Greuell, W. and Smeets, P., 2001. Variations with elevation in the surface energy balance of the Pasterze (Austria). *Journal of Geophysical Research*, **106**(D23), 31717–31727.

Grinsted, A., 2013. An estimate of global glacier volume. *The Cryosphere*, **7**, 141–151.

Grudd, H. and Schneider, T., 1996. Air temperature at Tarfala Research Station 1946–1995. *Geografiska Annaler*, **78A**(2–3), 115–120.

Gulley, J.D., Benn, D.I., Screaton, E. and Martin, J., 2009. Mechanisms of englacial conduit formation and their implications for subglacial recharge. *Quaternary Science Reviews*, **28**(19–20), 1984–1999.

Gulley, J.D., Walthard, P.D., Martin, J., Banwell, A.F., Benn, D.I. and Catania, G., 2012a. Conduit roughness and dye-trace breakthrough curves: why slow velocity and high dispersivity may not reflect flow in distributed systems. *Journal of Glaciology*, **58**(211), 915–925.

Gulley, J.D., Grabiec, M., Martin, J.B., Jania, J., Catania, G. and Glowacki, P., 2012b. The effect of discrete recharge by moulins and heterogeneity in flow-path efficiency at glacier beds on subglacial hydrology. *Journal of Glaciology*, **58**(211), 926–940.

Gulley, J.D., Spellman, P.D., Covington, M.D., Martin, J.B., Benn, D.I. and Catania, G., 2013. Large values of hydraulic roughness in subglacial conduits during conduit enlargement: implications for modeling conduit evolution. *Earth Surface Processes and Landforms,* **39**(3), 296–310.

Gusmeroli, A., Murray, T., Jansson, P., Petterson, R., Aschwanden, A. and Booth, A.D., 2010. Vertical distribution of water within the polythermal Storglaciären, Sweden. *Journal of Geophysical Research*, **115**(F4), doi: 10.1029/2009JF001539.

Gusmeroli, A., Jansson, P., Pettersson, R. and Murray, T., 2012. Twenty years of cold surface layer thinning at Storglaciären, sub-Arctic Sweden, 1989-2009. *Journal of Glaciology*, **58**(207), 3–10.

Hagen, J.O., Etzelmuller, B. and Nuttall, A-M., 2000. Runoff and drainage pattern derived from digital elevation models, Finsterwalderbeen, Svalbard. *Annals of Glaciology*, **31**(1), 147–152.

Hambrey, M.J., Murray, T., Glasser, N.F., Hubbard, A., Hubbard, B., Stuart, G., Hansen, S. and Kohler, J., 2005. Structure and changing dynamics of a polythermal valley glacier on a centennial timescale: Midre Lovénbreen, Svalbard. *Journal of Geophysical Research*, **110**, F01006.

Hanson, B. and Hooke, R.LeB., 1994. Short-term velocity variations and basal coupling near a bergschrund, Storglaciären, Sweden. *Journal of Glaciology*, **40**(134), 67–74.

Hanson, B., Hooke, R.LeB. and Grace, E.M. Jr., 1998. Short-term velocity and water-pressure variation down-glacier from a riegel, Storglaciären, Sweden. *Journal of Glaciology*, **44**(147), 359–367.

Herzfeld, U.C., Eriksson, M.G. and Holmlund, P., 1993. On the influence of kriging parameters on the cartographic output – a study in mapping subglacial topography. *Mathematical Geology*, **25**(7), 881–900.

Hewitt, I.J., 2011. Modelling distributed and channelized subglacial drainage: the spacing of channels. *Journal of Glaciology,* **57**, 302–314.

Hewitt, I.J., Schoof, C. and Werder, M.A., 2012. Flotation and free surface flow in a model for subglacial drainage. Part II: channel flow. *Journal of Fluid Mechanics*, **702**, 157–187.

Hock, R., 1999. A distributed temperature index ice and snow melt model including potential direct solar radiation. *Journal of Glaciology*, **45**(149), 101–111.

Hock, R., 2003. Temperature index melt modelling in mountain areas. *Journal of Hydrology*, **282**(1–4), 104–115.

Hock, R., 2005. Glacier melt: A review of processes and their modelling. *Progress in Physical Geography,* **29**(3)*,* 362–391.

Hock, R. and Hooke, R.LeB., 1993. Evolution of the internal drainage system in the lower part of the ablation area of Storglaciären, Sweden. *Geological Society of America Bulletin*, **105**(4), 537–46.

Hock, R. and Holmgren, B., 1996. Some aspects of energy balance and ablation of Storglaciären, northern Sweden. *Geografiska Annaler*, **78A**(2–3), 121–131.

Hock, R. and Noetzli, C., 1997**.** Areal melt and discharge modelling of Storglaciären, Sweden. *Annals of Glaciology*, **24**, 211–216.

Hock, R. and Holmgren, B., 2005. A distributed surface energy-balance model for complex topography and its application to Storglaciären, Sweden. *Journal of Glaciology*, **51**(172), 25–36.

Hock, R. and Jansson, P., 2005. *Modeling Glacier Hydrology*. In: **Anderson, M.G. and McDonnell, J. (Eds.)**, 2005. *Encyclopedia of Hydrological Sciences*. Chichester: Wiley. pp.2647–2655.

Hock, R., Iken, A. and Wangler, A., 1999. Tracer experiments and borehole observations in the over-deepening of Aletschgletscher, Switzerland. *Annals of Glaciology*, **28**, 253–260.

Hock, R., Radić, V. and de Woul, M., 2007. Climate sensitivity of Storglaciären, Sweden: an intercomparison of mass-balance models using ERA-40 re-analysis and regional climate model data. *Annals of Glaciology*, **46**, 342–348.

Hodgkins, R., Cooper, R., Tranter, M. and Wadham, J., 2013. Drainage-system development in consecutive melt seasons at a polythermal, Arctic glacier, evaluated by flow-recession analysis and linear-reservoir simulation. *Water Resources Research*, **49**, 1–14.

Holmlund, P., 1987. Mass balance of Storglaciären during the 20th century. *Geografiska Annaler*, **69A**(3–4), 439–444.

Holmlund, P., 1988a. An application of two theoretical melt water drainage models on Storglaciären and Mikkaglaciären, northern Sweden. *Geografiska Annaler*, **70A**(1–2), 1–7.

Holmlund, P., 1988b. Internal geometry and evolution of moulins, Storglaciären, Sweden. *Journal of Glaciology*, **34**(117), 242–248.

Holmlund, P. and Hooke, R.LeB., 1983. High water-pressure events in moulins, Storglaciären, Sweden. *Geografiska Annaler*, **65A**(1–2), 19–25.

Holmlund, P. and Eriksson, M., 1989. The cold surface layer on Storglaciären. *Geografiska Annaler*, **71A**(3–4), 241–244.

Holmlund, P. and Jansson, P., 1999. The Tarfala mass balance program. *Geografiska Annaler*, **81A**(4), 621–631.

Holmlund, P., Karlén, W. and Grudd, H., 1996. Fifty years of mass balance and glacier front observations at the Tarfala Research Station. *Geografiska Annaler*, **78A**(2–3), 105–114.

Holmlund, P., Jansson, P. and Petterson, R., 2005. A re-analysis of the 58-year mass balance record of Storglaciären, Sweden. *Annals of Glaciology*, **42**, 389–394.

Hooke, R.LeB., 1984. On the role of mechanical energy in maintaining subglacial water conduits at atmospheric pressure. *Journal of Glaciology*, **30**(105), 180–187.

Hooke, R.LeB., 1991. Positive feedbacks associated with erosion of glacial cirques and overdeepenings. *Geological Society of America Bulletin*, **103**(8), 1104–1108.

Hooke, R.LeB. and Pohjola, V.A., 1994. Hydrology of a segment of glacier situated in an overdeepening, Storglaciären, Sweden. *Journal of Glaciology*, **40**(134), 140–148.

Hooke, R.LeB., Brzozowski, J. and Bronge, C., 1983. Seasonal variations in surface velocity, Storglaciären, Sweden. *Geografiska Annaler*. **65A**(3–4), 263–277.

Hooke, R.LeB., Miller, S.B. and Kohler, J., 1988. Character of the englacial and subglacial drainage system in the upper part of the ablation area of Storglaciären, Sweden. *Journal of Glaciology*, **34**(117), 228–231.

Hooke, R.LeB., Calla, P., H, P., Nilsson, M. and Stroeven, A., 1989. A 3-year record of seasonal variations in surface velocity, Storglaciären, Sweden. *Journal of Glaciology*, **35**(120), 235–247.

Hooke, R.LeB., Laumann, T. and Kohler, J., 1990. Subglacial water pressures and the shape of subglacial conduits. *Journal of Glaciology*, **36**(122), 67–71.

Howat, I.M., Joughin, I., Fahnestock, M., Smith, B.E. and Scambos, T.A., 2008. Synchronous retreat and acceleration of southeast Greenland outlet glaciers 2000–06: ice dynamics and coupling to climate. *Journal of Glaciology*, **54**, 646–660.

Hubbard, B. and Nienow, P., 1997. Alpine subglacial hydrology. *Quaternary Science Reviews*, **16**(9), 939–955.

Hubbard, B. and Glasser, N., 2005. *Field Techniques in Glaciology and Glacial Geomorphology*. Chichester: Wiley.

Hubbard, B., Sharp, M, Willis, I.C, Nielsen, M. and Smart, C.C., 1995. Borehole water level variations and the structure of the subglacial hydrological system of Haut Glacier d'Arolla, Switzerland. *Journal of Glaciology*, **41**(139), 572–583.

Hubbard, B., Heald, A., Reynolds, J.M., Quincey, D., Richardson, S.D., Luyo, M.Z., Portilla, N.S. and Hambrey, M.J., 2005. Impact of a rock avalanche on a moraine-dammed lake: Laguna Safuna Alta, Cordillera Blanca, Peru. *Earth Surface Processes and Landforms*, **30**(10), 1251–1264.

Huss, M., 2011. Present and future contribution of glacier storage change to runoff from macroscale drainage basins in Europe. *Water Resources Research*, **47**(W7), W07511.

Huss, M. and Farinotti, D., 2012. Distributed ice thickness and volume of 180,000 glaciers around the globe. *Journal of Geophysical Research*, **117**, F04010.

Huss, M., Bauder, A., Werder, M., Funk, M. and Hock, R., 2007. Glacier-dammed lake outburst events of Gornersee, Switzerland. *Journal of Glaciology*, **53**(181), 189–200.

Iken, A., 1981. The effect of subglacial water pressure on the sliding velocity of a glacier in an idealized numerical model. *Journal of Glaciology*, **27**(97), 407–421.

Iken, A. and Bindschadler, R.A., 1986. Combined measurements of subglacial water pressure and surface velocity of the Findelengletscher, Switzerland: conclusions about drainage system and sliding mechanism. *Journal of Glaciology*, **32**(110), 101–19.

Iken, A., Röthlisberger, H., Flotron, A. and Haeberli, W., 1983. The uplift of Unteraargletscher at the beginning of the melt season, a consequence of water storage at the bed? *Journal of Glaciology,* **29**(101), 28–47.

Iken, A., Fabri, K. and Funk, M., 1996. Water storage and subglacial drainage conditions inferred from borehole measurements on Gornergletscher, Valais, Switzerland. *Journal of Glaciology*, **42**, 233–248.

IPCC, 2013. *Summary for Policymakers*. In: **Stocker, T.F., Qin, D., Plattner, G-K., Tignor, M., Allen, S.K., Boschung, J., Nauels, A., Xia, Y., Bex, V. and Midgley, P.M. (Eds.),** 2013. *Climate Change 2013: The Physical Science Basis. Contribution of Working Group I to the Fifth Assessment Report of the Intergovernmental Panel on Climate Change.* Cambridge University Press: Cambridge, United Kingdom and New York, NY, United States of America.

Irvine-Fynn, T.D.L, Hodson, A.J., Moorman, B.J., Vatne, G. and Hubbard, A.L., 2011. Polythermal glacier hydrology: a review. *Reviews of Geophysics*, **49**(4), RG000350.

Iverson, N.R., Jansson, P. and Hooke, R.LeB., 1994. In situ measurement of strength of deforming subglacial sediment. *Journal of Glaciology*, **40**, 497–503.

Iverson, N.R, Hanson, B., Hooke, R.LeB. and Jansson, P., 1995. Flow mechanisms of glaciers on soft beds. *Science*, **267**, 80–81.

Jacobsen, D., Milner, A.M., Brown, L.E. and Dangles, O., 2012. Biodiversity under threat in glacier-fed river systems. *Nature Climate Change*, **2**, 361–364.

Jain, S. and Sudheer, K., 2008. Fitting of hydrologic models: a close look at the Nash-Sutcliffe Index. *Journal of Hydrologic Engineering*, **13**(10), 981–986.

Jansson, P., 1995. Water pressure and basal sliding, Storglaciären, northern Sweden. *Journal of Glaciol*ogy, **41**(138), 232–240.

Jansson, P., 1996. Dynamics and hydrology of a small polythermal glacier. *Geografiska Annaler*, **78A**(2–3), 169–174.

Jansson, P., 1999. Effects of uncertainties in measured variables on the calculated mass balance of Storglaciären. *Geografiska Annaler*, **81A**(4), 633–642.

Jansson, P. and Pettersson, R., 2007. Spatial and temporal characteristics of a long mass balance record, Storglaciären, Sweden. *Arctic, Antarctic and Alpine Research*, **39**(3), 432–437.

Jansson, P. and Näslund, J-O., 2009. *Spatial and temporal variations in glacier hydrology on Storglaciären, Sweden*. SKB TR-09-13, Swedish Nuclear Waste Management Company. 53pp.

Jansson, P., Hock, R. and Schneider, T., 2003. The concept of glacier storage: a review. *Journal of Hydrology*, **282**, 116–129.

Jobard, S. and Dzikowski, M., 2006. Evolution of glacial flow and drainage during the ablation season. *Journal of Hydrology*, **330**(3), 663–671.

Jonsell, U., Hock, R. and Holmgren, B., 2003. Spatial and temporal variations in albedo on Storglaciären, Sweden. *Journal of Glaciology*, **49**(164), 59–68.

Kamb, B., 1970. Sliding motion of glaciers: theory and observation. *Reviews of Geophysics and Space Physics*, **8**(4), 673–728.

Kamb, B., 1987. Glacier surge mechanism based on linked cavity configuration of the basal water conduit system. *Journal of Geophysical Research*, **92**, 9083–9100.

Kamb, B., Raymond, C., Harrison, W., Engelhardt, H., Echelmeyer, K., Humphrey, N. and Pfeffer, T., 1985. Glacier surge mechanism: 1982–1983 surge of Variegated Glacier, Alaska. *Science*, **227**, 469–479.

Kavanaugh, J.L. and Clarke, G.K.C., 2001. Abrupt glacier motion and reorganization of basal shear stress following the establishment of a connected drainage system. *Journal of Glaciology*, **47**(158), 472–480.

Kerr, R.A., 2013. Melting glaciers, not just ice sheets, stoking sea-level rise. *Science*, **340**(6134), 798.

Klok, E.J. and Oerlemans, J., 2002. Model study of the spatial distribution of the energy and mass balance of Morteratschgletscher, Switzerland. *Journal of Glaciology*, **48**(163), 505–518.

Knighton, A.D., 1981. Channel form and flow characteristics of supraglacial streams, Austre Okstindbreen, Norway. *Arctic Alpine Research*, **13**(3), 295–306.

Knighton, A.D., 1985. Channel form adjustment in supraglacial streams, Austre Okstindbreen, Norway. *Arctic Alpine Research*, **17**(4), 451–466.

Koblet, T., Gärtner-Roer, I., Zemp, M., Jansson, P., Thee, P., Haeberli, W. and Holmlund, P., 2010. Reanalysis of multi-temporal aerial images of Storglaciären, Sweden (1959-99) – Part 1: Determination of length, area, and volume changes. *The Cryosphere*, **4**(3), 333–343.

Kohler, J., 1992. *Glacial Hydrology of Storglaciären, Northern Sweden*. Unpublished Ph.D. Thesis, University of Minnesota, Minneapolis, USA.

Kohler, J., 1995. Determining the extent of pressurised flow beneath Storglaciären, Sweden, using results of tracer experiments and measurements of input and output discharge. *Journal of Glaciology*, **41**(138), 217–231.

Krause, P., Boyle, D.P. and Bäse, F., 2005. Comparison of different efficiency criteria for hydrological model assessment. *Advances in Geoscience*, **5**, 89–97.

Krimmel, R.M., 1999. Analysis of difference between direct and geodetic mass balance measurements at South Cascade Glacier, Washington. *Geografiska Annaler*, **81A**(4), 653–658.

Legates, D.R. and McCabe G.J.Jr., 1999. Evaluating the use of "goodness-of-fit" measures in hydrologic and hydroclimatic model validation. *Water Resources Research*, **35**(1), 233–241.

Linderholm, H.W. and Jansson, P., 2007. Proxy data reconstructions of the Storglaciären (Sweden) mass-balance record back to AD 1500 on annual to decadal timescales. *Annals of Glaciology*, **46**, 261–267.

Lliboutry, L., 1968. General theory of subglacial cavitation and sliding of temperate glaciers. *Journal of Glaciology*, **7**(49), 21–58.

Lüthje, M., Pedersen, L.T., Reeh, N. and Greuell, W., 2006. Modelling the evolution of supra-glacial lakes on the western Greenland ice sheet margin. *Journal of Glaciology*, **52**, 608–618.

Mader, H.M., 1992. Observations of the water-vein system in polycrystalline ice. *Journal of Glaciology*, **38**(130), 333–347.

Mair, D., Nienow, P., Sharp, M., Wohlleben, T. and Willis, I., 2002. Influence of subglacial drainage system evolution on glacier surface motion: Haut Glacier d'Arolla, Switzerland. *Journal of Geophysical Research*, **107**(B8), EPM8-1–EPM8-13.

Mair, D., Willis, I., Hubbard, B., Fischer, U., Nienow, P. and Hubbard, A., 2003. Hydrological controls on patterns of surface, internal and basal velocities during three "spring events": Haut Glacier d'Arolla, Switzerland. *Journal of Glaciology*, **49**(167), 555–567.

Male, D.H. and Gray, D.M., 1981. Snow cover ablation and runoff. In: **Gray, D.M. and Male, D.H. (Eds.),** 1981. *Handbook of Snow*. Pergamon, Toronto, pp.360–436.

Marzeion, B., Jaorsch, A. and Hofer, M., 2012. Past and future sea-level change from the surface mass balance of glaciers. *The Cryosphere*, **6**, 1295–1322.

McCuen, R., Knight, Z. and Cutler, A., 2006. Evaluation of the Nash-Sutcliffe Efficiency Index. *Journal of Hydrologic Engineering*, **11**(6), 597–602.

McMillan, M., Nienow, P., Shepherd, A., Benham, T. and Sole, A., 2007. Seasonal evolution of supra-glacial lakes on the Greenland Ice Sheet. *Earth and Planetary Science Letters*, **262**(3–4), 484–492.

Meier, M.F., 1984. Contribution of small glaciers to global sea level. *Science*, **226**, 1418–1421.

Meier, M.F., Dyurgerov, M.B., Rick, U.K., O'Neel, S., Pfeffer, W.T., Anderson, R.S., Anderson, S.P. and Glazovsky, A.F., 2007. Glaciers dominate eustatic sea-level rise in the 21st century. *Science*, **317**(5841), 1064–1067.

Mercer, A., 2004. *An investigation of the englacial and subglacial drainage pattern in Storglaciären's ablation area*. Tarfalakursen Studentrapporter. Unpublished Master's Thesis, University of Stockholm, Stockholm, Sweden.

Müller, F. and Keeler, C.M., 1969. Errors in short-term ablation measurements on melting ice surfaces. *Journal of Glaciology*, **8**(52), 91–105.

Murray, T. and Clarke, G.K.C., 1995. Black-box modeling of the subglacial water system. *Journal of Geophysical Research: Solid Earth*, **100**(B6), 10231–10245.

Nash, J.E. and Sutcliffe, J.V., 1970. River flow forecasting through conceptual models, Part I. A Discussion of principles. *Journal of Hydrology*, **10**, 282–290.

Nick, F.M., Vieli, A., Howat, I.M. and Joughin, I., 2009. Large-scale changes in Greenland outlet glacier dynamics triggered at the terminus. *Nature Geoscience*, **2**, 110–114.

Nienow, P.W. and Hubbard, B.P., 2005. Surface and Englacial Drainage of Glaciders and Ice Sheets. In: **Anderson, M.G. (Ed.)**, 2005. *Encyclopedia of Hydrological Sciences.* John Wiley and sons.

Nienow, P., Sharp, M. and Willis, I., 1996. Velocity-discharge relationships derived from dye-tracer experiments in glacial meltwaters: implications for subglacial flow conditions. *Hydrological Processes*, **10**, 1411–1426.

Nienow, P., Sharp, M. and Willis, I., 1998. Seasonal changes in the morphology of the subglacial drainage system, Haut Glacier d'Arolla, Switzerland. *Earth Surface Processes and Landforms,* **23**, 825–843.

Nilsson, J. and Sundblad, B., 1975. The internal drainage of Storglaciären and Isfallsglaciären described by an autoregressive model. *Geografiska Annaler*, **57A**(1–2), 73–98.

Nye, J.F., 1976. Water flow in glaciers: Jökulhlaups, tunnels and veins. *Journal of Glaciology*, **17**(76), 181–207.

Oerlemans, J., 1992. Climate sensitivity of glaciers in southern Norway: application of an energy-balance model to Nigardsbreen, Hellstugbreen and Alfotbreen. *Journal of Glaciology*, **38**(129), 223–232.

Oerlemans, J., 1993. A model for the surface balance of ice masses: part I. Alpine glaciers. *Z. Glestscherkd. Glazialgol.*, **27/28**(1991/1992), 63–83.

Oerlemans, J. and Hoogendoorn, N., 1989. Mass-balance gradients and climatic change. *Journal of Glaciology*, **35**(121), 399–405.

Östling, M. and Hooke, R.LeB., 1986. Water storage in Storglaciären, Kebnekaise, Sweden. *Geografiska Annaler*, **68A**(4), 279–290.

Østrem, G. and Brugman, M., 1991. *Glacier mass-balance measurements. A manual for field and office work*. Saskatoon, Sask., Environment Canada. National Hydrology Research Institute (NHRI Science Report 4).

Pälli, A., Moore, J.C., Jania, J., Kolondra, L. and Głowacki, P., 2003. The drainage pattern of Hansbreen and Werenskioldbreen, two polythermal glaciers in Svalbard. *Polar Research*, **22**(2), 355–371.

Petterson, R., Jansson, P. and Holmlund, P., 2003. Cold surface layer thinning on Storglaciären, Sweden, observed by repeated ground penetrating radar surveys. *Journal of Geophysical Research*, **108**(F1).

Petterson, R. Jansson, P. and Blatter, H., 2004. Spatial variability of water content at the cold-temperate transition surface of the polythermal Storglaciären, Sweden. *Journal of Geophysical Research*, **109**(F2), F02009.

Pettersson, R., Jansson, P., Blatter, H. and Huwald, H., 2007. Spatial pattern and stability of the cold surface layer of Storglaciären, Sweden. *Journal of Glaciology*, **53**(180), 99–109.

Pimentel, S. and Flowers, G., 2011. A numerical study of hydrologically driven glacier dynamics and subglacial flooding. *Proceedings of the Royal Society A: Mathematical, Physical and Engineering Science*, **467**(2126), 537–558.

Pohjola, V. A., 1993. TV-video observations of bed and basal sliding on Storglaciären, Sweden. *Journal of Glaciology*, **39**(131), 111–118.

Pohjola, V.A., 1994. TV-video observations of englacial voids in Storglaciären, Sweden. *Journal of Glaciology*, **40**(135), 231–240.

Purdie, H.L., Brook, M.S. and Fuller, I.C., 2008. Seasonal variation in ablation and surface velocity on a temperate maritime glacier: Fox Glacier, New Zealand. *Arctic, Antarctic and Alpine Research*, **40**(1), 140–147.

Radić, V. and Hock, R., 2006. Modeling future glacier mass balance and volume changes using ERA-40 reanalysis and climate models: a sensitivity study at Storglaciären, Sweden. *Journal of Geophysical Research*, **11**, F03003, doi:10.1029/2005JF000440.

Radić, V. and Hock, R., 2011. Regionally differentiated contribution of mountain glaciers and ice caps to future sea-level rise. *Nature Geoscience*, **4**(2), 91–94.

Radić, V., Bliss, A., Beedlow, A.C., Hock, R., Miles, E. and Cogley, J.G., 2013. Regional and global projections of 21st century glacier mass changes in response to climate scenarios from global climate models. *Climate Dynamics*, doi:10.1007/s00382-013-1719-7.

Raymond, C.F. and Harrison, W.D., 1975. Some observations on the behavior of the liquid and gas phases in temperate glacier ice. *Journal of Glaciology*, **14**(71), 213–233.

Reijmer, C.H. and Hock, R., 2008. Internal accumulation on Storglaciären, Sweden, in a multi-layer snow model coupled to a distributed energy- and mass-balance model. *Journal of Glaciology*, **54**(184), 61–72.

Richards, K.S., Sharp, M.J., Arnold, N., Gurnell, A., Clark, M., Tranter, M., Nienow, P., Brown. G.H., Willis, I.C. and Lawson, W.J., 1996. An integrated approach to modelling hydrology and water quality in glacierised catchments. *Hydrological Processes*, **10**, 479–508.

Rippin, D., Willis, I., Arnold, N., Hodson, A., Moore, J., Kohler, J. and Björnsson, H., 2003. Changes in geometry and subglacial drainage of Midre Lovénbreen, Svalbard, determined from digital elevation models. *Earth Surface Processes and Landforms*, **28**(3), 273–298.

Rippin, D.M., Willis, I.C., Arnold, N.S., Hodson, A.J. and Brinkhaus, M., 2005. Spatial and temporal variations in surface velocity and basal drag across the tongue of the polythermal Midre Lovenbreen, Svalbard. *Journal of Glaciology*, **51**(175), 588–600.

Roesner, L.A., Aldrich, J.A. and Dickinson, R.E., 1988. *Storm Water Management Model User's Manual Version 4: EXTRAN Addendum.* US Environmental Protection Agency, Athens, Georgia, 188pp.

Röthlisberger, H., 1972. Water pressure in intra- and subglacial channels. *Journal of Glaciology*, **11**(62), 177–203.

Röthlisberger, H. and Lang, H., 1987. Glacial hydrology. In: **Gurnell, A.M and Clark, M.J. (Eds.),** 1987. *Glaciofluvial Sediment Transfer*. Chichester: Wiley. pp.207-284.

Rye, C.J., Arnold, N.S., Willis, I. and Kohler, J., 2010. Modelling the surface mass balance of a High Arctic glacier using ERA-40 reanalysis. *Journal of Geophysical Research: Earth Surface*, doi: 10.1029/2009JF001364.

Schaner, N., Voisin, N., Nijssen, B. and Lettenmaier, D.P., 2012. The contribution of glacier melt to streamflow. *Environmental Research Letters*, **7**(3).

Scherler, D., Bookhagen. B. and Strecker, M., 2011. Spatially variable response of Himalayan glaciers to climate change affected by debris cover. *Nature Geoscience*, **4**, 156–159.

Schneeberger, C., Albrecht, O., Blatter, H., Wild, M. and Hock, R., 2001. Modelling the response of glaciers to a doubling in atmospheric CO2: a case study of Storglaciären, northern Sweden. *Climate Dynamics*, **17**(11), 825–834.

Schneider, T., 1999. Water movement in the firn of Storglaciären, Sweden. *Journal of Glaciology*, **45**(150), 286–294.

Schneider, T., 2001. *Hydrological Processes in Firn on Storglaciären, Sweden.* Unpublished Ph.D. Thesis, University of Stockholm, Stockholm, Sweden.

Schneider, T. and Bronge, C., 1996. Suspended sediment transport in the Storglaciären drainage basin. *Geografiska Annaler*, **78A**(2–3), 155–161.

Schneider, T. and Jansson, P., 2004. Internal accumulation in firn and its significance for the mass balance of Storglaciären, Sweden. *Journal of Glaciology*, **50**(168), 25–34.

Schoof, C., 2007. Ice sheet grounding line dynamics: Steady states, stability, and hysteresis. *Journal of Geophysical Research: Earth Surface*. **112**(F3), doi: 10.1029/2006JF000664.

Schoof, C., 2010. Ice-sheet acceleration driven by melt-supply variability. *Nature*, **468**(7325), 803–806.

Schoof, C. and Hewitt, I.J., 2013. Ice-sheet dynamics. *Annual Reviews of Fluid Mechanics*, **45**, 217–239.

Schoof, C., Hewitt, I.J. and Werder, M.A., 2012. Flotation and open water flow in a model for subglacial drainage. Part I: linked cavities. *Journal of Fluid Mechanics*, **702**, 126–156.

Schuler, T., Fischer, U.H. and Gudmundsson, G.H., 2004. The diurnal variability of subglacial drainage conditions as revealed by tracer experiments. *Journal of Geophysical Research*, **109**(F2).

Schytt, V., 1959. *The glaciers of the Kebnekajse-massif*. *Geografiska Annaler*, **41A**(4), 213–227.

Schytt, V., 1973. Snow densities on Storglaciären in spring and summer. *Geografiska Annaler*, **55A**(3–4), 155–158.

Schytt, V., 1981. The net mass balance of Storglaciären, Kebnekaise, Sweden, related to the height of the equilibrium line and to the height of the 500 mb surface. *Geografiska Annaler*, **63A**(3–4), 219–223.

Seaberg, S.Z., Seaberg, J.Z., Hooke, R.LeB. and Wiberg, D., 1988. Character of the englacial and subglacial drainage system in the lower part of the ablation area of Storglaciären, Sweden, as revealed by dye trace studies. *Journal of Glaciology*, **34**(117), 217–227.

Sharma, A.N., Luo, D., and Walter, M.T., 2012. Hydrological tracers using nanobiotechnology: proof of concept. *Environmental Science and Technology*, **46**, 8928–8936, doi: 10.1021/es301561q.

Sharp, M.J., 2005. *Subglacial Drainage*. In: **Anderson, M.G. and McDonnell, J. (Eds.)**, 2005. *Encyclopedia of Hydrological Sciences*. Chichester: Wiley.

Sharp, M., Richard, K.S., Arnold, N., Willis, I.C., Nienow, P. and Tison, J-L., 1993. Geometry, bed topography and drainage system structure of the Haut Glacier d'Arolla, Switzerland. *Earth Surface Processes and Landforms*, **18**(6), 557–571.

Shepherd, A., Ivins, E.R., Geruo, A., Barletta, V.R., Bentley, M.J., Bettadpur, S., Briggs, K.H., Bromwich, D.H., Forsberg, R., Galin, N., Horwath, M. Jacobs, S., Joughin, I., King, M.A., Lenaerts, J.T.M., Li, J., Ligtenberg, S.R.M., Luckman, A., Luthcke, S.B., McMillan, M., Meister, R., Milne, G., Mouginot, J., Muir, A., Nicolas, J.P., Paden, J., Payne, A.J., Pritchard, H., Rignot, E., Rott, H., Sørensen, L.S., Scambos, T.A., Scheuchl, B., Schrama, E.J.O., Smith, B., Sundal, A.V., van Angelen, J.H., van de Berg, W.J., van den Broeke, M.R., Vaughan, D.G., Velicogna, I., Wahr, R., Whitehouse, P.L., Wingham, D.J., Yi, D., Young, D. and Zwally, H.J., 2012. A reconciled estimate of ice-sheet mass balance. *Science*, **338**(6111), 1183–1189.

Shreve, R.L., 1972. Movement of water in glaciers. *Journal of Glaciology,* **11**(62), 205–214.

Smart, C.C., 1996. Statistical evolution of glacier boreholes as indicators of basal drainage systems. *Hydrological Processes*, **10**(4), 599–613.

Span, N. and Kuhn, M., 2003. Simulating annual glacier flow with a linear reservoir model. *Journal of Geophysical Research*, **108**(D10), doi: 10.1029/2002JD002828.

Spring, U. and Hutter, K., 1981. Numerical studies of Jökulhlaups. *Cold Regions Science and Technology*, **4**, 227–244.

Spring, U. **and Hutter, K.,** 1982. Conduit flow of a fluid through its solid phrase and its application to intraglacial channel flow. *International Journal of Engineering Science*, **20**, 327–363.

Stenborg, T., 1965. Problems concerning winter run-off from glaciers. *Geografiska Annaler*, **47A**(3), 141–184.

Stenborg, T., 1969. Studies of the internal drainage of glaciers. *Geografiska Annaler*, **51A**(1–2), 13–41.

Stenborg, T., 1970. Delay of run-off from a glacier basin. *Geografiska Annaler*, **52A**(1), 1–30.

Stone, D.B. and Clarke, G.K.C., 1996. In situ measurements of basal water quality and pressure as an indicator of the character of subglacial drainage systems. *Hydrological Processes*, **10**(4), 615–628.

Stuart, G., Murray, T., Gamble, N., Hayes, K. and Hodson, A., 2003. Characterization of englacial channels by ground-penetrating radar: an example from austre Brøggerbreen, Svalbard. *Journal of Geophysical Research*, **108**(B11).

Sundal, A., Shepherd, A., Nienow, P., Hanna, E., Palmer, S. and Huybrechts, P., 2011. Melt-induced speed-up of the Greenland ice sheet offset by efficient sub-glacial drainage. *Nature*, **469**(7331), 521–524.

Svenonius, F., 1910. Studien über den Kårso- und die Kebnegletscher nebst Notizen über andere Gletscher im Jukkasjärvigebirge. In Die Gletscher Schwedens im Jahre 1908. *SGU*, **5**, 1–54.

Swift, D.A., Nienow, P.W., Hoey, T.B. and Mair, D.W.F., 2005. Seasonal evolution of runoff from Haut Glacier d'Arolla, Switzerland and implications for glacial geomorphic processes. *Journal of Hydrology*, **309**(1–4), 133–148.

Tranter, M., 2005. Sediment and Solute Transport in Glacial Meltwater Streams. In: **Anderson, M.G. (Ed.)**, 2005. *Encyclopedia of Hydrological Sciences*. Volume 4. Chichester: Wiley.

Tranter, M., Brown, G.H., Hodson, A. and Gurnell, A.M., 1996. Hydrochemistry as an indicator of subglacial drainage system structure: a comparison of Alpine and Sub-Polar environments. *Hydrological Processes*, **10**(4), 541–556.

UNIRAS, 1990. *Unimap 2000 user's manual. Version 6.* Søborg, Denmark, UNIRAS Ltd.

van der Veen, C.J., 2007. Fracture propagation as a means of rapidly transferring surface meltwater to the base of glaciers. *Geophysical Research Letters*, **34**(1), L028035.

Vaughan, D.G., Comiso, J.C., Allison, I., Carrasco, J., Kaser, G., Kwok, R., Mote, P., Murray, T., Paul, F., Ren, J., Rignot, E., Solomina, O., Steffen, K. and Zhang, T., 2013. *Observations: Cryosphere*. In: **Stocker, T.F., Qin, D., Plattner, G.-K., Tignor, M., Allen, S.K., Boschung, J., Nauels, A., Xia, Y., Bex, V. and Midgley, P.M. (Eds.),** 2013. *Climate Change 2013: The Physical Science Basis. Contribution of the Working Group I to the Fifth Assessment Report of the Intergovernmental Panel on Climate Change.* Cambridge University Press, Cambridge, United Kingdom and New York, NY, United States of America.

Vieli, A., Jania, J., Blatter, H. and Funk, M., 2004. Short-term velocity variations on Hansbreen, a tidewater glacier in Spitsbergen. *Journal of Glaciology*, **50**(170), 389–398.

Walder, J.S., 1986. Hydraulics of subglacial cavities. *Journal of Glaciology,* **32**, 439–445.

Walder, J.S. and Hallet, B., 1979. Geometry of former subglacial water channels and cavities. *Journal of Glaciology*, **23**(89), 335–346.

Walder, J.S. and Fowler, A.C., 1994. Channelized subglacial drainage over a deformable bed. *Journal of Glaciology*, **40**(134), 3–15.

Weertman, J., 1964. The theory of glacial sliding. *Journal of Glaciology*, **5**(39), 287–303.

Weertman, J., 1972. General theory of water flow at the base of a glacier or ice sheet. *Reviews of Geophysics,* **10**(1), 287–333.

Werder, M.A., Hewitt, I.J., Schoof, C.G. and Flowers, G.E., 2013. Modeling channelized and distributed subglacial drainage in two dimensions. *Journal of Geophysical Research*, **118**(4), 2140–2158.

Williamson, A.G., 2013. T*he subglacial drainage system structure and morphology of Storglaciären, Sweden*. Unpublished B.A. Thesis, University of Cambridge, Cambridge, UK.

Willis, I.C., 1995. Intra-annual variations in glacier motion: a review. *Progress in Physical Geography*, **19**(11), 61–106.

Willis, I.C., 2005. *Hydrology of Glacierised Basins*. In: **Anderson, M.G. (Ed.)**, 2005. *Encyclopedia of Hydrological Sciences*. Volume 4. Chichester: Wiley.

Willis, I.C., 2011. Hydrographs. In: **Singh, V.P., Singh, P. and Haritashya, U.K. (Eds.),** 2011. *Encyclopedia of Snow, Ice and Glaciers*, Part 17, 918–922.

Willis, I. and Bonvin, J-M., 1995. Climate change in mountain environments: hydrological and water resource implications. *Geography*, **80**(33), 247–261.

Willis, I.C., Sharp, M.J. and Richards, K.S., 1990. Configuration of the drainage system of Midtdalsbreen, Norway, as indicated by dye-tracing experiments. *Journal of Glaciology*, **36**(122), 89–101.

Willis, I.C., Sharp, M.J. and Richards, K.S., 1993. Studies of the water balance of Midtdalsbreen, Hardangerjokulen, Norway. I. The calculation of surface water inputs from simple meteorological data. *Z. Gletscherkd. Glazialgeol.*, **27/28**(1991/1992), 97–115.

Willis, I., Arnold, N. and Brock, B., 2002. Effect of snowpack removal on energy balance, melt and runoff in a small supraglacial catchment. *Hydrological Processes,* **16**(14), 2721–2749.

Willis, I., Lawson, W., Owens, I., Jacobel, B. and Autridge, J., 2008. Subglacial drainage system structure and morphology of Brewster Glacier, New Zealand. *Hydrological Processes*, **23**(3), 384–396.

Willis, I.C., Fitzsimmons, C., Melvold, K., Andreassen, L.M. and Giesen, R.H., 2012. Structure, morphology and water flux of a subglacial drainage system, Midtdalsbreen, Norway. *Hydrological Processes*, **26**(25), 3810–3829.

Wright, A.P., Siegert, M.J., Le Brocq, A.M. and Gore, D.B., 2008. High sensitivity of subglacial hydrological pathways in Antarctica to small ice-sheet changes. *Geophysical Research Letters*, **35**(17), 1–5.

Zhang, Y., Fujita, K., Liu, S., Liu, Q. and Numimura, T., 2011. Distribution of debris thickness and its effect on ice melt at Hailuogou glacier, southeastern Tibetan Plateau, using in situ surveys and ASTER imagery. *Journal of Glaciology*, **57**(206), 1147–1157.

Zimmerer, S., 1987. *A study of the englacial and subglacial hydrology of Storglaciären, northern Sweden.* Unpublished M.S. Thesis. University of Minnesota, Minneapolis, USA.

Zwally, H.J., Abdalati, W., Herring, T., Larson, K., Saba, J. and Steffen, K., 2002. Surface melt-induced acceleration of Greenland ice-sheet flow. *Science*, **297**(5579), 218–222.